ENC 2007

European Nuclear Conference

16-20 September 2007, Brussels, Belgium

TRANSACTIONS

inspire yourself ■ and others

www.euronuclear.org www.enc2007.org enc2007@euronuclear.org

european nuclear society
largest nuclear society for science and industry

in cooperation with the Belgian Nuclear Society

in cooperation with the IAEA

IAEA
International Atomic Energy Agency

in cooperation with the OECD/NEA

AEN NEA

in association with the American Nuclear Society

with the support of the Vrije Universiteit Brussel

Vrije Universiteit Brussel

Rue de la Loi 57
1040 Brussels, Belgium
Phone + 32 2 505 30 54
Fax +32 2 502 39 02
E-mail ens@euronuclear.org
Internet www.euronuclear.org
ISBN 978-92-95064-14-0
These transactions contain all contributions submitted by 14 September 2007.

Track 3

Medical applications

Session 17.3.1:

Diagnostics in Nuclear Medicine

Session 17.3.2:

Therapeutic Applications 2

POTENTIAL RADIONUCLIDES FOR RADIOSYNOVIORTHESIS. DOSIMETRIC CRITERIA FOR THEIR SELECTION

TORRES BERDEGUEZ M. B., AYRA PARDO F. E., ALBUERNE ALFONSO O.

Radiation Protection Department, Isotopes Centre
Havana, Cuba

MONTANO DELGADO M. A.

Hospital General Docente Enrique Cabrera
Havana, Cuba

ABSTRACT

The objectives of this work are to make a comparison of ^{32}P, ^{90}Y, ^{188}Re, ^{177}Lu, ^{51}Cr, ^{153}Sm, and ^{169}Er and determine the influence of the variation of the thickness of the synovial membrane and the shape of the synovium in the S values. We modelled spheres, cylinders and ellipsoids using MCNPX code to assess the therapeutic and maximum ranges, the S values and the influence of the mentioned variations on it. The results achieved with this work indicate that an approach to the patient – specific dosimetry in RSV will improve the prescription of the dose to the patient. The selection of the radionuclide should be a function of the inflammation of the joint and not of its size. An adequate diagnostic of the damaged joint, could help assessing the relationship dose – effect of the treatment. The optimal radionuclide does not exist in RSV.

1. Introduction

The treatment of inflammatory arthropaties is aimed to diminish the inflammation, relieve the pain, improve the functional capability and induce the remission of the disease. Although every illness requires specific therapeutic guidelines [1], some joints may not experience clinical improvement, so other complementary therapies should be used. Most commons are intrarticular corticoids, chemical synovectomy, surgical synovectomy and radiosynoviorthesis (RSV). The first published reports of this last treatment are as back as to 1924 [2]. In the clinical practice, the first results were published in 1952 [3] and were followed during the 60s with the inclusion of the Y-90 [4, 5].

The RSV is the injection of a radioactive substance inside any synovial cavity, in such way that the injected radionuclide makes contact with the synovial membrane. This substance is rapidly phagocytized by the synovial lining cells. During the radioactive decay of the injected radionuclide, a therapeutic dose will be delivered to the synovial tissue destroying it. The beta emitters used in radiosynoviorthesis range energies between 0.34 MeV (0.33 mm penetration in tissue) in the case of Er-169 and 2.27 MeV (3.6 mm penetration in tissue) for the Y-90. The half life of these isotopes goes from 2.3 hrs (Dy-165) to 27.8 days (Cr-51)[6]. Nowadays, the selection of the radionuclide to be used depends on the size of the joint to be treated. Thus, the smaller the joint, the lower should be the energy and therefore the penetration. These facts led to the use of fixed radionuclides for specific joints. The first works on the assessment of doses to the patients in RSV were published in the 80s and beginning of the 90s [7, 8, 9, 10].

We've focused our attention in radionuclides that have been used or tested in animal and human models: ^{32}P, ^{90}Y, ^{188}Re, ^{177}Lu, ^{51}Cr, ^{153}Sm and ^{169}Er. Two were the objectives of this work. First, to compare these radionuclides from the dosimetric point of view so we can provide selection criteria depending on the kind and damage of the joint to be treated. Dosimetric parameters taken into account were the therapeutic and maximum range of the beta and electronic emission in the pannu tissue, as well as the absorbed dose in the synovial surface for different sizes of the synovium.

The second objective was to determine the influence in the S values of the proposed model, varying the thickness of the synovial membrane and the shape of the synovium. The method used to assess the dosimetry in radioactive synovectomy is known as the Monte Carlo method. The simulation in Monte

Carlo is the best alternative available nowadays to solve the problem of the radiation transport in the matter when we're dealing with complex geometries.

2. Materials and methods.

The synovial joint is basically the articular cartilage, bone and tissue (synovial membrane). In table 1 is shown the composition and density of every constituent according to Johnson and Yanch [9].

ELEMENTS	H	C	N	O	Na	Mg	P	S	Ca	Cl	ρ (g/cm^3)
BONE (%)	3.4	15.5	4.2	43.5	0.1	0.2	10.3	0.3	22.5	-	1.92
ARTICULAR CARTILAGE (%)	9.6	9.9	2.2	74.4	0.5	-	2.2	0.9	-	0.3	1.1
TISSUE (%)	10.0	14.9	3.5	71.6	-	-	-	-	-	-	1.0

Table 1. Composition and density of components of the synovial joint.

The energy of beta particles used in RSV should be enough to destroy the synovial tissue yet not as high as to expose unnecessarily the cartilage and bone. In table 2 are listed the energetic characteristics of the radionuclides assessed in this work.

Radionuclides	Y-90	P-32	Re-188	Lu-177	Sm-153	Er-169	Cr-51
$T_{1/2}$	64.1 hours	14.3 days	16.98 hours	6.71 days	46.7 hours	9.4 days	27.7 days
Emission type	Beta	Beta	Beta, gamma, electron	Beta, gamma, electron	Beta, gamma, electron	Beta, gamma, electron	electron, gamma

Table 2. Energetic characteristic of the evaluated radionuclides

The beta spectrum of each of these radionuclides was downloaded from www.doseinfo-radar.com and the characteristics of the gamma and/or electronic emission are the ones in the software RADIATION DECAY [11].

The S values have been calculated for different pair of source-target organs and for a number of radionuclides of interest in Nuclear Medicine. Here, the S factors for each proposed model was obtained by the calculation of the mean absorbed energy by disintegration (tally f8*) in the volume of the cell using the MCNPX code (problem geometry)[12], thru the equation 1:

$$S = \frac{f8^*}{m} * 576.7 * 10^{-3} \quad \text{(Gy/h*MBq)} \quad (1)$$

Where:

m: mass in grams of the cell.

*f8: results of the tally (MCNPX).

To determine the therapeutic range (X_{90}), a point isotropic source was simulated in the centre of various concentric spheres of different radii. These radii went from 1 mm to 10 mm with 1 mm increment for all radionuclides but for Er-169 and Cr-51. In the case of the Erbium, the radii went from 0.1 mm to 1 mm with 0.1 mm increments. For Chromium, from 0.1 µm to 1 µm with 0.1 µm increments.

The mathematical model to calculate the maximum range (X_{max}) was a point source in the centre of a sphere. Simulations were made using spheres of different radii, from 1 mm to 10 mm, with 1 mm increments for all the radionuclides but for the Er-169 and the Cr-51. In the case of the Erbium, the radii went from 0.1mm to 1mm with 0.1mm increments. For Chromium, from 0.1µm to 1µm with 0.1µm increments.

The S values for the synovial membrane were calculated using as a model a cylinder with the source uniformly distributed in its volume. This model was simulated varying the radius of the cylinder (from 0.5cm to 9cm, with 0.5cm increments) and its height (from 0.01cm to 0.04cm with 0.005cm increments). The radii represent different sizes of the synovial surface (the area in the base of the cylinder) for small, medium and large joints. The height represent different stages of the progression of the rheumatoid arthritis (RA)[8].

To assess the influence of the variation of the shape of the synovium in the S factors, spheroid elongations with fixed mass were simulated. Keeping the mass constant at 5, 10, 30, 70 and 100

grams, the radii were changed at a rate ($\frac{R_{long\ axis}}{R_{short\ axis}}$) of 1, 3, 5 and 10 every time. The source is distributed uniformly in the surface of the spheroid.
For the variation of the thickness of the synovial membrane, the model chosen was different pairs of concentric spheres with masses of the smaller one of 5, 10 and 30 grams. The radius of the second sphere will be 0.02 cm bigger than the first one. The source is uniformly distributes between the radii of two spheres. The variation of the thickness of the membrane is simulated moving the inner sphere in the X axis from 0 to 0.01 cm.

3. Analysis and discussion of results.

The selection of the radionuclide for the treatment will depend on the thickness of the synovium to be treated and the proximity of the non target organs of the joint (bone and articular cartilage), so it will be based in the absorbed dose and the penetration of the radiation emitted by the radionuclide. It is particularly important that the deepness of the target volume be in the therapeutic range (X_{90})and that the non target structures such as bone and cartilage be exposed the less possible to the radiation [10].
The therapeutic range is defined as the deepness at which the absorbed dose equals the 10 % of the maximum dose deposited in the synovial surface. In figure 2 there is a comparison between X_{90} and X_{max} for the assessed radionuclides. The therapeutic range is the one that determines the synovial thickness that can be treated and not the maximum range.

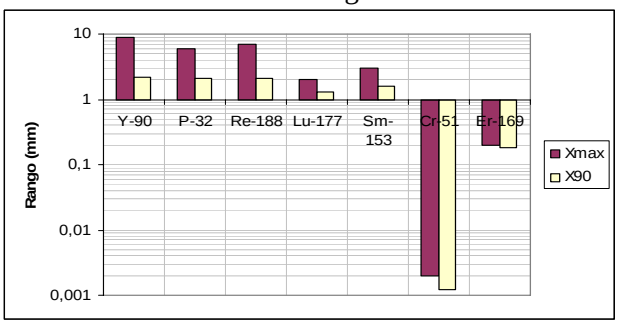

Figure 1. X_{90} and $X_{máx}$ for the ^{90}Y, ^{32}P, ^{188}Re, ^{177}Lu, ^{153}Sm, ^{51}Cr and ^{169}Er.

As the area of the inflamed synovium increases, diminishes the value of the absorbed dose rate in the synovial membrane (figure 3). For example, if we consider that 5 mCi of Y-90 delivers approximately 100 Gy of absorbed dose in an arthritic knee with a synovium surface of 250 cm^2, only 3 mCi of Y-90 will be needed to treat an arthritic wrist of about 50 cm^2 and achieve the same therapeutic effect [10]. In this case it is considered that the radionuclide decays completely in the joint, so no escape is taken into account, important aspect to keep in mind. No significant differences in the S values (Gy/h*MBq) obtained for different synovial membrane thickness and for each assessed radionuclide were observed.
The results obtained allow the estimation of the dose that will be delivered to the synovial membrane for different sizes of the joint and different stages of the disease. The values of X_{90} allow the estimation of the absorbed dose to the treated synovium (pannu tissue). Nevertheless, the relationship dose – effect of the treatment is far from been effectively assessed using this simple model due to factors not taken into account in it and that will be analyzed bellow.

Variation of the synovium shape.

The variation of the shape of the synovium depends on the kind of joint and the inflammatory nature of the RA. As shown in picture 5, the mayor influence in the variation of S value is observed for Y-90, P-32 and Re-188. For the rest of radionuclides, this variation is twice as less and for the Cr-51 is barely perceptible. For all the radionuclides this influence diminishes gradually as the synovium size increases.

Variation of the thickness of the synovial membrane.

As shown in figure 4, the variation of the thickness of the synovial membrane for Y-90 and a very small synovium volume (5 g), produces a considerable increment in the variation of S value in this volume. As the volume of the synovium increases this influence disappears.

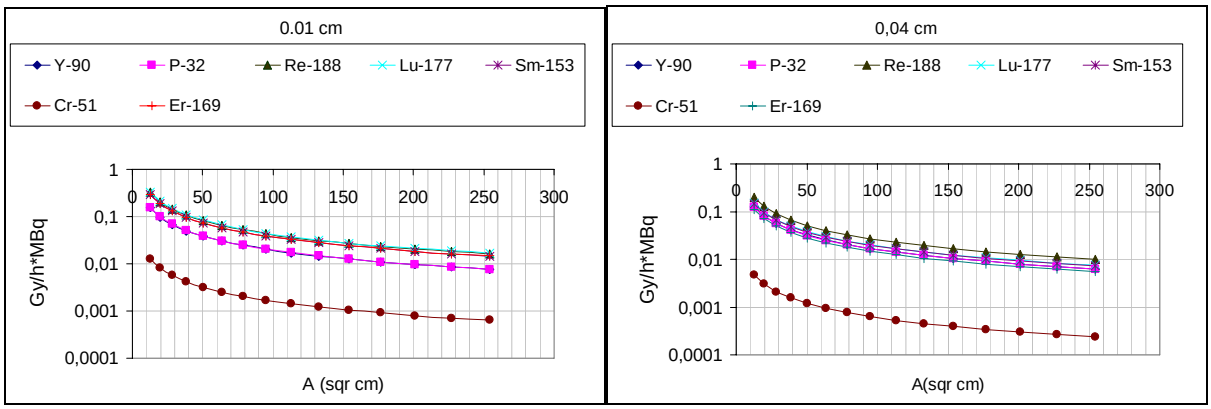

Figure 2. S Value for different size and thickness of synovial membrane

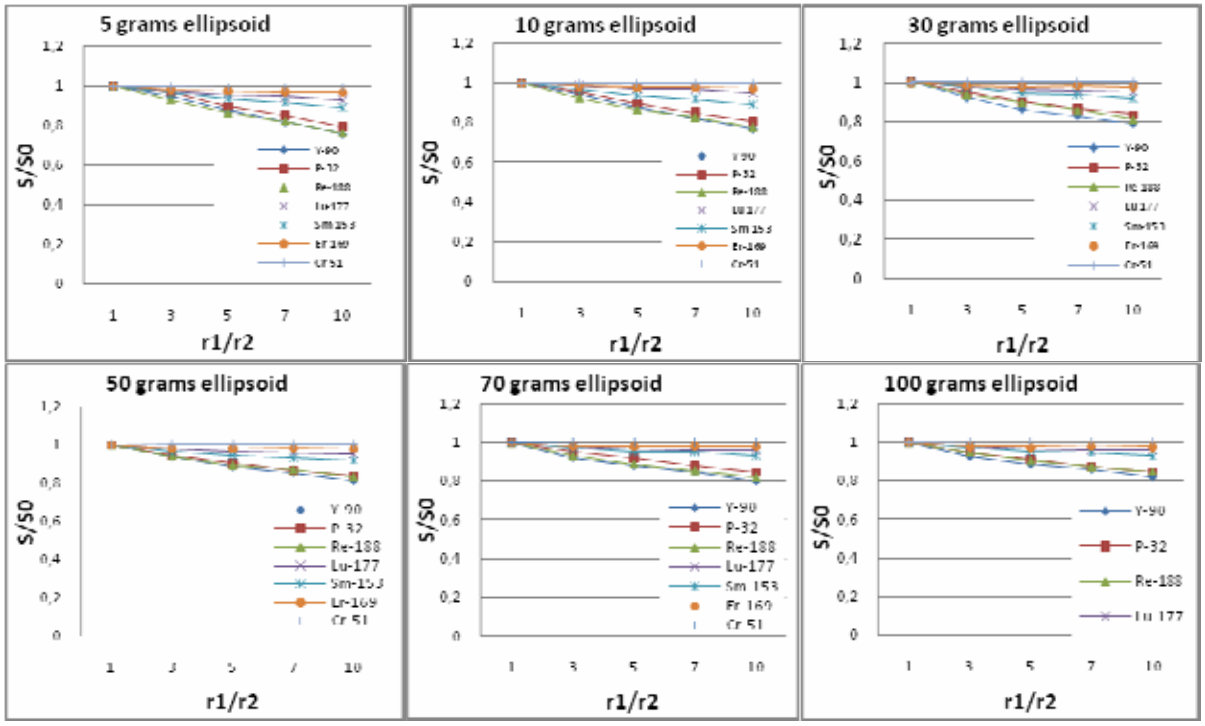

Figure 3. S-value fraction. Influence of the variation of the synovium shape.

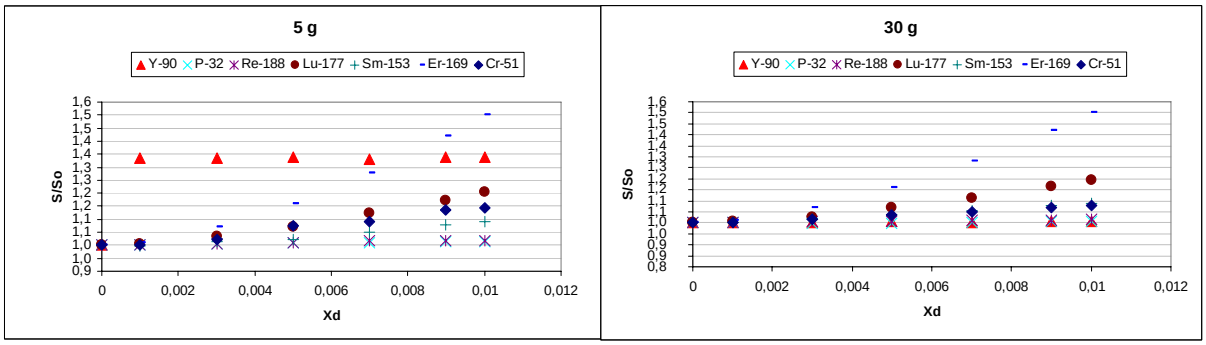

Figure 4. Variation of the synovial membrane thicknees. S-value influencing

Phosphorus 32 and Rhenium 188 have a similar behaviour between them. Here, the variation of the thickness of the membrane will not affect the variation of the S factors in the synovium. In the case of Er-169, Lu-177, Sm-153, and Cr-51, the gradual increase in the variation of the thickness of the synovial membrane (Xd), leads to an increment in the variation of the S factors for every volume of the synovium (5, 10 and 30 grams) been the Erbium the one that affects the most.

4. Conclusions.

The results achieved with this work indicate that the use of a simple model of the joint could lead to an overestimation or an underestimation of the dose to the damaged synovium. Nevertheless, an approach to the patient – specific dosimetry in RSV will improve the prescription of the dose to the patient, eliminating the practice of fixed radionuclides and doses for the treatment of different kind of joints, methodology applied in many clinics in Europe [14]. The selection of the radionuclide should be a function of the inflammation of the joint and not of its size.

An adequate diagnostic of the inflammatory characteristics of the damaged joint, could help assessing the relationship dose – effect of the treatment.

The optimal radionuclide does not exist in RSV. The planning of the treatment will be more effective as more real is the dosimetric model used. The debate is opened.

5. References.

1. Manual Merck, 17.ª Edición 1999
2. Ishido C. Über die Wirkung des radiothoriums auf die Gelenke. Strahlentherapie 1924;27:188-96
3. Fellinger K, Schmid J. Local therapy of rheumatics diseases. Wien Z Inn Med 1952;33:351-63
4. Delbarre F, Menkes C et al, Synoviorthesis with radioisotopes, Press med. 76 (1968) 1045.
5. Delbarre F, Le Go A, Menhes C, Aignan M, et al, Double Blind statistical study of therapeutics effect of a radioactivity yttrium (90Y) charged colloid on rheumatoid arthritis of the knee. C R Acad Sci Hebd Seances Acad Sci D 1974;279:1051-4
6. Clunie. G. A survey of radiation synovectomy in Europe, 1991-1993. European Journal of Nuclear Medicine. (Sep 1995) V.22 (9).p.970-976.
7. Martti Hannelin, "A dosimetric study of Dysprosium-165 macroaggreagates used in treating rheumatoid arthritis", Commentationes physico-mathematicae 87/1988, Dissertationes No. 16, Central Hospital of Etela-Saimaa, Lappeenranta, Finland.
8. Harling et al. Radiation synovectomy. Treatment of rheumatoid arthritis. Nucleat scince and engineering. Vol 110 apr 1992
9. L.Scott Johnson and Jacquelyn C. Yanch, "Absorbed dose profiles for radionuclides of frequent use in radiation synovectomy", Arthritis and Rheumatism, Vol 34. No 12, December 1991.
10. Johnson L.S, Yanch J.C, Shortkroff S, et.al, "Beta-particle dosimetry in radiation synovectomy", European Journal of Nuclear Medicine, (Sep 1995) V.22 (9).p.977-988.
11. Radiation decay version 2 March 1997. Charles Hacker, Engineering and Applied Science, Griffith University, Australia.
12. Judith F. Briesmeister, Editor. LA-12625-M, Version 4B Manual. MCNPTM. A general Monte Carlo N-particle transport code.
13. Clunie. G, "A survey of radiation synovectomy in Europe", European Journal of Nuclear Medicine, V.22 (9).p.970-976, Sep 1995.

Session 18.3.1:

Instrumentation

NOVEL SOLID STATE PHOTOMULTIPLIERS AND THEIR APPLICATION TO VERY HIGH RESOLUTION PET AND HYBRID SYSTEMS

G. LLOSÁ, N. BELCARI, G. COLLAZUOL, A. DEL GUERRA, S.MARCATILI, S.MOEHRS
Department of physics,University of Pisa and INFN - Pisa
Largo B. Pontecorvo 3, I-56127 Pisa – Italy

C. PIEMONTE
FBK-irst, Divisione Microsistemi,
Via Santa Croce 77, I-38100 Trento – Italy

T.A. CARPENTER, R.C. HAWKES, A.J. LUCAS, J.W. STEVICK
Wolfson Brain Imaging Centre, University of Cambridge
Addenbrookes Hospital, CB2 2QQ Cambridge – UK

ABSTRACT

Photomultipliers (PMTs) have been employed for many years as photodetectors in medical imaging. Position sensitive PMTs are currently used in the last generation of PET scanners, that achieve high resolution and efficiency, and they are also successfully employed in combined scanners like PET/SPECT or PET/CT. However their sensitivity to magnetic fields and their size limit their use in certain applications, such as the combination of PET and MRI. Solid state photomultipliers present an alternative to vacuum photomultipliers, with important advantages. They have higher quantum efficiency, reduced size and weight, and they can operate in magnetic fields. In addition, their cost is potentially lower, since they can undergo a mass production process. The SiPM is a novel type of photodetector that operates in Geiger mode and has a gain of the order of 10^6. The active area is segmented in small microcells (typical size 25-100 μm) in order to obtain a signal proportional to the particle energy. The use of SiPMs in PET offers the possibility to obtain depth of interaction information and to improve the spatial resolution. In addition, the implementation of combined PET/MRI scanners is possible. Silicon photomultipliers produced by FBK-irst are being evaluated for their use in PET and PET/MR scanners. Results are presented.

1. Introduction

For more than six decades photodetectors have been employed in high energy physics, astrophysics and medical imaging, among other fields. Still they are an active area of research, in the seek of improved photon detection efficiency (PDE), reduced size, larger area, improved spatial resolution or optimization for different applications. PMTs continue to be the photodetector of choice for many experiments. Position sensitive PMTs (PSPMTs) have been employed in the construction of the last generation of small animal commercial PET scanners, achieving a spatial resolution close to 1 mm and 10% efficiency [1].

Solid state photodetectors have gained much attention in the last years. Compared to PMTs, they offer a potentially higher quantum efficiency, reduced size, and insensitivity to magnetic fields. The mature and well established silicon technology allows mass production, which can reduce significantly the cost with respect to vacuum technologies. In the case of the avalanche photodiodes (APDs), these advantages are at the cost of some drawbacks, such as lower gain (<1000), that makes necessary the use of low noise electronics, worse timing properties and a strong dependence of the gain on the temperature and bias voltage.

A novel type of photodetector, the multicell Geiger-mode avalanche photodiode or silicon photomultiplier (SiPM) has experienced a very fast development in the last ten years. In addition to the advantages of silicon detectors previously mentioned, SiPMs offer high gain (~10^6) at low bias voltage (<100 V) and excellent timing properties. The low power consumption results in less heating. These advantages makes them an ideal photodetector to be employed in high energy and space physics, astrophysics and medical imaging. Their potential use in numerous experiments is currently being evaluated.
Silicon photomultipliers are being developed in several institutes and research centres, and are currently commercially available from SensL [http://www.sensl.com] and Hamamatsu [http://www.hamamatsu.com]. Different structure and size is being investigated. In spite of their recent development, excellent performance has already been achieved with these devices.
The Center for Scientific and Technological Research, FBK-irst, in Trento, Italy [http://www.itc.it] has been one of the first centres to develop this technology, producing high performance devices. In addition, they are fabricating matrices of SiPMs in a common substrate. The performance of silicon photomultipliers from FBK-irst is being evaluated at the University of Pisa for their use in the construction of a very high resolution PET and a combined PET/MR scanner for small animals.

2. Silicon photomultipliers

A SiPM consists of a 2D array of *microcells*, i.e. p-n structures made of several layers of different doping concentrations in a common substrate [2]. When reverse bias voltage a few volts above the breakdown voltage is applied to the detector, a very high field region is created in each microcell, that acts as an independent detector. If a photon interacts in a microcell, the electrons or holes created drift towards the high field region, where an avalanche is produced. A resistor placed in series with the microcell is employed to quench the avalanche. The microcells work in limited Geiger mode, and its output is independent of the number of photons that interact in it. In order to obtain information proportional to the energy deposited in the detector, the output of the SiPM is given by the sum of the outputs of all the microcells that fire. The proportionality of the output signal with energy holds as long as the number of microcells in the device is large compared to the number of photons detected. The dynamic range of the device is thus related to the number of microcells per SiPM unit, and to the photon detection efficiency (PDE) of the device.
The gain is determined by the product of the microcell capacitance and the overvoltage, i.e. the voltage above the breakdown, and therefore it is linear with the bias voltage.
The PDE in a SiPM is given by the product of three parameters: the quantum efficiency (QE), the triggering probability (Pt), and the geometrical efficiency (GF).
The QE is given by the intrinsic QE or probability of photoabsorption, and the reflectivity of the SiPM coating. Both factors are wavelength dependent. Short wavelength photons are absorbed in the first 500 nm of the detector, while long wavelengths (red light) penetrate deeper in the silicon substrate. This effect must be taken into account in the detector design.
The triggering probability (Pt) is the probability that the electrons or holes created in the photon interaction initiate an avalanche. The Pt will be higher if the avalanche is triggered by electrons [3]. This factor depends on the SiPM structure, and on the depth at which the photon interacts, and therefore on the wavelength.
The geometrical factor (GF) is the ratio of the active to total area of the microcell. This parameter is related to the microcell size, since a larger microcell size leads generally to a higher GF, and therefore to a higher PDE. However, for a fixed SiPM size, increasing the microcell size also results in a reduction of the dynamic range of the device.
The SiPM application will determine the most appropriate structure, that depends on the wavelength of the radiation to be detected, the dynamic range (related to the number of microcells) and the microcell size, among others. A smaller number of big microcells per unit area with high GF are suitable for applications where low light levels have to be detected. For applications where a high number of photons is involved, a larger number of microcells is necessary to avoid the saturation of the device. Different types and structures are being investigated [2,4].

3. FBK-irst SiPMs for PET applications.

The first Silicon photomultipliers developed by FBK-irst have an active area of 1mm x 1 mm, with 625 microcels of 40 μm x 40 μm size [5]. Their gain is of the order of 10^6, and their breakdown voltage around 30 V. Their structure has been carefully studied in order to improve the quantum efficiency in the blue region, with a very thin (4 μm) epitaxial layer. An anti-reflective coating optimized for 420 nm wavelength has also been implemented with the same purpose. In addition, test structures of SiPM matrices have been fabricated and tested. The matrices consist of an array of 2x2 pixel elements in the same substrate, of the same size and characteristics as the single SiPMs (Fig 1).
Recently, new SiPMs with improved characteristics such as lower noise and higher GF (44-50%) have been developed, and are currently being tested. These include single SiPMs of various sizes and matrices of 16 (4x4) elements.

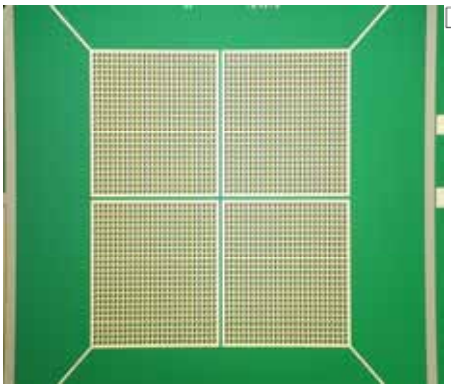

Fig 1. SiPM matrix consisting of four (2x2) pixel elements of 1 mm x 1mm in a common substrate.

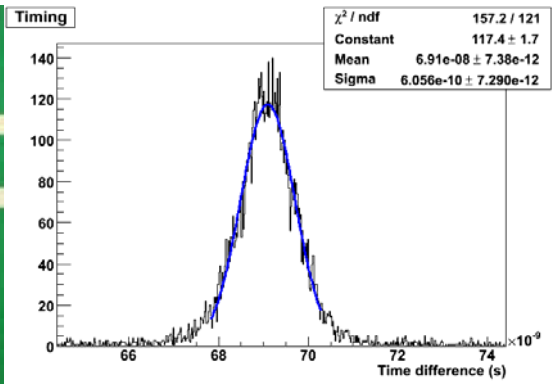

Fig 2. Coincidence timing resolution of two SiPMs with two LSO crystals.

3.1 Electro-optical characterization

The SiPMs from FBK-irst show a very good uniformity in their properties, which is essential for the fabrication of the matrices [5]. They have very good single photoelectron resolution, and a gain ranging from $4x10^5$ to $2x10^6$. The dark rate is about 1-3 MHz at the level of 1-2 photoelectrons, and drops rapidly to kHz as the threshold is increased to 3-4 photoelectrons.
A QE above 95% for blue light has been measured employing a diode structure produced in the same wafer as the SiPMs. The overall PDE is reduced due to the low triggering probability. Still, for a detector with 20% GF, the PDE is about 10% for 420 nm, and 14% at 550 nm. This parameter is enhanced for the SiPMs with 30% GF, and for the ones recently fabricated with 44% GF, for which a PDE around 20% is expected.

3.2 Timing

Both the intrinsic timing and the coincidence timing with two LSO crystals coupled to the SiPMs have been measured.
The intrinsic timing has been measured at the photoelectron (p.e.) level, employing a laser emitting 60 fs pulses at 80 MHz rate (i.e, T=12.34 ns) with less than 100 ps jitter. Two wavelengths were tested, 400±7 nm and 800±15 nm. The analysis of the data estimates the time difference of contiguous signals corresponding to 1 p.e. The time difference distribution is fitted with a Gaussian function. A timing resolution around 60 ps sigma is obtained for 3-4 V overvoltage at 400 nm. Also, the timing dependence on the square root of the number of photoelectrons has been verified up to 15 photoelectrons, for which the measured timing resolution is 20 ps sigma [6].
For the coincidence timing measurement, two small (1mm x 1 mm x 10 mm) LSO crystals have been coupled to two SiPMs, and the time difference is plotted. The fit of the peak with a Gaussian function results in a timing resolution of 600 ps sigma (Fig 2).

3.3 SiPMs and SiPM matrices as photodetectors

The SiPM performance as readout for scintillators has also been tested. A ^{22}Na energy spectrum was obtained with a 1 mm x 1 mm x 10 mm LSO crystal coupled to SiPMs with 30% GF, and operated in time coincidence with a second device. The fit of the 511 keV photopeak with a Gaussian function gives an energy resolution of 20% FWHM.
The performance of the SiPM matrices has also been evaluated. In this case, the SiPMs that compose the matrix have lower GF (20%), and therefore less PDE. In this case, the resolution obtained coupling the crystal to one of the SiPMs in the matrix is 30%, the same as the one obtained with single SiPMs of similar characteristics. Next, the same crystal has been placed in the centre of the matrix, covering part of each of the SiPMs. The signals coming from the four SiPMs are summed and histogrammed. The resulting spectrum has the same energy resolution as the one obtained with a single SiPM (Fig 3). The results show that the matrix development and operation does not degrade the performance of the SiPMs.

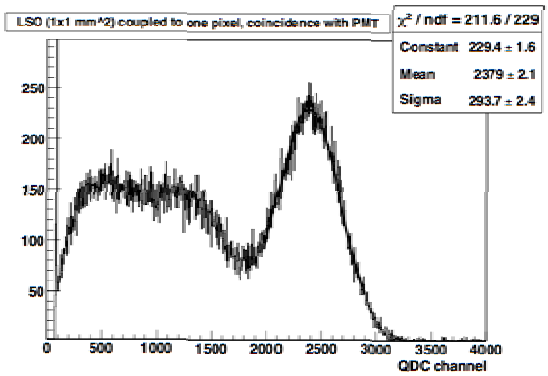

Fig 3. ^{22}Na energy spectrum obtained with a SiPM matrix, adding up the signals from the four pixels.

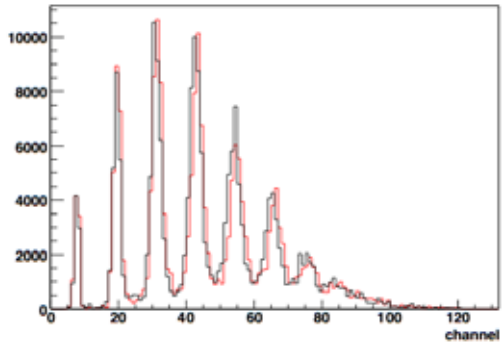

Fig 4. Single photoelectron spectrum obtained with the gradient fields on (red line) and off (black line). No difference is appreciated.

3.4 Tests in an MR system

The effect of MR static magnetic, pulsed gradient and radiofrequency (RF) fields on SiPM performance has been studied. The interaction of the MR system with the electronics necessary to drive the SiPM was minimized by shielding the electronics in a box. The SiPM was left uncovered and exposed to the magnetic fields. The tests were performed both with the electronics box inside and outside the MR system. In the latter case, the SiPM was connected to the electronics by means of a 1 m long shielded coaxial cable.
The performance of the SiPMs in an MR scanner has been evaluated by acquiring single photoelecton spectra and ^{22}Na energy spectra whilst switching magnetic fields with the SiPM positioned in the MR system. The resulting spectra show no degradation of the data with respect to those taken outside the MR system (Fig 4).
The interference between the two systems results in a pickup in the SiPM baseline simultaneous to the switch-on of the gradient fields or RF pulses, that must be minimized. Also, the temperature changes in the MR system result in gain variations in the SiPM that should be monitored and corrected for.

4. Application to small animal imaging

Silicon photomultipliers open new possibilities in medical imaging. A very high resolution PET scanner for small animals employing SiPMs has been proposed and is under construction at the

university of Pisa [7]. The tomograph consists of four 4 cm x 4 cm detector heads that rotate around the object to be imaged. A detector head is made of a stack of three layers. Each layer is composed of a 5 mm thick scintillator slab read out by a SiPM matrix structure, with 1 mm x 1mm pixels in a 1.5 mm pitch. The distance between opposite heads is variable, ranging from 10 to 15 cm. The total scintillator thickness is 15 mm, ensuring a high detection efficiency for 511 keV photons, while the 3 layer structure provides discrete depth of interaction information that reduces the parallax error and improves the spatial resolution. The use of continuous scintillators instead of pixellated blocks allows to improve the spatial resolution, while avoiding the problems of light collection efficiency that are related to fine pixellation of the crystals. Additionally, the cost of the detector is reduced.
In order to estimate the performance of the device, simulations have been carried out with GEANT4, that take into account the characteristics of the FBK-irst photomultipliers. For a detector head, an intrinsic spatial resolution of 0.3 mm FWHM, and 70% efficiency have been obtained. If the positions are determined with center-of-gravity algorithms, this value degrades in the final 5 mm, near the edges of the detectors. Skewness and barycentre based likelihood methods have been applied that allow to correct for the displacement error and maintain its value well below the parallax error. For the proposed tomograph, a spatial resolution of less than 1 mm^3 at the centre of the FOV, and a sensitivity above 4% are expected. The sensitivity can easily be enhanced by adding more detector pairs.
The combination of PET/CT has allowed the simultaneous acquisition of functional and structural images. However, the superior resolution and soft tissue contrast of MRI would provide a much better anatomical reference for the functional data of PET. At the same time, it would avoid the radiation dose due to CT, that is significant in the case of small animal imaging where a submillimetre spatial resolution is required.
The main limitations for the combination of PET and MR imaging technologies are the space constraint inside the magnet, and the sensitivity of PMTs to magnetic fields. In addition, technical problems arise from the interference of both imaging modalities. Progress in this field has been achieved following two main approaches. One is the use of light guides to carry the light to positions where the magnetic field is low enough for the PMTs to be operated [8]. The second one is the use of APDs that are insensitive to magnetic fields [9]. In this second approach, the shielding of the electronics results in a decrease of the signal-to-noise ratio of the MR images.
The reduced size and modularity of the SiPMs, together with their insensitivity to magnetic fields makes possible their operation inside an MR system. In addition, their high signal-to-noise ratio can be profited from to find the best configuration and shielding that would minimize the interference between the two modalities. The development of a PET insert based on SiPMs to be operated inside a small animal MR scanner will allow simultaneous PET/MR imaging.

5. Conclusions

Silicon photomultipliers are an alternative photodetector that can offer significant advantages in many fields. Being compact, light, insensitive to magnetic fields and providing high spatial resolution, they open new possibilities in medical imaging.
FBK-irst has fabricated high performance SiPMs and matrices of SiPMs in a common substrate. New devices with reduced noise and larger active area have recently been produced.
At the University of Pisa SiPMs are being studied for the construction of a very high resolution, high sensitivity small animal PET, and a combined PET/MR scanner.

6. Acknowledgements

This project is partially supported by the European Commission's Sixth Framework programme through a Marie Curie Intra-European Fellowship.

7. References

[1]http://www.medical.siemens.com/siemens/en_US/gg_nm_FBAs/files/multimedia/inveon/index.htm
[2] C. Piemonte, “A new Silicon Photomultiplier structure for blue light detection”, Nucl. Instr. Meth. A 568, 224-232 (2006).

[3] W. G. Oldham et al, “Triggering phenomena in Avalanche diodes”, IEEE Trans. Elec. Dev., ED-19(9) (1972) 1056.
[4] N. Otte “The silicon photomultiplier: A new device for High Energy Physics, Astroparticle Physics, Industrial and Medical applications. Proc. SNIC-2006-0018.
[5] C. Piemonte, et al., “Characterization of the first prototypes of Silicon Photomultiplier fabricated at ITC-irst”, IEEE Trans. Nucl. Sci. 54(1), 236-244 (2007).
[6] G. Collazuol et al. “Single timing resolution and detection efficiency of the ITC-irst Silicon photomultipliers”. Presented at the XI VCI, Vienna 19-24 Feb. 2007 and to be published in Nucl. Instr. Meth. A (2007).
[7] S. Moehrs, A. Del Guerra, D. Herbert, M. Mandelkern, “A detector head design for small animal PET with silicon photomultipliers”, Phys. Med. Biol. (2006), 1113-1127.
[8] A.J. Lucas et al. “Development of a combined microPET/MR system”. Technol. Cancer Res. Treat. 5, 337-41 (2006).
[9] B. Pichler et al. “Performance test of an LSO-APD detector in a 7T MRI scanner for simultaneous PET/MRI”. J. Nucl. Med. 47, 639-47 (2006).

HIGH SENSITIVITY PET DETECTOR DESIGN USING MONOLITHIC SCINTILLATOR CRYSTALS

P. BRUYNDONCKX, C. *LEMAITRE*, S. TAVERNIER
Department of physics, Vrije Universiteit Brussel
Pleinlaan 2, 1050 Brussels– Belgium

D.J. VAN DER LAAN, M. MAAS, D. SCHAART
IRI, Technische Universiteit Delft
Mekelweg 15, 2629 JB Delft– The Netherlands

ABSTRACT

Using undivided scintillator blocks yields an effective manner to significantly increase the sensitivity of high-resolution PET systems. A neural network based positioning scheme is able to localize perpendicular incident photons with an accuracy 1.7 mm FWHM for a 10 mm thick LSO block and 2.0 mm FWHM for a 20 mm thick LSO block. Because the positioning algorithm determines the incidence position as opposed to the interaction position, no separate measurement of the interaction depth is required to obtain parallax corrected coordinates. Energy and time resolution were 12% FWHM and 1.6 ns FWHM respectively.

1. Introduction

Positron emission tomography (PET) is an imaging modality for measuring the spatial and temporal distribution of an administered radio-labelled substance within the body of a patient. The quality of PET images is usually given by three physical characteristics : spatial resolution (ability to see details), contrast (ability to see differences in radio-tracer levels) and noise (statistical fluctuations in the measured radio-tracer concentrations). Despite the fact that these characteristics describe different aspects of the image quality, they are not independent. The improvement of one parameter very often leads to the degradation of one of the others. Over the last decade a lot of effort has been put into improving the spatial resolution. Small animal PET scanners now have an image resolution well below 2 mm FWHM and some get close to 1 mm FWHM. To completely utilize the resolving power of high resolution PET scanners, clinical or small animal, the signal to noise ratio (SNR) in the images should be kept at a sufficiently low level. Otherwise small details that could be discerned are swamped in the noise. For a given number of detected annihilation photon pairs in a PET scan, the squared SNR in the image is inversely proportional to the fourth power of the image voxel size (or detector pixel size). Hence an enhancement of the intrinsic detector resolution without an increase in the number of detected events is detrimental for the image noise. Depending on the PET study and object, a longer scanning time or a higher tracer dose are not always possible. The newest clinical PET scanners now also offer time-of-flight (TOF) capability. Using the measured arrival time difference of the two annihilation photons in the image reconstruction process allows a reduction of the image variance. Given a time resolution of 600 ns, TOF PET imaging is currently only useful in clinical whole body imaging [1].
Another way of improving the sensitivity of a PET scanner is to increase the packing fraction (fraction of sensitive material compared to the total detector volume). Classical PET scanner designs are based on matrices of small scintillating pixel elements that are optically separated and read out by a position sensitive photo detector. Reducing the size of the detector pixels to enhance the spatial resolution also reduces the packing fraction because of the relative higher presence of material to optically separate the crystals. The packaging of the photo detector itself also introduces some dead area unless the scintillation crystals are decoupled from the photo detector using optical fibers [2]. In this case the crystal matrices can be mounted side-by-side at the expense of some scintillation light loss in the optical fibers, resulting in a lower energy resolution. The spatial resolution gain obtained by using

smaller individual crystals is also partially offset by increased inter-crystal scatter and parallax errors for photons impinging at non-perpendicular angles.
To overcome the above obstacles while trying to simultaneously improve spatial resolution and sensitivity, we studied an alternative detector design based on monolithic scintillator blocks read out by pixelated photo detectors. The philosophy behind our approach to localize the impinging photons is to make use of the scintillation light distribution that is generated when a photon interacts in the scintillator block. This shape obviously depends on the 3D interaction position of the photon. Because we rely on the spreading of the scintillation light, the scintillator block can be larger than the sensitivity area of the photo detector en hence also cover the packaging of the photo detector.

2. Materials and methods

2.1 Detector components and experimental set-up

In this study two different continuous LSO scintillator blocks were used: a rectangular 20x10x10 mm block and a thicker rectangular 20x10x20 mm. The LSO blocks were wrapped with Teflon on 4 sides (20 mm thick blocks) or 5 sides (10 mm thick block) to maximize the light output. The scintillation light distribution emerging at the bottom of the 10 mm thick block is sampled by an 8x4 S8550 Hamamatsu avalanche photo diode (APD) array on the top side (Fig. 1 left). The pixel size of this device is 1.6 x 1.6 mm and the pixel pitch is 2.3 mm. In case of the 20 mm thick blocks, the top and bottom surface were read out by APDs (Fig. 1 middle).
To extract the position of an impinging photon from the sampled scintillation light distribution we used a neural network (NN). The NN needs to be trained using a set of training events before it can be used. A ~1 mm FWHM electronically collimated 511 keV photon beam that can be positioned at any known point on the front surface of the LSO block using a motorized XZΩ stage (Fig. 1 right) was used to generate these training events. More details about the experimental set-up can be found in [3]. The beam was stepped along the central x-axis of the front surface using 250 μm steps. At each beam position a number of events were measured, the 32/64 APD pixel values were summed along the rows and columns to obtain the light distribution projections and stored together with the incidence photon position (i.e. the centre of the known beam position).

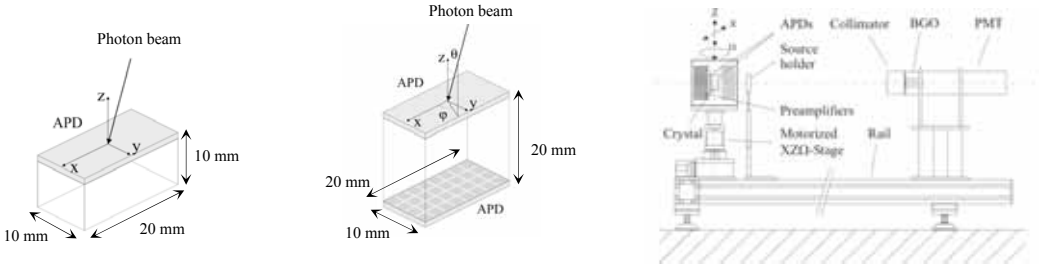

Fig. 1 : (*left*) A 20x10x10mm LSO block with an APD readout on the top surface, (*middle*) A 20x10x20 mm LSO block with a double APD readout, (right)) Schematic representation of the experimental set-up. The photon beam is defined by coincidence measurements with a 35 mm thick BGO crystal mounted to a PMT at some distance. The 60 mm thick lead collimator has a hole diameter of 5.0 mm

2.2 Parallax-free positions

Usually a measurement of the depth at which a photon interacts in a scintillation crystal forms the basis for parallax correction. This can either be achieved in a discrete way (e.g. phoswich [4] or a pixel encoding scheme [5]) or in a continuous way (e.g. using the ratio of the signals measured on the top and bottom side of the scintillator [6]). Hence the accuracy on the estimated true interaction position in the scintillator depends on the accuracy of the estimated position of the photon in the plane of the photo detector and on the accuracy of the depth-of-interaction (DOI) measurement.
Because we trained the NN to reproduce the incidence position instead of the interaction position within the scintillator block, there is no need for a separate DOI measurement and DOI calibration of the detector module because the incidence position is independent of the incidence angle. Hence it

does not suffer from parallax problems. However the relation between the measured scintillation light distribution and the incidence position depends on the incidence angle. Therefore algorithms have to be trained for different incidence angles. We set $\varphi=0^o$ while θ was varied from 0^o to 30^o in 10^o (Fig. 1).

2.3 Positioning algorithm

The neural networks used to compute the incidence position consist of an input layer, one or more hidden layers and an output layer. The neurons in the input layer accept the APD pixel signals while the neuron in the output layer yields the corresponding photon impinging position once the network has been trained. The neural network computation of a coordinate x using a single hidden layer network can be written as

$$\begin{aligned} x &= \mathbf{v}^T \sigma[\mathbf{W} \cdot \mathbf{p} + \mathbf{d}] \\ &= \mathbf{v}^T \sigma[\mathbf{n}] \end{aligned} \qquad (1)$$

where **p** is the vector of APD signals, **W** is the matrix of input-to-hidden layer weights, **d** is the vector of hidden node biases, **v** is the vector of hidden-to-output layer weights. The term $\sigma[\mathbf{n}]$ indicates an element-by-element evaluation of **n** using a sigmoidal function.

The classical way to train a neural network is by using error back propagation [7]. For each event in the training data set, the predicted position x_i is compared with the known incidence (i.e. beam centre) position y_i. There are various algorithms which tune the network parameters such that the root mean square error is minimal. In general the neural network minimization problems are often very ill-conditioned. For these kind of problems the Levenberg-Marquardt algorithm is usually a good choice because of its higher robustness. The training of a NN with a single 10 neuron hidden layer was implemented using the neural network package of the Mathematica [8].

3. Results

3.1 Position information content in scintillation light profiles

The Cramér-Rao inequality gives a lower bound on the variance of an efficient estimator [9,10]. We used this theory to obtain a lower limit on the accuracy with which a photon can be localized from the scintillation light distribution it generates in the scintillator blocks. Figure 2 shows the lower variance bounds on a 20x10x10 mm and 20x10x20 mm LSO block. The light distributions used in the computation of these lower bounds were generated by a Geant4 [11] based Monte Carlo simulation of scintillation point sources placed on a grid in the LSO block. In most regions of the block the lower variance bound is less than 0.5 mm. In general the position estimation accuracy degrades as the photon interacts further away from the APD array (z=-5 in fig. 2 left). Therefore we have to use a read out on both top and bottom side of monolithic scintillator blocks that have a thickness larger than 1 cm (e.g. to further optimize the stopping power and sensitivity) in order to retain good overall spatial

resolution (Fig. 2 right).

Fig.2: Distribution of the Cramér-Rao lower variance that can be achieved by an efficient position estimator in a 20x10x10 mm LSO block with top one-sided read out (left) and a 20x10x20 mm LSO block with a double sided read out (right).

3.2 Detector resolution and nonlinearity

Figure 3 left shows the overall intrinsic FWHM resolution measured at all beam positions along the x-axis for the 20x10x10 mm LSO block, as a function of the incidence angle and energy threshold. For perpendicular incident photons, the measured FWHM detector resolution is 1.75 for a threshold of 100 keV and 1.60 mm for a threshold of 380 keV. When the photon incidence angle increases to 30°, the spatial resolution degrades slightly to 2.0 mm and 1.85 mm FWHM respectively. Increasing the threshold from 100 keV to 250 keV or 380 keV reduces the detector sensitivity by respectively 11.8 % and 26.4 %.

The FWHM obtained using the signals from the top and bottom APD on the 20x10x20 mm thick LSO block is shown in figure 3 middle. The measured detector resolutions are worse compared to the thinner 20x10x10 mm LSO block. This could be due to the fact that the scintillation light is now spread over 64 APD pixels in stead of only 32 pixels. Hence the statistical fluctuation of the number of photons per pixel will be larger. In addition each of the 32 extra readout channels will also contribute electronic noise to the data.

The deviation from linearity for the NN estimated coordinate is shown in figure 3 right. The nonlinearity is negligible except for photons impinging within 1 mm from the edge of the scintillator block.

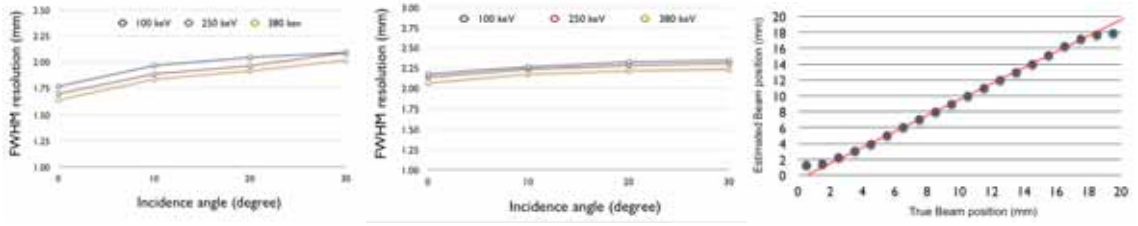

Figure 3: (Left) FWHM resolution for a 20x10x10 mm LSO block, (Middle) FWHM resolution for a 20x10x20 mm LSO block, (Right) deviation from linearity of the NN positioning algorithm for the 20x10x10 mm LSO block.

3.3 Energy and time resolution

Figure 4 left shows the energy spectrum for the 20x10x10 mm LSO block obtained from the events measured at all beam positions. The average energy resolution is 12% FWHM and does not vary significantly as a function of the photon impinging position.

Time resolution measurements were performed against a BaF_2 crystal coupled to an XP2020Q PMT. The PMT signal and the analogue sum of the 32 APD signals were both fed into a constant fraction discriminator for time pick off. The time spectrum (fig 4 right) was obtained using a time-to-analog convertor followed by an analog-to digital convertor. The time resolution obtained had a resolution of 1.6 ns FWHM. A similar measurement on the 20x10x20 mm LSO block yielded a 2.2 ns FWHM time resolution.

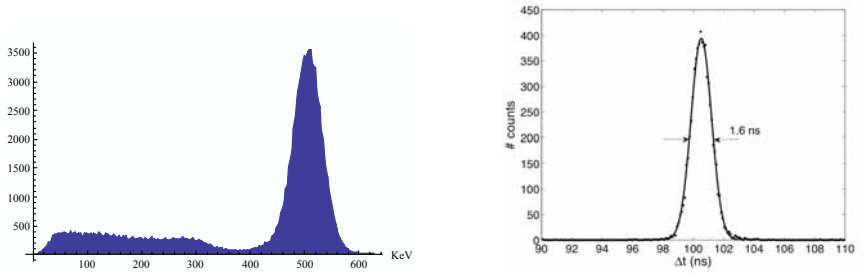

Figure 4: (Left) Energy spectrum for a 20x10x10 mm LSO block, (Right) Time spectrum of a 20x10x10 mm LYSO block measured against a BaF2 crystal coupled to an XP2020Q PMT. The solid line represents a Gaussian fit through the data

3.4 Image resolution

A 250 µm diameter ^{22}Na point source (50 µCi) was placed at radial distance of 1, 6, 11 and 16 mm respectively from the centre of a simulator set-up. The simulator consists of two detector modules equipped with 20x10x10 mm LSO blocks. The detector modules are mounted on a rotating gantry with a diameter of 130 mm [12]. The estimated continuous coordinates of the impinging annihilation

photons, obtained with neural networks, were first rebinned in 1x1 mm virtual pixels. The coordinates of the centre of these pixels were then used to fill up the sinograms. Table I gives the radial and tangential resolution at the different positions of the point source in FBP or OSEM reconstructed images. A square filter function with a cut-off at the Nyquist frequency was used in the FBP reconstruction. The OSEM algorithm used 8 subsets and 5 iterations. In both cases the image matrix consisted of 0.5 mm^3 voxels. Close to the centre, the resolution is 1.7 mm FWHM in the FBP reconstructed image and 1.3 mm FWHM in the OSEM reconstructed image. The degradation of the radial resolution at some distance from the centre is probably due to the fact that the incidence position of the photons was estimated using only the neural network trained for perpendicular incident photons, i.e. non-parallax corrected positions.
The axial resolution was obtained from the width of the profile showing the number of coincidences measured in 0.5 mm thick transaxial slices. The FWHM of this distribution was 1.8 mm.

	FBP		OSEM	
Position	Radial	Tangential	Radial	Tangential
1 mm	1.7 mm	1.7 mm	1.3 mm	1.3 mm
6 mm	1.8 mm	1.7 mm	1.4 mm	1.3 mm
11 mm	1.9 mm	1.7 mm	1.45 mm	1.3 mm
16 mm	2.0 mm	1.8 mm	1.6 mm	1.4 mm

Table I : FWHM radial and tangential resolution in FBP and OSEM reconstructed images of a point source at various radial distances from the centre

4. Conclusion

A high-sensitivity, high-resolution PET detector concept using a neural network positioning algorithm was evaluated. We achieved a 1.7 mm FWHM resolution in a 10 mm thick LSO block and 2.0 mm FWHM resolution in a 20 mm thick LSO block. These results still include the influence of the finite size of the collimated photon beam used in the set-up. The study also indicates that a PET scanner design based on continuous blocks should preferably be build using a double layer of 10 mm thick LSO blocks coupled to a single APD in stead of a single 20 mm thick LSO blocks read out on both sides. The nonlinearity in the position estimation is negligible up to 1 mm from the edge of the LSO block. The corresponding resolution near the center of a PET image acquired on a simulator set-up was 1.7 mm FWHM using FBP and 1.3 mm FWHM using OSEM.
When training data sets are acquired for different incidence angles, we observed a slight degradation of the intrinsic detector resolution from 1.7 mm FWHM at 0^o to 2.0 mm FWHM at 30^o when a 350 keV threshold is applied.
The absence of multiple reflections due to the light piping effect found in the traditional crystal pixel matrices results in a larger light output and hence a better energy resolution of 12 % that remains rather uniform over the length of the block. Despite the summing of the 32 APD pixels signals to trigger an event, we achieved a time resolution of 1.6 ns.
Given the above performances, we see this photon detection and localization principle as a viable alternative to the classical designs. Because of the high sensitivity and parallax-free photon detection property, we foresee the implementation of this technology in a future BrainPET system.

5. References

[1] “Performance of Philips Gemini TF PET/CT Scanner with Special Consideration for Its Time-of-Flight Imaging Capabilities”, Suleman Surti, Austin Kuhn, Matthew E. Werner, Amy E. Perkins, Jeffrey Kolthammer and Joel S. Karp, The journal of nuclear medicine, Vol. 48, No. 3, pp471-480

[2] “MicroPET II: an ultra-high resolution small animal PET system”, Y.C. Tai et Al., Nuclear Science Symposium Conference Record, 2002 IEEE Volume 3, Issue , 10-16 Nov. 2002 Page(s): 1848 - 1852 vol.3

[3] “Experimental characterization of monolithic-crystal small animal PET detectors read out by APD arrays**”,** M.C. Maas, D.J. van der Laan, D.R. Schaart, J. Huizenga, J.C. Brouwer, P. Bruyndonckx, S. Leonard, C. Lemaitre, C.W.E. van Eijk, *IEEE Trans. Nucl. Sci.*, vol. 53, no. 3, pp. 1071-1077, June 2006

[4] “Digital pulse shape discrimination methods for phoswich detectors”, D. Wisniewski,M. Wisniewska, P. Bruyndonckx,M. Krieguer, S. Tavernier, O. Devroede, C. Lemaitre, J.B. Mosset and C. Morel, 2005 Nucl. Sci. Symp. Conf. record, Vol. 4, pp 2017-2021
[5] “Performance evaluation of a subset of a four-layer LSO detector for a small animal DOI PET scanner; JPET-RD”, T. Tsuda, H. Murayama, K. Kitamura, N. Inadama, T. Yamaya, E. Yoshida,F. Nishikido, M. Hamamoto, H. Kawai and Y. Ono, IEEE trans. Nucl. Sci., Vol 53 (2006), Issue 1, Part 1., pp 35-39
[6] “Design and evaluation of the Clear-PEM scanner for positron emission mammography”, M.C. Abrue et al, IEEE Trans, Nucl. Sci., Volume 53 (2006), Issue 1, Part 1, pp 71-77
[7] “Neural Networks : A comprehensive foundation”, S. Haykin, Prentice Hall, 1999
[8] www.wolfram.com
[9] “Performance optimization of continuous detector modules using Cramer-Rao theory combined with Monte Carlo simulations”, D.J. van der Laan, M.C. Maas, D.R. Schaart, P. Bruyndonckx, S. Leonard and C. van Eijk, 2004 Nucl. Sci. Symp. Conf. record, Vol. 4, pp 2417-2421
[10] “Influence of sensor arrangements and scintrillator crystal properties on the 3D precision of monolithic scintillation detectors in PET”, P. Ojala, A. Bousselham, L. Eriksson,A. Brahma and C. Bohm, 2005 Nucl. Sci. Symp. Conf. record, Vol. 5, pp 3018-3021
[11] “Geant4 – a simulation toolkit”, S. Agostinelli et al., Nucl. Instr. Mehods, A506 (2003), pp250
[12] “Performance of a PET prototype demonstrator based on non-pixelated scintillators”, P. Bruyndonckx, C. Lemaitre, S. Leonard, D. Schaart, D.J. van der Laan, M. Maas, Y. Wu, M. Krieguer, S. Tavernier and O. Devroede, 2004 Nucl. Sci. Symp. Conf. record, Vol. 6, pp 3924-2927

Session 18.3.2:

Radiolabelling of molecules

IN VIVO EVALUATION OF [^{18}F]-2-FLUOROMETHYL-L-PHENYLALANINE IN TUMOUR BEARING RATS WITH PET ACQUISITION.

KEN KERSEMANS, MATTHIAS BAUWENS, ANH THO NGUYEN, TONY LAHOUTTE, AXEL BOSSUYT, JOHN MERTENS

BEFY, Radiopharm. Chemistry, Vrije Universiteit Brussel
Laarbeeklaan 103, 1090 Brussels, Belgium

ABSTRACT

Currently there is a vast interest for [^{18}F]-labelled amino acid-analogues for tumour specific diagnosis with PET. We hereby present the in vivo evaluation in R1M tumour bearing rats of [^{18}F]-2-fluoromethyl-L-phenylalanineas a new tumour specific PET tracer.
The precursor, N-Boc-2-Bromomethyl-L-phenylalaine-tButylester, is radiofluorinated in conditions comparable to FDG synthesis with a good radiochemical yield. After HPLC separation and deprotection the [^{18}F]-2-fluoromethyl-L-phenylalanine is recovered in n.c.a. conditions. Traces of free radiofluoride were removed using a custom appatite filter before sterilisation. 3.7 – 10 MBq were injected into R1M tumour bearings rats and imaging was performed with a human PET camera from 5 to 45 minutes p.i.. The obtained tumour/background and tumour/blood ratios were at least 3 coupled to an appropriate biodistribution and cleaning pattern.
N.c.a.[^{18}F]2-fluoromethyl-L-phenylalanine is currently used in a Phase I study for tumour diagnosis with PET.

1. Introduction

Currently there is a vast interest for [^{18}F]-labelled amino acid-analogues for tumour specific diagnosis with PET because the widespread 2-[^{18}F]fluorodeoxyglucose ([^{18}F]FDG) lacks the tumour cell specificity required for control and follow-up after surgery, radiotherapy and chemotherapy [1,5]. A key-point in the development of this new type of tracers is the Na+-independent LAT1 amino acid transport system for neutral and lipophilic amino acids, which is overexpressed in tumour tissue relative to normal tissue[6-10]. We have already proven in vitro and in vivo that 2-I-L-phenylalanine, a SPECT tracer, is taken up for the major part by LAT1 system in a R1M rhabdomyosarcoma tumour cell line and in several types of human cancer cells [11]. This radio-iodinated amino acid shows a very high tumour selectivity when compared to the clinically routinely used [^{18}F]-FDG, which is taken up considerably in brain and inflammatory tissue [3-5]. On this basis we developed a new fluorinated phenylalanine analogue, [^{18}F]-2-fluoromethyl-L-phenylalanine, considering that the spatial volumes of FCH_3 and Iodine are comparable and that [^{18}F]-2-fluoromethyl-L-phenylalanine can be prepared with the ease of [^{18}F]-FDG to allow clinical routine. The challenge was to develop a suitable precursor and radiolabeling strategy that would reduce the chemistry to a simple aliphatic nucleophilic substitution on the methyl side chain, thus avoiding the difficult low-yield multistep radiolabeling procedures as often encountered in previous attempts to introduce a suitable PET amino acid for routinely use. The [$^{18}F^-$] for bromine substitution strategy that we developed at our lab allows to prepare the [^{18}F]-2-fluoromethyl-L-phenylalanine with the ease of [^{18}F]FDG in a clinical routine and thus filling the gap between radiolabeled amino acids and [^{18}F]FDG. The aim of this study was to evaluate in vivo n.c.a. 2-[^{18}F]fluoromethyl-L-phenylalanine in tumour-bearing rats by means of PET acquisition.

2. Materials and Methods

All the conventional products mentioned were at least analytical or clinical grade. The solvents were of HPLC quality and were all from Sigma-Aldrich unless stated otherwise.

2.1 Radiosynthesis

The labelling has been described in detail elsewhere (submitted Nucl Med Biol). In short: 10 µmoles of N-Boc-2-bromomethyl-L-phenylalanine-tButyl ester were labelled with [18F-] in presence of K_{222} and K_2CO_3 in ACN(400 µL) within 5 minutes at 120°C. The n.c.a. N-Boc-2-[18F]-fluoromethyl-L-phenylalanine-tButyl ester was recovered from HPLC speration..Complete deprotection was achieved in 400 µL of a dichloromethane/trifluoroacetic acid: 3/1 mixture in presence of $CaCl_2$ within 20 minutes at 50 °C. After removal of the original solvents by evaporation using the N2-flow at room temperature the 2-[^{18}F]Fluoromethyl-L-phenylalanine is recovered in an isotonic aqueous solution that is successively sent through a mini C18 column and a custom apatite column before sterilising through a 0.20 µ Cathivex filter for sterilization.

2.2 Quality and shelf-life control

Quality control of 2-[^{18}F]fluoromethyl-L-phenylalanine (spiked with a small amount of KF) was achieved by HPLC, using a Prevail C18-column (5 mm, 250 x 4 mm) (Alltech, Belgium) and ethanol/water (1/99, v/v) as eluent with a flow of 1 ml/min (k' = 5.6), while monitoring UV absorption (Shimadzu UV detector, 280 nm) and radioactivity (NaI(Tl)-detector, Harshaw Chemie, Belgium) at the same time.

2.3 In vivo experiments

2.3.1 Laboratory Animals

Water and food were ad libitum during the experimental period. For the tumour model, male Wag/Rij rats (Harlan, The Netherlands) were injected subcutaneously in the right flank (armpit region) with 15 x 10^6 R1M rhabdomyosarcoma cells. Imaging experiments with 2-[^{18}F]fluoromethyl-L-phenylalanine were performed 6 weeks after injection of the R1M cells. The average tumour size was 12 cm³. During all imaging experiments, the animals were anaesthetized intraperitoneal (IP) with 350 ml of a solution containing 60 mg pentobarbital/ml (Nembutal, 60 mg/ml, Ceva Sante´ Animale, Belgium). 2-[^{18}F]Fluoromethyl-L-phenylalanine was injected intravenously (IV) in the penis vein. The study protocol was approved by the ethical committee for animal studies of our institution. Guidelines of the National Institute of Health principles of laboratory animal care (NIH publication 86-23, revised 1985) were followed.

2.3.2 PET acquisition

The scanner is a 2D/3D human Accel PET camera (Siemens) with a resolution of 6mm at the centre of the field of view. R1M bearing Wag/Rij rats were injected with 3.7MBq of 2-[^{18}F]fluoromethyl-L-phenylalanine, which was eluted over a custom made appatite filter just before injection, and imaging was performed at 5, 15 and 30 min p.i. (1 acquisition sequence lasts about 10 min) in 3D mode. The rats were positioned crosswise to allow a faster acquisition so that coronal slices are seen as sagittal rat-slices. The injected activity was calculated as the amount of radioactivity in the syringe before and after injection (Capintec CRC-15R, Ramsey, NJ, USA). Quantification of activity uptake occurred by using the 3D-isocontour ROI feature of the medical imaging data analysis program Amide (VA Linux Systems), allowing accurate outlining of the tumour and tissues of interest. The ROIs for muscle were taken in the contra-lateral background region, while the heart was taken as a measure for the blood pool activity. Differential uptake ratios (DUR) were calculated as (mean tissue activity/voxel)/(mean total body activity/voxel).

3. Results and discussion

3.1. Radiosynthesis and formulation of 2-[^{18}F]fluoromethyl-L-phenylalanine

The labeling of Boc-2-bromomethyl-L-phenylalanine-tButylester with [$^{18}F^-$] provided the Boc-2-[^{18}F]fluoromethyl-Lphenylalanine- tButylester with a radiochemical yield of at least 85 %. After deprotection, adjusting the isotonicity and sterilising the solution, 2-[^{18}F]fluoromethyl-L-phenylalanine could be obtained ready for use with an overall average radiochemical yield of about 57 % (corrected for decay it is 83 % zelfde als artikel), with a radiochemical purity of at least 98%.
Radiodefluorination during deprotection and in the aqueous radiopharmaceutical formulation were major problems.
When applying deprotection on the ACN soluble compounds in the reaction mixture up to 50 % of radiofluorination was noticed. The presence of $CaCl_2$ reduces defluorination considerably.
Several shelf life tests, where 2-[^{18}F]Fluoromethyl-L-phenylalanine was incubated in milliQ water at room temperature for several hours, showed that n.c.a. 2-[^{18}F]Fluoromethyl-L-phenylalanine was not stable in aquaous solutions and showed a defluorination rate of 33 %/hour due to hydrolysis. A significant stabilisation could be achieved by adding non-radioactive 2-fluoromethyl-L-phenylalanine in a concentration of 50µM to the solution containing 2-[^{18}F]Fluoromethyl-L-phenylalanine, reducing the radiodefluorination rate to a mere 3 %/hour, as shown in Fig. 1. Applying this method should be at the cost of the n.c.a. characteristic. The Ca_2^+ ions already present from deprotection also inhibits the radiodefluorination of the n.c.a. 2-[^{18}F]Fluoromethyl-L-phenylalanine and represents an interesting alternative.

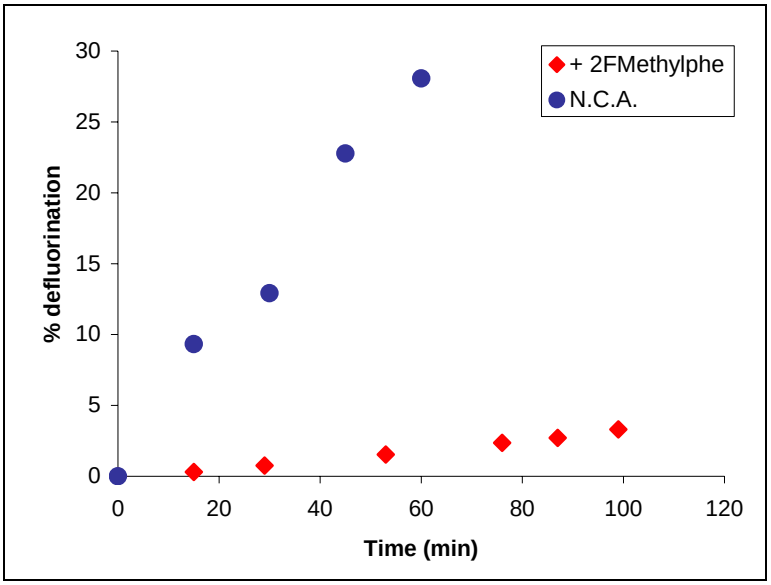

Fig. 1: Defluorination of [^{18}F]fluoromethyl-L-phenylalanine at room temperature in water as a function of time, n.c.a. or in presence of 50µM 2-Fluoromethyl-L-phenylalanine (+2FMethylphe)

In the animal experiments described in this work n.c.a. 2-[^{18}F]fluoromethyl-L-phenylalanine was injected n.c.a.

3.2. In vivo results: PET acquisition

Fig. 2 depicts the mean DUR values (3 R1M bearing rats) of the tumour and different tissues of interest at 5, 15 and 30 min p.i..

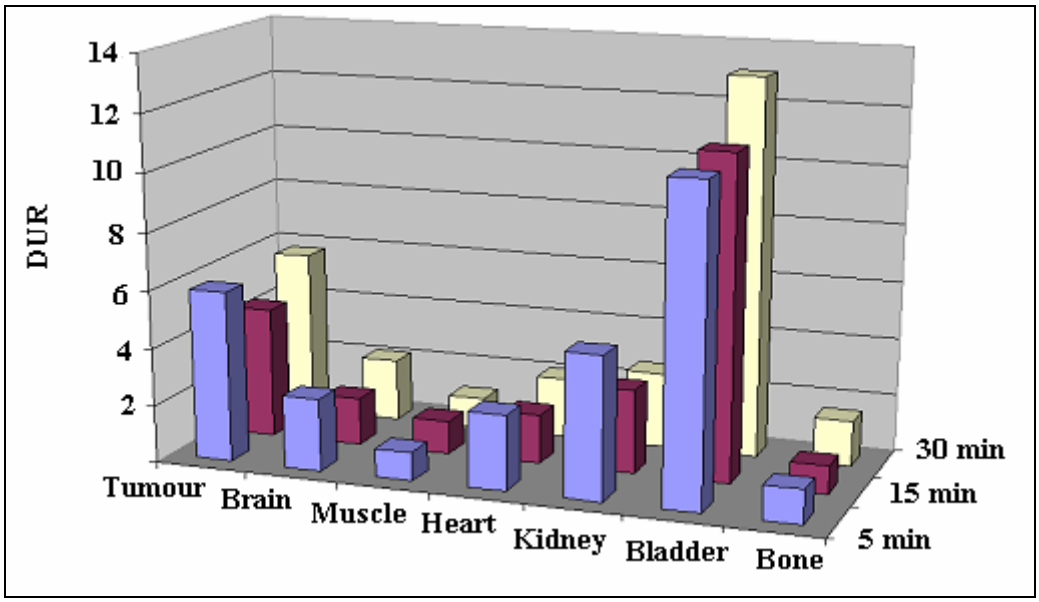

Fig. 2: Graph, showing the DUR values of the tumour and different tissues of interest at 5, 15 and 30 minutes p.i..

The PET acquisitions at three time points clearly show a high uptake in the tumour and a fast clearance of the tracer via the kidney to the bladder without renal accumulation. The tumour/background (contralateral shoulder or flank) ratios were about 5, tumour/heart ratios about 2.5 and the tumour/brain ratios about 3 at 30 min p.i. The latter shows that this new tracer allows to obtain good contrast for brain tumour imaging.

4. Conclusion

The new PET-tracer 2-[^{18}F]fluoromethyl-L-phenylalanine can be obtained in a reasonable yield with a high radiochemical purity using a radiochemistry similar to [^{18}F]FDG. However, in order to establish a reproducible procedure which can be adapted into a routine procedure, a considerable reduction of radiodefluorination during radiosynthesis and in the radiopharmaceutical formulation is of major priority. The new tracer is taken up in a high amount in the tumours in the rats and also shows a favourable biodistribution and clearance. The results coupled to the fact that this compound shows no toxicity allow that n.c.a. 2-[^{18}F]Fluoromethyl-L-phenylalanine could be used in Phase I clinical studies.

5. Acknowledgements

The authors thank FWO-Vlaanderen (project G.0299.04N) and GOA-Vrije Universiteit Brussel (GOA28) for financial support.

6. References

[1] P.I. Jager, W.V. Vaalburg, J. Pruim, E.G.E. de Vries, K.-J. Langen, D.A. Piers, J. Nucl. Med. 42 (2001) 432–445.
[2] P. Laverman, O.C. Boerman, F.H.M. Cortens, W.J.G. Oyen, Eur. J. Nucl. Med. 29 (2002) 681–690.
[3] D. Pauleit, A. Zimmermann, G. Stoffels, D. Bauer, J. Risse, M.O. Fluss, K. Hamacher, H.H. Coenen, K.J. Langen, J. Nucl. Med. 47 (2)
(2006) 256–261.
[4] C. Rau, W.A. Weber, H.J. Wester, M. Herz, I. Becker, A. Kruger, et al., Eur. J. Nucl. Med. Mol. Imag. 29 (2002) 1039–1046.
[5] T. Miyagawa, T. Oku, H. Uehara, R. Desai, B. Beattie, J. Tjuvajev, et al., J. Cereb. Blood Flow Metab. 18 (1998) 500–509.

[6] O. Yanagida, Y. Kanai, A. Chairoungdua, et al., Biochim. Biophys. Acta 1514 (2001) 291–302.
[7] D.B. Shennan, J. Thomson, M.C. Barber, M.T. Travers, Biochim. Biophys. Acta 1611 (2003) 81–90.
[8] H. Ohkame, H. Masuda, Y. Ishii, Y. Kanai, J. Surg. Oncol. 78 (2001) 265–271.
[9] T. Lahoutte, V. Caveliers, S.M.R. Camargo, R. Franca, T. Ramadan, E. Veljkovic, J.J.R. Mertens, A. Bossuyt, F. Verrey, J. Nucl. Med. 45 (9) (2004) 1591–1596. [10] F. Verrey, Pflugers Arch. 445 (2003) 529–533.
[10] F. Verrey, Pflugers Arch. 445 (2003) 529–533.
[11] V. Kersemans, B. Cornelissen, K. Kersemans, M. Bauwens, E. Achten, R.A. Dierckx, J.J.R. Mertens, G. Slegers, J. Nucl. Med.46 (5) (2005) 32–539.

Session 18.3.3

HEALTH EFFECTS OF LOW DOSES OF IONISING RADIATIONS

M.H. BOURGUIGNON
Commissioner, French nuclear safety authority (ASN)
6 Place du Colonel Bourgoin, 75572 Paris Cedex 12 – France
michel.bourguignon@asn.fr

ABSTRACT

The health effects of low doses of ionising radiations are controversial since the concept of low doses remains ambiguous. However, it is clearly established that the risk of the corresponding stochastic effects, i.e., cancers or hereditary disease, if it exists, is very small. The linear no threshold hypothesis cannot be retained to establish a collective risk. Thus progress can only result from research in radiation biology. DNA lesions have been documented at doses as low as 1 mGy, but the pathway between one DNA lesion and a cancer is not known yet. On the basis that ionising radiations are genotoxic, the regulator must apply the current rules of radiation protection and look forward to the development of new radiation biology paradigm.

1. Introduction

Low doses of ionising radiations are usually defined as the doses below which no health effects have been observed, i.e., an effective dose of about 200mSv. This definition raises numerous issues:

- Epidemiologic studies have shown that lower values should probably be retained, about 100mSv in adults and 50mSv in children.
- These values do not take into account the dose rate and the duration of exposure; indeed a total dose of 100 mSv delivered in a few seconds and in one year are not identical in terms of effects because the number and type of DNA lesions and the rate at which they are produced are totally different and the corresponding repair mechanisms of DNA are not involved in the same way in the 2 situations.
- The confusion regarding the definition appears in many publications which are impossible to categorize : the authors claim the use of low dose of ionizing radiations in experimental animals and it appears clearly that the total dose delivered can be greater than 200 mSv although delivered at low doses.

With such an ambiguous definition of low doses of ionising radiations, it is not surprising that the potential corresponding health effects are so controversial. By definition, it is not known if below the level of dose setting up the upper limit of the low dose domain some stochastic effects do appear. Epidemiology will remain unable to make such a demonstration because of a lack of statistical power. Therefore, since it has not been possible to demonstrate health effects of low doses of ionising radiations, one can clearly state that the risk of low doses of ionising radiations, if it exists, is very small. At this level of doses, only stochastic effects, i.e., cancers or hereditary diseases might be observed.

2. The linear no treshold hypothesis

A linear relationship between health effects and doses has been observed at high doses and dose rates and has been extended as an hypothesis to the low dose domain for radiation protection purposes. The linear no treshold hypothesis (LNT) is by definition a hypothesis; since it states that each ray has an health effect, it is over-evaluating the risk of ionising radiations. Consequently, the subsequent radiation protection rules, i.e., justification, optimisation and limitation of doses, have proved useful in the sense that they help protect the workers and the population by decreasing the dose of exposures.

However it is very clear that the LNT remains an hypothesis and a simplification: it is not established as a scientific fact ; consequently collective doses must not be used to evaluate the risks related to low doses and this has been clearly stated by ICRP in its last recommendations (still to be published).

3. Progress in radiation biology

How to make further progress regarding the potential health effects (cancer or hereditary effect) of low doses of ionising radiations ? We have seen above that it is not possible to clearly answer this question with epidemiologic studies in humans. The only way to progress is to better understand the mechanisms of the effects of ionising radiations at the molecular/cellular/tissular level: progress can only result from the research in radiation biology.

Variation in individual sensitivity to ionising radiation has emerged as a new critical issue (1,2). It is clearly linked to the DNA repair mechanisms and signalling pathways. However the significance of individual sensitivity to low doses of ionising radiations needs to be confirmed by further research.

The demonstration of the existence of non targeted effects, i.e., bystander effects and genomic instability, has challenged the existing paradigm that DNA is the prime target of concern (3,4). These findings raise more than ever the possibility that the LNT hypothesis may not be appropriate in many cicumstances.

Numerous experiments have demonstrated the potential benefits of low doses of ionising radiations, this phenomenon of adaptive reponse being known as hormesis. These experiments which have been highlighted in the report of the French academies show real effects (5). There are no reason not to accept these results which have been clearly published in peer review journals. However it is also clear that these effects appear in some paradigms of exposure to ionising radiations, and this does not mean that they appear in all type of exposures. Furthermore, many of these effects are not true beneficial effects but appear as a decrease of the detriment caused by a large dose of ionising radiations delivered after chronic exposures at low “training” doses in comparison with “untrained” animals.

On another hand, one can observe in the litterature the numerous reports describing cellular and molecular effects of ionising radiations. One of these reports must be highlighted. The demonstration by Rothkamm (6) that DNA double strand breaks can be demonstrated by anti γH2AX fluorescent antibodies and appear at doses as low as 1 mGy constitutes a major event because this level of dose is about 100 times lower than previously reported. Indeed it is not a true surprise that ionising radiations create DNA lesions, but it is the first time that it is demonstrated for such low doses. It must be noticed that 1mGy is the level of dose currently delivered by medical imaging examinations (radiology and nuclear medicine).

However, there is a very large gap between one DNA lesion and a cancer. An adverse biological effect at the cellular or molecular level does not necessarily mean the appearance of adverse health consequences. So far it has been said that about 10 gene mutations are necessary to produce a cancer. Recent findings indicate that it is likely that many more gene mutations are necessary, up to 100. Indeed “cancer genes” are not equivalent : the activation of oncogenes is more powerful than the inactivation of tumor suppressor genes. Because gene mutations and cancer incidence increase in the elderly, mostly because of the inactivation of tumor suppressor genes, it is wise /necessary to limit the exposure to all genotoxic compounds e.g., chemicals, radiations..., which can contribute to these mutations.

Radio-induced hereditary effects have never been demonstrated in humans but have been observed in plants and animals exposed to rather high doses of ionising radiations (range of 1 Gy). The last scientific results which have been validated by UNSCEAR indicate that the risk of hereditary effects in humans is lower than initially expected. Consequently, ICRP has retained for its new coming recommendation an estimation of risk for the hereditary effects 10 times lower than the risk of radio-induced cancer.

Finally, the most recent researches in genomics and proteomics tend to indicate that there might be some signature of radio-induction of cancers. Further research in these domains will certainly bring new insights on the effects of ionising radiations at the molecular and cellular levels, and on the cellular responses to the initial injuries.

4. The position of a regulator

On the basis of the current knowledge regarding the effects of ionising radiations, what can be the position of a regulator ?

Although the health risk related to the exposure to low doses of ionising radiations is small, it is also very clear that ionising radiations are genotoxic. Genotoxicity does not mean health effects, i.e., cancer or hereditary disease. But since a cancer results from an accumulation of gene lesions, there are no reason to remain voluntarily exposed to ionising radiations, especially when it is not so difficult to decrease the level of exposure. This is the case for both medical exposures and radon exposures which are respectively number one in the artificial and natural exposures to ionising radiations, far greater than any other type of exposure such as industrial exposure.

Consequently, the regulator must apply the current rules of radiation protection to protect the public, the patients and the workers and inform the population of the potential risks of exposure to ionising radiations.

In terms of policy challenge, the development of new radiation biology paradigm, including targeted and non-targeted effects and individual susceptibility to ionising radiations, may require changes to the current system of radiation protection in the future (7).

References

1- Bourguignon MH, Gisone PA, Perez MR, Michelin S, Dubner D, Giorgio MD, Carosella ED. Genetic and epigenetic features in radiation sensitivity. Part I : cell signalling in raidation response. Eur J Nucl Med Mol Imaging 2005, 32(2): 229-246

2- Bourguignon MH, Gisone PA, Perez MR, Michelin S, Dubner D, Giorgio MD, Carosella ED. Genetic and epigenetic features in radiation sensitivity. Part II : implications for clinical practice and radiation protection. Eur J Nucl Med Mol Imaging 2005, 32(3): 351-368

3- Morgan WF. Non targeted and delayed effects of exposure to ionising radiations: I. Radiation induced genomic instability and bystander effects *in vitro*, Radiation Research 2003, 159: 567-580

4- Morgan WF. Non targeted and delayed effects of exposure to ionising radiations: II. Radiation induced genomic instability and bystander effects *in vivo*, Clastogenic factors and transgenerational effects. Radiation Research 2003, 159: 581-596

5- Tubiana M. Dose effect relationship and estimation of the carcinogenic effects of low doses of ionising radiation : the joint report of the Académie des Sciences (Paris) and of the Académie nationale de médecine. Int.J. Radiation Oncology Biol.Phys. 2005,63,n°2, 317-319

6- Rothkamm K, Lobrich M. Evidence for a lack of DNA double-strand break repair in human cells exposed to very low x-ray doses. Proc Natl Acad Sci U S A. 2003 ; 100(9):5057-62

7- Scientific issues and emerging challenges for radiation protection. Report of the Expert Group on the Implications of Radiation Protection Science (EGIS). OECD/NEA editor, 2007

ENC 2007 European Nuclear Conference
16-20 September 2007, Brussels, Belgium

Session 18.3.4

New developments in nuclear imaging

PINHOLE SPECT

CHRISTIAN VANHOVE
Department of nuclear medicine, University Hospital Brussels
Laarbeeklaan 101, 1090 Brussels – Belgium

ABSTRACT

Single-photon emission computed tomography (SPECT) is one of the image modalities within a clinical environment. This technique is based on the detection of gamma photons that originate from injected radioactive tracers to image the body's physiology. Nearly all clinical SPECT uses parallel-hole collimation as the image-forming aperture. These collimators are a limiting component for the spatial resolution, typically >1cm. In recent years, SPECT has become a very attractive modality for in-vivo imaging of physiological functions in small animals. Although, one might be pessimistic about the utility of SPECT for imaging small animals due to its inadequate spatial resolution, SPECT imaging using pinhole collimators can provide sub-millimetre spatial resolution. Pinhole collimation is based on the camera obscura principle. Through magnification, pinhole imaging reduces the apparent intrinsic resolution of the gamma detector. This paper demonstrates that pinhole SPECT combined with advanced software algorithms can provide high-quality three-dimensional images of small animals.

1. Introduction

Single-photon emission computed tomography (SPECT) is one of the image modalities within a clinical environment. This technique is based on the detection of gamma photons that originate from injected radioactive tracers to image the body's physiology in a three-dimensional manner. Nearly all clinical SPECT uses parallel-hole collimation as the image-forming aperture. These collimators are a limiting component for the spatial resolution, which are typically larger than 1cm. A recent trend in nuclear medicine is the growing interest for the application of SPECT in small animal studies. The development of new experimental therapies, such as stem cell therapy and gene therapy, and of new cardiovascular drugs requires several stages of animal testing before proceeding to clinical trials. Although in-vitro imaging is a common tool in this field, it requires sacrificing the animals. This can be a severe limitation because a same animal cannot be followed by sequential studies over time. Furthermore, the cost of in-vitro studies is dramatically higher than that of in-vivo studies, because a larger number of animals are needed, not only because sacrificed animals cannot be reused, but also because a larger number of experiments must be carried out in order to eliminate variability due to small physiological differences between normal animals. The understanding of the advantages of non-invasive in-vivo imaging has given rise to the need for high resolution imaging devices that can image low concentrations of biochemical agents on very small scales. Although, one might be pessimistic about the utility of SPECT for imaging small animals due to its inadequate spatial resolution, SPECT imaging using pinhole collimators can provide this required high spatial resolution (*1, 2*).
Historically, the pinhole collimator was the very first collimator used on a gamma camera. Pinhole collimation is based on the camera obscura principle as shown in Fig 1.

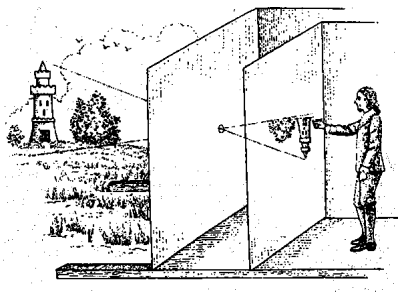

Fig 1. Pinhole collimation is based on the camera obscura principle. Here you can see an artist's impression using early pinhole imaging. However, in a clinical setting, pinhole imaging is not used to shrink an image, but to magnify it with the intention to improve the spatial resolution.

Through magnification, pinhole imaging reduces the apparent intrinsic resolution of the gamma detector, resulting in an overall spatial resolution predominantly determined by the diameter of the pinhole opening (Fig 2). Although, sub-millimetre spatial resolution can be obtained by using pinhole inserts with a sufficiently small diameter, the use of pinhole SPECT has been mainly hampered due to a trade-off between the spatial resolution, the sensitivity, and the size of the field-of-view (FOV).

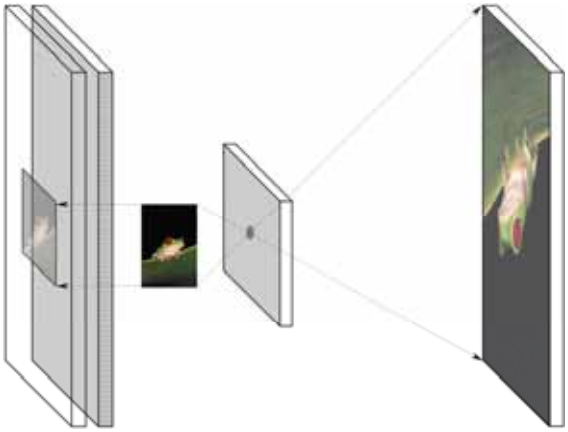

Fig 2. With parallel-hole collimation (left) the image obtained of the small frog is degraded by the intrinsic camera resolution. With pinhole collimation (right), the information loss due to intrinsic camera blurring is suppressed by the magnification.

When a system is desired with high spatial resolution, very small pinhole diameters should be used and the object should be positioned close to the pinhole opening to obtain large magnification. However, small pinhole diameters will reduce the efficiency of photon detection and the large magnification will reduce the size of the FOV. Moreover, the high spatial resolution will make the system very sensitive to imperfect camera motion, which is necessary to perform a tomographic acquisition. This is equivalent to camera shake when taking pictures in conventional photography using large zoom lenses.

Alternatively, when a system is required that efficiently detect gamma photons, large pinhole diameters should be used and the object should be acquired close to the pinhole opening. This is because the solid angle, at which the gamma photons from each point in the object are able to pass through the pinhole opening, increases enormously for points close to the pinhole opening and also increases when the pinhole diameter increases. However, the large magnification obtained in this way will reduce the size of the FOV and the large pinhole diameter will deteriorate the spatial resolution.

Finally, when a large FOV is required, one should acquire an object far away from the pinhole opening to reduce the magnification, which will result in poor spatial resolution and sensitivity.

The aim of this paper is to demonstrate that with the development of advanced software algorithms pinhole SPECT imaging can provide high-quality three-dimensional images of small animals, even though its resolution/sensitivity/FOV trade-off.

2. Image reconstruction

Tomographic reconstruction algorithms are necessary to transform the acquired two-dimensional projection images into a three-dimensional volume. As is done in Computed Tomography (CT), the reconstruction of pinhole SPECT projection images can be performed analytically using a filtered back projection algorithm (*3*). Although, these algorithms are fast because they have a low computational burden, they are not very adaptable to incorporate the physical properties of the imaging system and to model the transport of the gamma photons from the object to the imaging system. Therefore, at present, most pinhole SPECT systems use iterative reconstruction based on the Maximum-Likelihood Expectation-Maximization (MLEM) algorithm (*4*). Fig 3 illustrates the basic

steps involved in this iterative reconstruction approach. The slow convergence of the MLEM algorithm results in long reconstruction times, which restricts its practical application. With the introduction of the Ordered-Subsets Expectation-Maximization (OSEM) approach (*5*, *6*), the algorithm was made more efficient and could generate usable results within clinically acceptable time limits. The OSEM algorithm was modified by our group (*7*) to allow iterative reconstruction of pinhole SPECT images, by modelling the pinhole SPECT acquisition geometry.

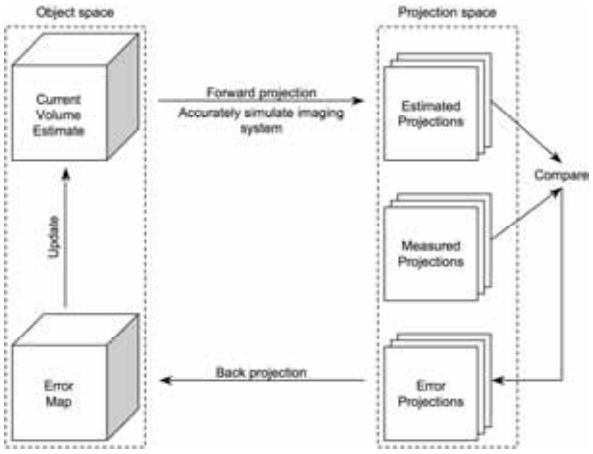

Fig 3. Iterative reconstruction. Projection images simulated from the current reconstruction estimate are arithmetically compared with the measured projections and the result is back projected to update the reconstruction estimate. The physical properties of the imaging system and image degrading effects can be modelled in the forward and the back projector.

3. Characterization of pinhole SPECT acquisition geometry

When a system is desired with sub-millimetre spatial resolution, very small pinhole diameters should be used and the object should be positioned close to the pinhole opening to obtain large magnification. This high spatial resolution will make the system very sensitive to imperfect camera motion, motion that is necessary to perform a tomographic acquisition. To avoid loss of resolution, the reconstruction of the data acquired with a pinhole camera requires a detailed description of the camera geometry, which has to be incorporated into the iterative reconstruction algorithm. This can be achieved by doing a geometric calibration of the pinhole SPECT system (*8*, *9*). The technique first acquires circular orbit SPECT projection data of a calibration object consisting of three point sources, which form a triangle with known dimensions. The location of the three sources on each projection image is then determined using simple segmentation techniques. By iteratively fitting analytically calculated locations to the measured locations, three intrinsic and six extrinsic parameters can be determined to accurately describe the pinhole acquisition geometry. The three intrinsic parameters are independent of the position of the detector during the pinhole SPECT acquisition and give information about the focal length of the pinhole collimator and the two coordinates of the orthogonal projection of the pinhole opening onto the surface of the gamma detector. For each position of the gamma detector during a tomographic acquisition, six extrinsic parameters give information about the three-dimensional location of the pinhole opening in space together with three angles to determine the orientation of the gamma detector. Fig 4 shows the effect of accurately describing the pinhole acquisition geometry during reconstruction.

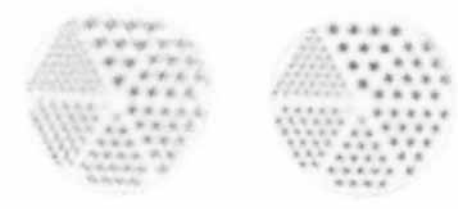

Fig 4. Trans-axial slice of a phantom containing hot rods with diameters varying from 2mm down to 1mm in steps of 0.2mm. On the left, three intrinsic parameters and only one extrinsic parameter was used to describe the pinhole geometry, on the right side three intrinsic parameters and six extrinsic parameter were used to describe the pinhole SPECT acquisition geometry.

4. Modelling the finite dimensions of the pinhole opening

When a system is required that efficiently detect gamma photons, a large pinhole diameter should be used and objects should be scanned close to the pinhole opening, to increase the solid angle at which the gamma photons from each point in the object are able to pass through the pinhole opening. However, a large pinhole diameter will deteriorate the spatial resolution. This resolution-sensitivity trade-off can be improved by modelling the finite dimension of the pinhole opening during iterative reconstruction. During the process of reconstruction it is usually assumed that the pinhole opening is infinitesimally small. This assumption is acceptable for very small pinhole openings but may introduce artefacts when using larger pinhole openings. To incorporate the finite dimension of the pinhole opening an approach based on multi-ray projections can be used (*10*). The method is based on the theory of Gaussian quadratures and prescribes a set of rays that can be incorporated in the forward and back projector of an iterative reconstruction algorithm to model the pinhole opening. Instead of using one ray, when assuming an infinitesimally small pinhole diameter, typically seven or twenty-one rays are used in the forward and back projector of the OSEM algorithm to model the finite dimension of the pinhole opening. The effect of resolution recoveryis illustrated in Fig 5.

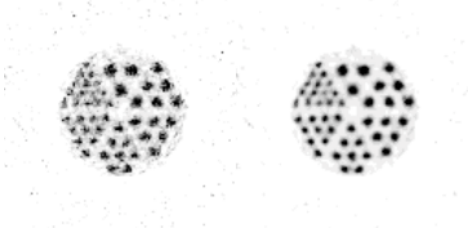

Fig 5. Trans-axial slice of a phantom containing hot rods with diameters varying from 3mm down to 1.5mm in steps of 0.3mm, reconstructed assuming that the pinhole opening was infinitesimally small (*left*) and reconstructed using the multi-ray technique modelling a 3mm pinhole opening (*right*).

5. Multiple-pinhole SPECT

As mentioned above, the pinhole collimator can deliver high spatial resolution and improved detection efficiency when imaging small subjects close to the pinhole aperture. However, this comes at the expense of a severely reduced FOV. By setting up additional pinholes and focus them on different regions in the FOV, it is possible to increase the size of the FOV. We have developed a three-pinhole collimator to obtain an axial FOV of 160 mm (*11*), allowing to reconstruct three-dimensional whole-body images of rats. Fig 6 illustrates the principle of image formation using this three-pinhole collimator. To characterize such a three-pinhole system, the calibration procedure described in the third paragraph can be used. However, the three intrinsic parameters should be defined for each of the individual pinhole openings.

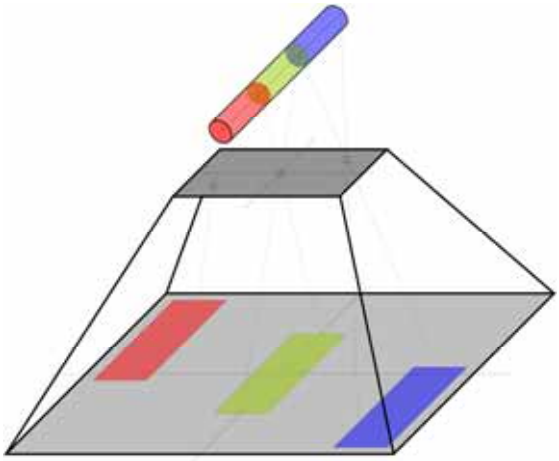

Fig 6. Principle of image formation when using a three-pinhole collimator, each pinhole focussing on another part of the object. The detector surface is tiled with three different projections of the object.

6. Conclusions

The resolution/sensitivity/FOV trade-off in pinhole SPECT can be improved using advanced software algorithms. Multiple-pinhole systems, geometrically characterized with calibration software, used in combination with iterative reconstruction algorithms that allows incorporating this pinhole acquisition geometry, can extend the axial FOV. By modelling the finite dimensions of the pinhole apertures during the iterative reconstruction process, larger pinhole openings can be used to improve the efficiency gamma photons detection while remaining good spatial resolution.

7. References

1. Beekman F, van der Have F. The pinhole: gateway to ultra-high-resolution three-dimensional radionuclide imaging. *European Journal of Nuclear Medicine and Molecular Imaging.* Feb 2007;34(2):151-161.

2. Madsen MT. Recent advances in SPECT imaging. *J Nucl Med.* Apr 2007;48(4):661-673.

3. Feldkamp LA, Davis LC, Kress JW. Practical cone-beam algorithm. *J Opt Soc Am.* 1984;A1:612-619.

4. Lange K, Carson R. Em Reconstruction Algorithms for Emission and Transmission Tomography. *Journal of Computer Assisted Tomography.* 1984;8(2):306-316.

5. Hudson HM, Larkin RS. Accelerated Image-Reconstruction Using Ordered Subsets of Projection Data. *Ieee Transactions on Medical Imaging.* Dec 1994;13(4):601-609.

6. Hutton BF, Hudson HM, Beekman FJ. A clinical perspective of accelerated statistical reconstruction. *European Journal of Nuclear Medicine.* Jul 1997;24(7):797-808.

7. Vanhove C, Defrise M, Franken PR, Everaert H, Deconinck F, Bossuyt A. Interest of the ordered subsets expectation maximization (OS-EM) algorithm in pinhole single-photon emission tomography reconstruction: a phantom study. *European Journal of Nuclear Medicine.* Feb 2000;27(2):140-146.

8. Beque D, Nuyts J, Bormans G, Suetens P, Dupont P. Characterization of pinhole SPECT acquisition geometry. *Ieee Transactions on Medical Imaging.* May 2003;22(5):599-612.

9. Defrise M, Vanhove C, Nuyts J. Perturbative refinement of the geometric calibration in pinhole SPECT. *Ieee Transactions on Medical Imaging.* 2007:In Press.

10. Vanhove C, Andreyev A, Defrise M, Nuyts J, Bossuyt A. Resolution recovery in pinhole SPECT based on multi-ray projections: a phantom study. *European Journal of Nuclear Medicine and Molecular Imaging.* Feb 2007;34(2):170-180.

11. Vanhove C, Defrise M, Bossuyt A. Three-pinhole collimator to improve axial spatial resolution and sensitivity in pinhole SPECT. *J Nucl Med.* 2007;48:428P.

EXPERIENCE WITH A COMBINED PET/SPECT SCANNER FOR SMALL ANIMAL IMAGING

N. BELCARI, A. DEL GUERRA, A BARTOLI, S. FABBRI, D. PANETTA
Department of Physics "E. Fermi" and Center of Excellence AmbiSEN, University of Pisa and INFN
Largo Bruno Pontecorvo, 3, 56127 Pisa – Italy

ABSTRACT

This paper reports a brief review of the state of the art in PET, SPECT and multi-modality scanners for small animals. At the University of Pisa a prototype version of the PET/SPECT scanner for small animal YAP-(S)PET II is available. The performance in both PET and SPECT modalities are reported together with some examples of experimental applications on small animals. X-ray transmission images of a mouse obtained with a high resolution CT prototype are also shown. This CT scanner will be soon plugged on the YAP-(S)PET II.

1. Introduction

The study of biochemical processes at a molecular level is of great importance for pharmacology, genetic, and pathology investigations. This field of research is usually called "molecular imaging" [1]. In-vivo imaging techniques for small animals [2] have demonstrated to be very valuable investigation methods for molecular imaging in the pre-clinical phase. Among the various imaging techniques Positron Emission Tomography (PET) and Single Photon Emission Computed Tomography (SPECT) have a great success that is largely due to the continuous development of high resolution, high sensitivity instrumentation for gamma ray detection. The latest advances in radiation detection technology have strongly improved the performance of small animal scanners with respect to the clinical ones. This is especially true for the spatial resolution figure of merit so as to fulfil the requirements for small size animal study. On the shadow of the successful application of combined PET-CT scanners in the clinical environment this combined technique has been recently transferred to small animal scanners.

2. State-of-the art in PET and SPECT

The relatively small size of the objects under study in small animal imaging (small organs or brain regions of rats and mice), makes it difficult the use of imaging instruments developed for human subjects, i.e., the spatial resolution of the available clinical PET scanners is not satisfactory for the quantitative and qualitative assessment of in vivo gene expression [1]. Molecular small animal imaging requires instruments with a finer spatial resolution than that of the available clinical scanners, that is not better than 4-6 mm FWHM. In small animals, it is usually acceptable to work with a spatial resolution better than 2 mm FWHM for rats (for example for the imaging of the brain), whilst for mice it would be ideal to use instruments with a resolution better than 1 mm FWHM.

2.1 PET

The best achievable spatial resolution in PET is limited because of both the physics of the β+ decay (positron range and angular deviation from collinearity) and the available technology for the position detection of two gamma rays in coincidence (crystal size, crystal position readout coding and image reconstruction algorithm). The best spatial resolution of a PET scanner can be expressed in terms of the FWHM of the point spread function (PSF) after a filtered backprojection (FBP) reconstruction with the following formula [3]:

$$FWHM = 1.2\sqrt{\left(\frac{d}{2}\right)^2 + b^2 + (0.0022D)^2 + r^2 + p^2}$$

where: 1.2 = degradation factor due to tomographic reconstruction; d = crystal pitch; b = coding error; D = tomograph ring diameter; r = effective source diameter including positron range; p = parallax error. Considering all the contributions included in the formula it can be found that the spatial resolution in PET is intrinsically limited and cannot be better than 0.7-0.8 mm FWHM. The present best scanners offers a spatial resolution which is of the order of 1.4-1.6 mm FWHM at the center of the field-of-view (FOV). This is good enough for most cases (especially for rats). On the other hand, the sensitivity of small animal PET scanners has now reached values of the order of 8-10% at the center of the FOV.

Siemens MicroPET® FocusTM 120 (http://www.medical.siemens.com/) and GE eXplore Vista (http://www.gehealthcare.com/usen/fun_img/pcimaging/products/vista.html) systems represent the state-of-the-art in high resolution small animal PET scanners. These systems offer a very high resolution and a good sensitivity. For both systems a special care is devoted to keep the spatial resolution as constant as possible over the whole FOV. Two different approaches are used: microPET® FocusTM 120 uses thinner crystal elements with a larger gantry aperture, while GE eXplore Vista makes use of a more complex phoswich technology to limit the parallax error. The performance of these systems (expressed as the best value measured at the center of the FOV) offers a spatial resolution of 1.3 mm FWHM and 1.4 mm FWHM and a sensitivity of 6.5% and 4% for the Siemens and GE scanners, respectively. Other examples of small animal PET scanners available on the market are the HIDAC-PET (http://www.oxpos.co.uk/), that uses a detector technology based on gas multiwire proportional chambers coupled to solid, high Z, converters and the LabPET from Advanced Molecular Imaging (AMI Inc.), that is based on a one-to-one coupling between APD's and phoswich LYSO/LGSO crystal assembly.

2.2 SPECT

SPECT does not suffer from intrisic spatial resolution limitations. On the other hand, the main goal is to find the optimal compromise between spatial resolution, sensitivity and size of the field-of-view that drives the choice of the collimator type and dimensions as well as the source to collimator distance and detector intrinsic resolution. For example, the use of pinhole collimators is a solution for ultra high resolution SPECT. A pinhole collimator consists in a single hole shaped like a double cone. This type of collimators are usually made of high Z materials (such as gold) in order to reduce the radiation penetration at the edge of the hole. For this type of collimators the FWHM of the spatial resolution is given by [4]:

$FWHM = D_e \cdot (d + b) / b$

where d is the distance between the object and the pinhole and b is the distance between the pinhole and the scintillator. D_e represents the effective diameter of the pinhole, depending also on the attenuation coefficient of the collimator material and on the hole aperture. Differently from parallel holes collimator, the sensitivity of a pinhole is proportional to $1/d^2$. Thus, the closer is the object to the hole the higher is the sensitivity. However, the sensitivity rapidly decreases as the distance increases. By using more holes (multi-pinholes) it is possible to enlarge the FOV to obtain "whole-body" high resolution images of small animals.

X-SPECT® by Gamma Medica-Ideas (http://www.gammamedica.com/X-SPECT.php) and NanoSPECT system by Bioscan (http://www.bioscan.com/product.php?p=nanospect) are examples of commercially available SPECT imaging system for small animals. They are both based on rotating NaI detectors. These systems can be equipped with a wide range of collimators in order to give access to the best spatial resolution/sensitivity/FOV size compromise for the protocol under study. By using high resolution pinhole collimators they can reach a spatial resolution in the submillimeter range.

2.3 Multi-modality systems

Multi-modality systems handle functional imaging provided by the SPECT and/or PET modalities, fused with high-resolution anatomical imaging provided by X-ray CT. In most cases the different modalities are combined by assembling two or more scanners that have the same axis. In this way the different systems are accessible with the same animal bed and the image fusion can be obtained by a

1-D translation. The CT part usually consists of a rotating flat-panel X-ray detector and a microfocus X-ray source.
An example of such a system is the X-FLEX preclinical imaging platform from Gamma Medica-Ideas. In this case the already mentioned X-SPECT (see section 2.2) is combined with a PET ring called X-PET and a CT scanner called X-O. A similar configuration is offered by the Siemens Inveon system that provides integrated small animal PET, SPECT and CT with multiple configuration options. The PET part is based on the MicroPET Focus technology upgraded in sensitivity (10 % at the center of the FOV) and in field-of-view (12.7 cm axially). The SPECT part is made up of two or four NaI pixellated detectors. Conversely to X-FLEX, the Inveon CT scanner is not separated from the SPECT scanner but they share the same rotation gantry and are co-planar. For this reason the CT is available with two SPECT head configuration only. Also the NanoSPECT is available with a CT scanner. In this case the CT shares the same rotational gantry with SPECT but it is displaced axially. It is made up with a CMOS flat panel detector coupled to a microfocus X-ray source.
Among the commercial systems, YAP-(S)PET II (http://www.ise-srl.com) is the only scanner that includes PET and SPECT on the same gantry [5]. This is possible because of the four-planar rotating scintillator detectors, made up of a pixellated, medium Z scintillator (YAP:Ce): each matrix is composed of a 4 cm × 4 cm YAP:Ce matrix of 27 × 27 elements, 1.5 × 1.5 × 20 mm^3 each, and is coupled to a PS-PMT. The SPECT imaging is obtained by simply adding a lead parallel hole collimator (0.6 mm Ø, 0.15 mm septum) in front of each crystal. Such architecture has the advantage of a reduction of number of detectors, meaning simplicity and affordability in terms of cost and maintenance, but at the same time maintaining the resolution and sensitivity as required for pre-clinical applications. The system operates in 3-D data acquisition mode and both FBP (Filtered Back Projection) and EM (Expectation Maximization) algorithms can be used for image reconstruction. For both PET and SPECT modalities the scanner has an axial field of view of 4 cm and the diameter of the transaxial FoV is 4 cm.

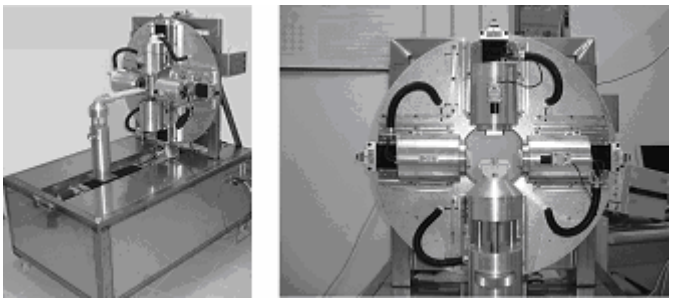

Fig 1. Pictures of the YAP-(S)PET II scanner prototype installed at the University of Pisa

3. The YAP-(S)PET scanner prototype of the University of Pisa

At the Department of Physics of the University of Pisa, a prototype version of the YAP-(S)PET II small animal scanner is installed (figure 1). In this version the distance between the opposing heads can be varied between 100 mm and 250 mm. In this way it is possible to tune the sensitivity-to-spatial resolution compromise according to the experiment requirements. In fact, the sensitivity in PET mode at the center of the FOV is 17 cps/kBq at 150 mm, 24 cps/kBq at 125 mm and 35 cps/kBq at 100 mm while the spatial resolution slightly improves as the distance increases. The peak NEC is nearly independent from the head-to-head distance (about 42 kcps) but it is reached for increasing values of activity with increasing distance. Figure 2 reports the spatial resolution measured at the standard head-to-head distance of 125 mm in the central plane. The FWHM of the images of a ^{22}Na point source (1 mm × 1 mm ∅ nominal size) reconstructed with FBP is plotted against the radial position of the source. On the other hand when working in SPECT mode the minimum distance, according to the animal size, is always preferable in order to maximize the spatial resolution. In the SPECT modality the spatial resolution measured on a glass capillary (1.0 mm nominal diameter) filled with a ^{99m}Tc solution is 2.9 mm FWHM using FBP. The measured SPECT sensitivity is 30 cps/MBq, in the 140-250 keV energy window, constant over the whole FOV.

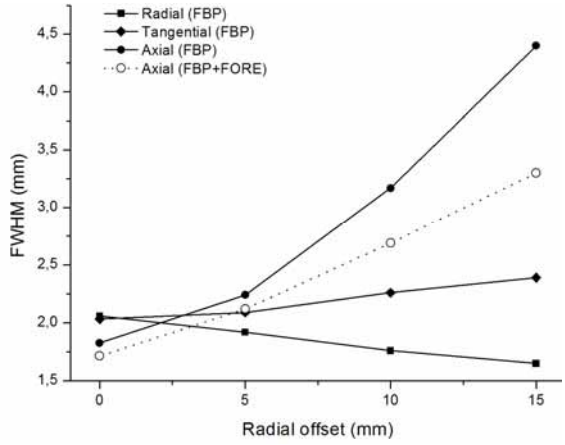

Fig 2. Plot of the spatial resolution measured in PET mode. The FWHM of the profile of the image of a ^{22}Na point-like source is plotted against the radial position in the FOV

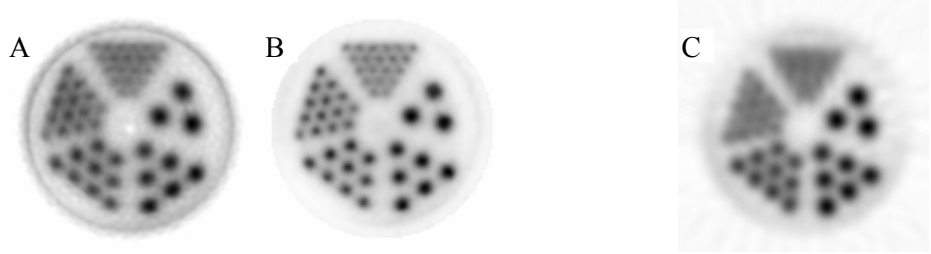

Fig 3. Images of the mini Derenzo phantom. The diameter of the rods are 3.0 mm, 2.5 mm, 2.0mm, 1.5 mm and 1.2 mm; the center-to-center distance is twice the diameter. Left: PET images (^{18}F) reconstructed with 2D-FBP+FORE (A) and 3-D OSEM (B). Right: SPECT image (^{99m}Tc) reconstructed with 2-D FBP (C).

As an example of the spatial resolution figure of merit in both PET (^{18}F) and SPECT (^{99m}Tc) modalities we have used a mini Derenzo phantom. Reconstructed images are shown in figure 3.
We have used the YAP-(S)PET II scanner prototype in PET and SPECT for animal imaging. The simple procedure for switching between the two modalities allow us the user to perform both PET and SPECT experiment in the same day. As an example of PET imaging, figure 4 shows the glucose metabolism of a normal rat obtained injecting 37 MBq of ^{18}F-FDG and acquiring for 45 min. after 30 min. of uptake. Principal structures such as cortex, thalamus and striatum are visible.

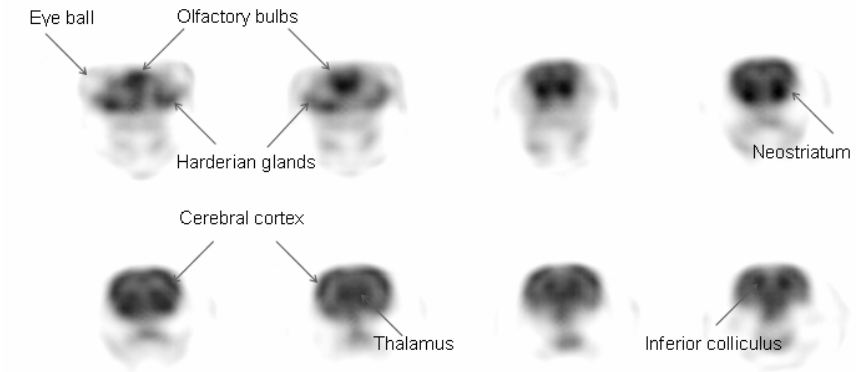

Fig 4. Coronal sections through a rat brain obtained in PET with [^{18}F]-FDG.

Examples of the experiments performed in SPECT mode on rats are shown in figure 5.
A CT scanner has been also developed using a CMOS flat panel detector (2048×1048 pixels, 48 μm pitch coupled to a Gd_2O_2S scintillator screen) and a microfocus X-ray source. The CT will be soon integrated with the YAP-(S)PET II prototype. An image of a mouse is shown in figure 6. The image was obtained with a scan time of 200 seconds (single view, axial FOV 40 mm).

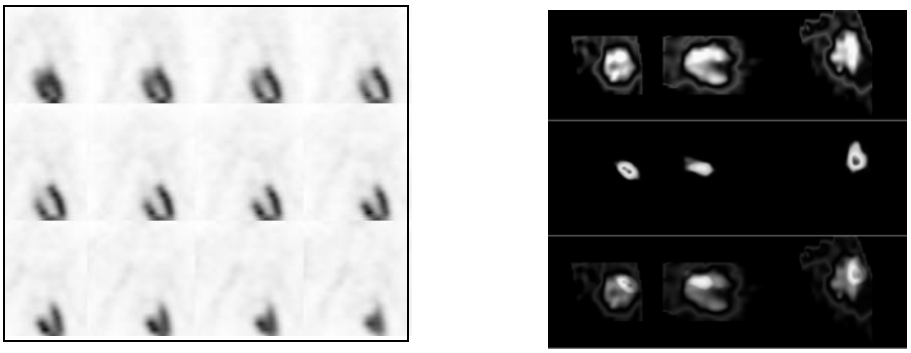

Fig 5. Left: rat myocardium perfusion studies performed in SPECT mode (^{99m}Tc-Myoview). Right: Double tracer study on a rat heart with ischemia and subsequent re-perfusion; short axis, vertical long axis and horizontal long axis projection are shown from left to right. Top row: perfusion study (^{99m}Tc-Myoview), central row ischemia study (^{99m}Tc-Annexin), bottom row: fused images.

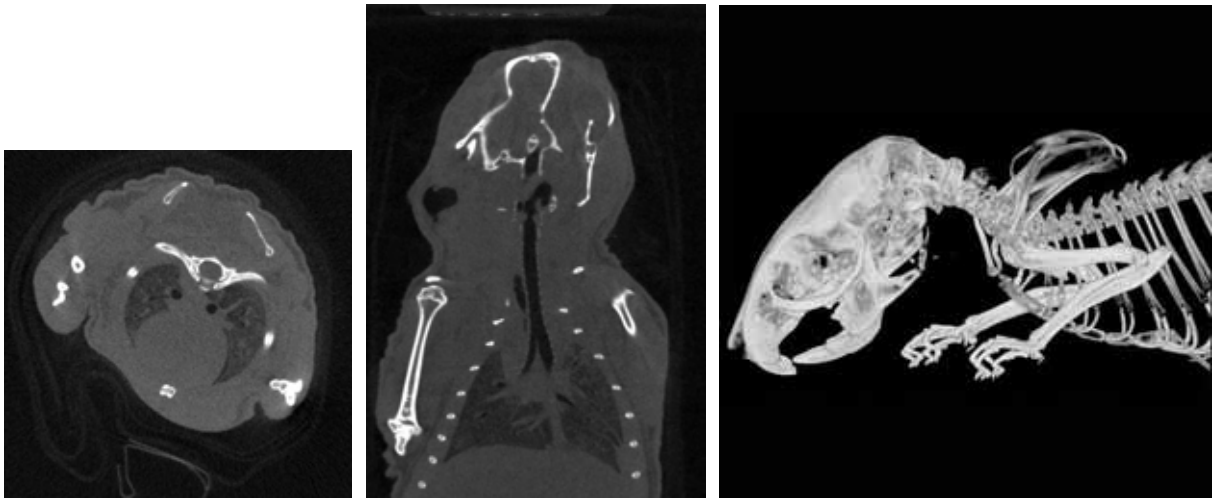

Fig 6. Left and center: transaxial and horizontal sections (80μm thick) of the mouse skull and thorax (single bed view). Right: side view of the volume rendering of the image. The acquisition parameters were 40kV, 250 μA, 1mm Al filtering, continuous rotation (500 views over 360°). Total acquisition time 200 s. Reconstruction parameters: 512^3image size (binning two), 80×80×80 μm^3 voxel size.

4. Conclusions

Our experience with the YAP-(S)PET II indicates that its spatial resolution and sensitivity are adequate for molecular imaging investigation in both PET and SPECT. The availability of both emission techniques on the same gantry allows multimodality study in a very easy and effective way. The future availability of an integrated CT will be a critical improvement for a better visualization of anatomical repere, attenuation correction and morphological characterization.

5. References

[1] T.F. Massoud, S. S. Gambhir, Genes & Development 17 (2003) 545-580.

[2] A. Del Guerra, N. Belcari, Quarterly Journal of Nuclear Medicine, 46(1) (2002) 35-47.

[3] S. Derenzo, W.W. Moses, "Critical instrumentation issues for resolution <2mm, high sensitivity brain PET", in Quantification of Brain Function, Tracer Kinetics & Image Analysis in Brain PET, ed. Uemura et al, Elsevier (1993) 25-40.

[4] G. Zavattini, A. Del Guerra, "Small animal scanners", in Ionizing Radiation Detectors for Medical Imaging, ed. A. Del Guerra, World Scientific (2004), 385-464.

[5] A. Del Guerra et al., IEEE Trans. Nucl. Sci. 53(3) 1078-1083 (2006)

ENC 2007 European Nuclear Conference
16-20 September 2007, Brussels, Belgium

Session 18.3.5

New developments in radiotherapy

TUMOUR MOTION TRACKING: EXPERIENCES WITH MICROSYSTEMS & SENSORS FOR RADIOTHERAPY

M. BANDALA, M. J. JOYCE
Engineering Department, Lancaster University
Lancaster LA1 4YR – United Kingdom

ABSTRACT

The objective of this research is to address a significant need that currently exists in medical radiotherapy. Radiotherapy is compromised by the mobility of tumours in the chest. The motion induced while breathing often makes it difficult to target tumours, meaning that patients often have to endure extended treatment times or carry out difficult breath-control techniques. A way to account for such motion is often desirable during radiotherapy treatments. By using tumour tracking, physicians can irradiate tumours more accurately without exposing the healthy tissue around the tumour to radiation.

A diminutive inertial sensor developed at Lancaster is capable of measuring position and orientation about three orthogonal axes. The sensor is intended for tracking the position and orientation of a medical target within the human body without the need for an external imaging system. Embodiments of this sensor may be applied to tumour tracking in radiation oncology.

1. Introduction

The major goal of radiotherapy is the delivery of a prescribed radiation dose as accurately as possible to a tumour region while minimising the dose distribution to the surrounding healthy tissue. There are several factors which tend to compromise this goal such as improper placement of shielding blocks, shifting of skin marks relative to internal anatomy, incorrect beam alignment and, of course, movement of internal organs and tumours. The source of internal organ motion varies from case to case, but generally falls into one of the following: organ filling and wriggling [1], peristalsis and digestive processes that alter the contents of the waste-disposal organs [2], standard behaviour of the skeletal muscular, cardiac or gastrointestinal systems [3], and finally and the more significant source of internal motion: the respiratory system.

It is well know that internal organs in the chest move due to breathing, and some tumours may move by as much as few centimetres [4]. Radiotherapy, has traditionally addressed the issue of tumour motion by treating what is known as the planning target volume (PTV). This includes not only the region where the clinical target volume (CTV) is during imaging and planning, but also where it might be during the treatment. These tumour definitions where formally adopted in 1993 [5] by the medical community.

2. Background

In an ideal case, treating the CTV would be preferable, because in doing so, healthy structures are not over-irradiated. Instead, the bigger and ‘static’ PTV is generally treated since no method to ‘view’ mobile tumours during treatment is normally utilized. X-rays imaging systems cannot sensibly be used to view tumour motion throughout therapy fractions because of the unwanted increase to the radiation dose that this would cause. Instead, surrogates [6], and respiration control methods [7] are sometimes employed.

Even though the use of surrogates (as in gated-radiotherapy) has demonstrated great effectiveness, these techniques raise another issue: the increase of the length of the treatment, which is never desirable in clinical practise. To account for such issues, alternative methods to track tumour motion are proposed by the scientific community.

The CALYPSO system [8] is a method to perform continuous target location tracking based upon AC electromagnetic technology. This system utilizes permanently implantable wireless transponders of 8 mm x 1.85 mm diameter, without the need of additional ionizing radiation. The PeTrack [9] proposes a real-time tumour tracking system using implanted positron emission markers, containing low activity positron emitting isotopes, such as ^{124}I, ^{74}As, or ^{84}Rb with half-lives comparable to the duration of radiation therapy (from a few days to a few weeks). The size of the proposed PeTrack marker will be 500-800 micrometres. Position detection requires external instrumentation for both the CALYPSO and the PeTrack systems.

3. Active navigational approach

The Powered, IN-vivo POsition Indication for Therapies (PINPOINT) system was developed at Lancaster University as an inexpensive method to detect position and orientation of a moving target. The system is comprised by a six-degrees-of-freedom sensor and an embedded DSP that conform an inertial navigation system (INS).

An INS uses accelerometers to measure the acceleration for object position and gyroscopes to measure the orientation of the object. Ideally, both are deployed in orthogonal triples (for 3D position in X; Y, and Z, and 3D orientation in roll, pitch, and yaw, in order to estimate 6D pose [10]. Fig. 1 illustrates the general operation of an INS.

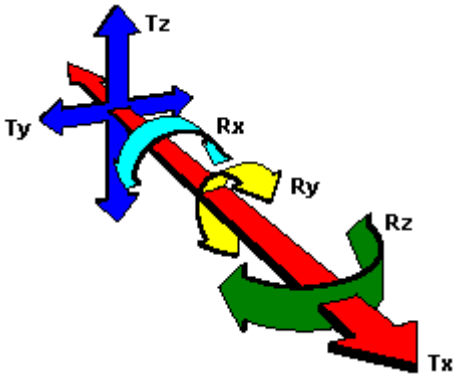

Fig 1. Inertial navigation performance defining the six degrees of freedom: three components of translation, and three components of rotation.

The prototype consists of two symmetrically- bonded PCB boards of size of 30 mm x 20 mm x 10 mm. With conditioned analog signals that are digitised, possessed, and transmitted wirelessly via Bluetooth; the power consumption is comparatively low, less than 20 mA at 3.3 V. The practical implementation of the sensor is shown in Fig. 3.

4. Tracking algorithm

Inertial sensors detect and measure motion based on the laws of nature and do not rely on external signals. Therefore, this tracking method does not require external instrumentation. The only drawback is the need of considering the gravity component.
In order to know how much gravity affects the axes where the accelerometers are, let us consider the relation between the sensor's reference frame and the earth's reference frame to witch the gravity

component is linked (see fig. 2). If the vectors associated to the accelerometers are $\mathbf{u_x}$, $\mathbf{u_y}$ and $\mathbf{u_z}$, it is necessary to establish a equation to know their components when the systems rotates around θ_1, θ_2 and θ_3. Therefore

$$u' = uR_\phi \tag{1}$$

Where **x**, **y** and **z** are the components of vector $\mathbf{u_x}$, $\mathbf{u_y}$ and $\mathbf{u_z}$. And

$$R_\phi = \begin{pmatrix} tx^2 + c & txy + sz & txz - sy \\ txy - sz & ty^2 + c & tyz + sx \\ txz + sy & tyz - sx & tz^2 + c \end{pmatrix} \tag{1}$$

If K_0 is the accelerometer scale factor given in *V/g*, then the accelerometers output is affected by the addition of the gravity offset V_G

$$V_G = K_0 \times \cos\theta \qquad \text{or} \qquad V_G = K_0 \times \frac{g \cdot u}{|g|} \tag{3}$$

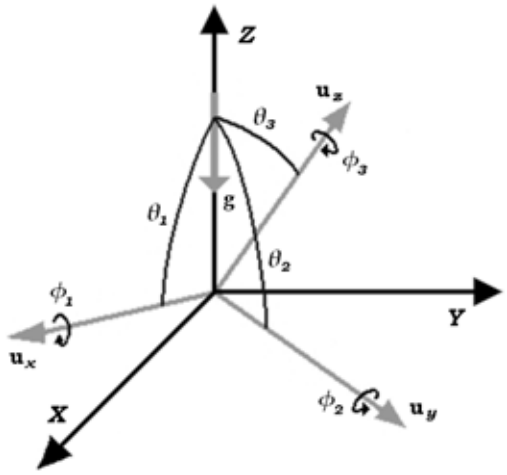

Fig 2. Representation of the earth's reference frame (black axes) against the sensor's reference frame (grey axes).

If V_0 is the accelerometer output voltage and V_Z the component when the device in immobile, then the final acceleration is:

$$A = \frac{V_0 + V_G - V_Z}{K_0} \tag{2}$$

The computation of velocity and position are made by software by implementing numerical integration algorithms:

$$v[t_n] = \frac{1}{2}\sum_{i=1}(t_n - t_{n-1}) \cdot (a[t_n] + a[t_{n-1}]) + v[t_{n-1}] \tag{4}$$

$$s[t_n] = \frac{1}{2}\sum_{i=1}(t_n - t_{n-1}) \cdot (v[t_n] + v[t_{n-1}]) + s[t_{n-1}] \tag{5}$$

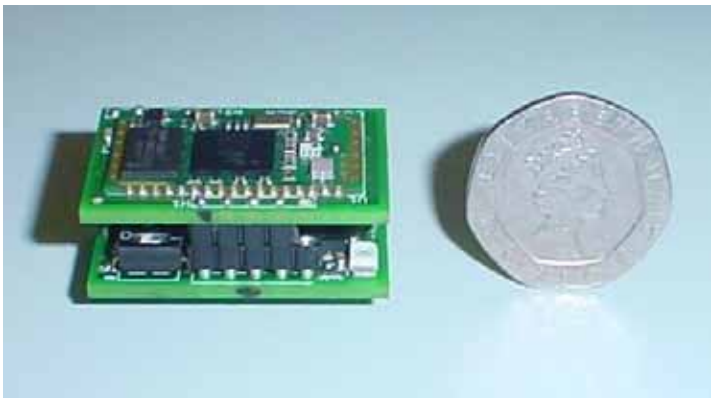

Fig 2. 30 mm x 20 mm x 10 mm prototype of the inertial sensor.

5. Experimental setup

The sensor was located inside a custom-made gimballed gyroscope (Lancaster University) for rotation tests (fig. 4a). Similarly, it was mounted on a 2-axis rig, capable of moving a small platform in two dimensions. Each individual degree of freedom was tested independently. Both the gimballed gyroscopes and the rig were marked using standard dimension measurement tools, so that the marks could be used to compare against the displacement and the angular motion of the sensor. The testing was repeated ten times. The results of this particular experiment have been submitted to publication [11].

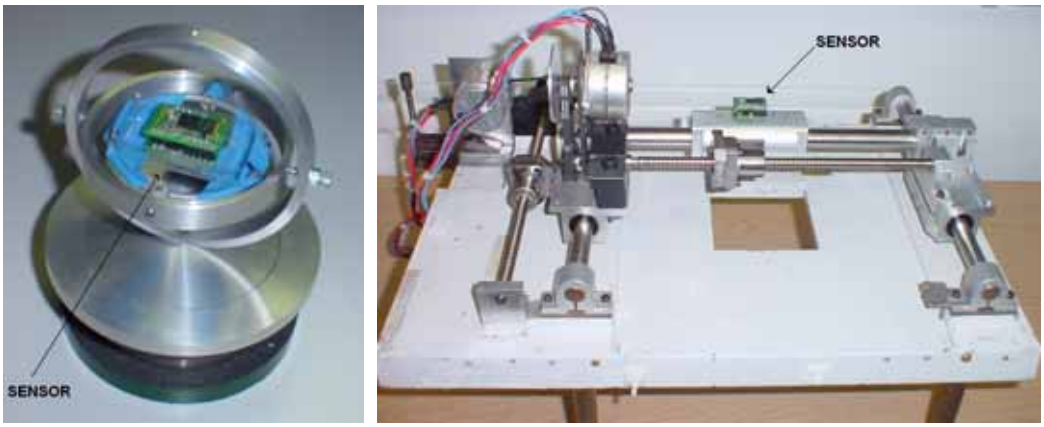

Fig 4. (a) The sensor in a gimballed gyroscope for testing. (b) The sensor in a 2-axis rig for testing.

6. Radiation effects

As the sensor will remain implanted during the course of treatment, the total radiation dose will be a factor that may limit the operational lifetime of the sensor internal electronics. The electrical properties of solid-state components change upon exposure to radiation [12]. As the dose accumulates, these changes drive the component parameters outside of the design range for the circuits in which they are used. Ultimately, these changes cause the circuit to cease proper functioning. We are carrying out a set of experiments to determine the hardness of the DPS core. The DSP will be given similar doses as a common treatment course. The results of this experiment will be presented in the ENC, September 2007.

7. References

[1] Jiang S. B. Radiotherapy of mobile tumors. Seminars in Radiation Oncology, 16:239–248, 2006.

[2] Webb S. Tumour motion: many solutions to one problem. Medical Physics Web, [Online]. Available: http://medicalphysicsweb.org/opinion, November 2006.

[3] Keall P. J. Mageras G. S. Balter J. M. Emery R. S. Forster K. M. Jiang S.B. Kapatoes J. M. Low D. A. Murphy A. J. Murray B. R. Ramsey C. R. VanHerk M. B. Vedam S. S. Wong J. W. Yorke E. The management of respiratory motion in radiation oncology. Medical Physics, 33(10):3874–3900, 2006.

[4] Murphy M. J. Tracking moving organs in real time. Seminars in Radiation Oncology, 14(1):91–100, 2004.

[5] ICRU Report 50. Prescribing, recording, and reporting photon beam therapy. International Commission on Radiation Units and Measurements, 1993.

[6] Webb S. Motion effects in (intensity modulated) radiation therapy a review. Physics in Medicine and Biology, 51:403–425, 2006.

[7] Keall P. J. Mageras G. S. Balter J. M. Emery R. S. Forster K. M. Jiang S.B. Kapatoes J. M. Low D. A. Murphy A. J. Murray B. R. Ramsey C. R. VanHerk M. B. Vedam S. S. Wong J. W. Yorke E. The management of respiratory motion in radiation oncology. Medical Physics, 33(10):3874–3900, 2006.

[8] J. M. Balter J. N. Wright L. J. Newell B. Friemel S. Dimmer Y. Cheng J. Wong Vertatschitsch E. Mate T.P. \Accuracy of a wireless localization system for radiotherapy," International Journal of Radiation Oncology, Biology, Physics, 61(3):933-7, 2005.

[9] T. Xu J. T. Wong P. M. Shikhaliev J. L. Ducote M.S. Al-Ghazi S. Molloi. Real-time tumor tracking using implanted positron emission markers: Concept and simulation study," Medical Physics, 33(7):2598{2609, 2006.

[10] M. S. Grewal L. R. Weill A. P. Andrews Global Positioning Systems, Inertial Navigation, and Integration. John Wiley and Sons, Inc., New York, p131, 2001.

[11] Bandala M. Joyce M. J. Tracking of internal organ motion with MEMS: concept and simulation Study. Meas. Sci. Technol. 2007

[12] Benson C. Price R. A. Silvie J. Jaksic A. Joyce M. J. Radiation-induced statistical uncertainty in the threshold voltage measurement of MOSFET dosimeters. Institute of Physics Publishing, Physics in Medicine and Biology, 49(2004) 3145-3159.

ENC 2007 European Nuclear Conference
16-20 September 2007, Brussels, Belgium

Session 19.3.1

Human performance in safety and maintenance

MAN, TECHNOLOGY AND ORGANISATION IN CURRENT UTILITY OPERATION AND PERSPECTIVE FOR FUTURE

TEA BILIĆ ZABRIC
Engineering, Nuclear Power Plant Krško
Vrbina 12, 8270 Krško –Slovenia

MILENA ČERNILOGAR RADEŽ
Inspection, Slovenian Nuclear Safety Administration
Železna cesta 16, 1001 Ljubljana –Slovenia

ABSTRACT

Man, technology and organisation are essential attributes of a healthy nuclear safety culture, with a goal of creating a framework for open discussion and continuing evolution of safety culture throughout the commercial nuclear electric generating industry.
A variety of operation experiences over the years have improved the safety culture at nuclear electric generating plants. The nuclear industry does not allow decreasing the safety margins, which could cause occurrences. Many fundamental principles involving hardware, procedures, training, and attitudes toward safety and regulation contributed to the error prevention.
Response from operation experience from both industry and regulatory organisations was extending. Improvements were made in standards, hardware, emergency procedures, processes, training (including simulators), emergency preparedness, design and configuration control, testing, human performance, and attitude toward safety.
But still, analysis of the available nuclear operating experience shows that human performance is a key factor in a large proportion of events.

1. Introduction

Safety culture, what is a safety culture? "*An organisation's values and behaviours – modelled by its leaders and internalised by its members – that serve to make nuclear safety the overriding priority*". Therefore, safety culture has to be inherent in the thoughts and actions of all the individuals at every level in an organization. The principles and associated attributes for a strong safety culture have a basis in plant events and operation experience. These principles and attributes influence values, assumptions, experiences, behaviours, beliefs, and norms that describe how things are done at specific utility.

Utility leading personnel have to be encouraged to make comparisons between established principles and their day-to-day policies and practices and to use any differences as a basis for improvement. Subcontractors, vendors, third-party engineering and authority support should be included in the efforts of improving safety culture. Safety culture awareness and recognition of the importance of nuclear safety and its value to the organisation should be reflected in supplemental personnel performance.

Analysis of the available nuclear operating experience shows that man - human performance is a key factor in a large proportion of events. The safety gains achievable through improved human performance become increasingly important in deciding where to apply resources; "*Arrives the time to invest in people, not only in equipment*". Plant management establishes performance standards and

requirements for the conduct of plant activities that are consistent with corporate policies and objectives, nuclear safety philosophy and other requirements. Management also establishes methods to communicate effectively upward, downward and horizontally within the organisation.
The organisation of the plant helps achieve a high level of performance and nuclear safety during plant operation and shutdown conditions through effective implementation and control of plant activities. The organisation provides the administrative and functional structure that determines where people are assigned and defines how they are expected to accomplish their tasks. The complexity of a nuclear generating plant requires that the organisation be clearly defined.
Policies, directives, procedures, goals and objectives and performance standards provide administrative controls and management direction to implement the organisational structure.
The basic assumptions that have worked well in current organisation should be considered as a valid to new organisation and facilities built in the future.

2. Men, technology and organisation

Earlier industry attempts to improve human performance focused on results and individual behaviour at the worker level, a common response to human error that exists today in many organisations. However, organisation and management influences on human behaviour are equally important, but often overlooked or underestimated. Experience has revealed that most causes of human performance problems exist in the work environment, indicating weaknesses in organisation and management.
To optimise successful performance, appropriate individual and leader behaviours must occur together with appropriate organisational processes and values. All three must work together during all phases of a work, from work identification through completion of documentation.

2.1 Man-Human Performance and Management

It was learned form industry: "*When a program agrees to spend less money or accelerate a schedule beyond what the engineers and program managers think is reasonable, a small amount of overall risk is added. These little pieces of risk add up until managers are no longer aware of the total program risk, and are, in fact, gambling*"
Human performance is a series of behaviours executed to accomplish specific task objectives (results). Behaviour is what people do. Results are achieved by behaviours, the mental and physical efforts to perform a task. Although results that add value are important, desired behaviour must be the target for improvement efforts.
We have to be aware that excellence in human performance becomes an important measure to reduce events. A key way to improve human performance is to focus on instilling in people the correct behaviour patterns in all stages of the NPP life cycle. The installation of this 'ethos' is of much greater importance than attempting to solve post event problems created by its lack. Human error is caused by a variety of conditions related to individual behaviour, management and leadership, organisational processes and values. Alignment involves facilitating organisational processes and values to support desired behaviour.

Particular organisation has to establish its own principles for excellence in human performance to promote behaviours throughout an organisation that support safe and reliable operation of the plant. Progress toward excellent human performance requires a work environment in which individuals and leaders routinely exhibit desired behaviours. Such behaviours must be clearly described, communicated and what is a most importantly reinforced. Open communication and positive reinforcement can establish a culture in which individuals, leaders and organisational processes eliminate barriers to excellent human performance, what results in reduce or even elimination of significant plant events due to human error. Experience with error prevention and human performance improvement has revealed that the most capable defences against events are open communication and positive reinforcement of desired behaviours.
How to reach environment where we can proudly say 'that is the way we do things here'?. Achievement of that goal includes:

- Systematic performance assessment of the operational experience related with human factors/human errors, following worldwide good practices criteria and specific experience of operators internationally
- Establishment of an analysis tool for human errors
- Establishment of measures for human error prevention
- Establishment of a system for near misses reporting and resolution
- Safety culture improvement and safety culture audits
- Establishment of basis for safety culture assessment.

2.2 Technology

Changes to plant design and improved equipment deliver high levels of safety. It based on the implementation of operating experience programme. This contributes to safe, reliable and efficient nuclear plant operation. Events, which occur today, reveal a completely new cause or failure mechanism. Most investigations find that external operating experience was available which, if used effectively, could have prevented recurrence of the event. The best use of operating experience is to look for similarities that could apply to particular plant, rather than look for differences that should lead to screen the experience out.
Effectively using operating experience includes analysing both internal and external operating experience to identify fundamental weaknesses and then determining appropriate plant specific corrective actions that will minimise the likelihood of similar events. Plants have to be encouraged to share operating experience.
The plant's goal for operating experience is, to effectively and efficiently use lessons learned from plant and external operating experience to improve plant safety and reliability. Learning and applying the lessons from operating experience is an integral part of plant safety culture and has to be encouraged by managers throughout the organisation. Plant personnel have to be encouraged to use operating experience information at every opportunity as a helpful. Strength methods of using operating experience assured provision of applicable information to the right personnel in write time. When plant personnel analyse the causes of plant events, operating experience has to be routinely reviewed to determine if and why previous lessons were not effectively learned.

2.3 Organisation

An effectively implemented organisational structure establishes the framework to accomplish the organisation's mission. Responsibilities and authorities for accomplishing assigned tasks have to be clearly defined and communicated in organisations. Various administrative elements have to be established to ensure that management's expectations are clearly communicated and understood and effectively implemented. Administrative elements include formally established goals and objectives. Administrative elements also include policies, procedures and methods to conduct plant activities and maintain nuclear safety. Policies and procedures have to be clearly written, technically correct and readily available so plant personnel can easily determine and properly implement actions required under varying circumstances. Management monitoring and assessment activities are an integral part of the administrative elements to identify strength and week performance area.

3. Safety Culture and Human Performance – Perspective for the future

The recent events like Davis-Besse Nuclear Power Station reactor vessel head and the severe damage to fuel external to the reactor at Paks Nuclear Power Plant have highlighted problems, which happened when the safety environment does not have sufficient attention. A common thing in these cases is that, that they are mostly result of the plant culture. If the weaknesses are recognised and resolved on time, the events could have been prevented or their severity lessened. The series of decisions and actions that resulted in these events can usually be traced to the shared assumptions, values, and beliefs of the organisation. Organisational culture is the shared basic assumptions that are developed in an organisation as it learns and copes with problems. The basic assumptions for strong culture have to be

taught to new employees of the organisation as the correct way to perceive, think, act, and feel. Culture is the sum total of a group's learning.
In addition to a healthy organisational culture, each nuclear power station, because of the special characteristics and unique hazards of the technology – radioactive products, concentration of energy in the reactor core, and decay heat – needs a strong safety culture.

Implied in the definition of the Safety Culture is the notion that nuclear power plants are designed, built, and operated to produce power in a safe, reliable, efficient manner; that the concept of safety culture applies to every employee in the nuclear organisation, from the board of directors to the individual contributor; that the focus is on nuclear safety, although the same principles apply to radiological safety, industrial safety, and environmental safety; and that nuclear safety is the first value adopted at a nuclear station and is never abandoned.

Even the nuclear plants are designed to perform safely under a full range of scenarios, events happened. Where is the problem? Corporate cultures must embrace the reality of human fallibility because even the best people make mistakes. The relieving factor is the fact that error-likely situations are predictable, manageable, and, preventable. Organizational processes and values influence individual behaviour. People achieve high levels of performance based largely on the encouragement and reinforcement received from leaders and subordinates. Events can be avoided by an understanding of the reasons mistakes occur and application of the lessons learned from past events.

The following statistic makes more clear answer why human performance:

- 100,000 people die every year due to medical errors
- 17,000 people are seriously injured or die every year due to driver errors
- 21 out of 26 fuel damaging events due to human error
- 75 % of all reportable nuclear power plant events are due to human error
- 70 % of causes are related to weaknesses in the organization

But it has to be clear that human error is not always a sign of poor safety culture.

Could we find if Safety culture is present or it is not present? Safety culture is present, when people feel good, when a well done work can be found, when the workers are satisfied, when open communication exists, etc. There are different indicators to "measure" safety culture and allow ongoing assessment of it. Each facility has to address their own indicators, depends on their culture, people, organisation. Some of them are: Compliance with rules and licensing requirements; Challenges to operation; Radiation protection programme effectiveness; Number of human factor related events; Number of self-assessments.

And what is perspective for future, what means improvement in human performance, what are next steps: emotional intelligence? What is emotional intelligence: *"The ability to monitor one's own and others' emotions, to discriminate among them, and to use the information to guide one's thinking and actions"* and why emotional intelligence: *"Business has become, in this last half-century, the most powerful institution on the planet -- the dominant institution in any society needs to take responsibility for the whole and emotional intelligence is emerging as a critical factor in high performance at work, school, and at home"*
Everyone has emotional intelligence. Research shows: can be taught or increased or can change leadership styles. We can increase emotional intelligence by:

- Practicing being more aware – Listening and Observing
- Being more conscious of our choices
- Deliberately blending our thinking plus feelings to generate better decisions

What is important emotional intelligence does not mean "being nice", it equals "Consciously and carefully processing and using emotional information and emotional energy".

If we value emotions as a source of information and energy, we will begin to get more positive results in our relationship with others and ourselves.

4. Conclusion

Commercial nuclear electric generating plants are designed, built, and operated to produce electricity. Safety, production, and cost control are necessary goals for the operation of such a plant. These outcomes are quite complementary, and most plants today achieve high levels of safety, impressive production records, and competitive costs, reinforced by decisions and actions made with a long-term view. This perspective keeps safety as the overriding priority for each plant and for each individual associated with it.
Nuclear safety is a collective responsibility. No one in the organisation is exempt from the obligation to ensure safety first. The following principles are important:

- Everyone is personally responsible for nuclear safety.
- Leaders demonstrate commitment to safety.
- Trust permeates the organisation.
- Decision-making reflects safety first.
- Nuclear technology is recognised as special and unique.
- A questioning attitude is cultivated.
- Organisational learning is embraced.
- Nuclear safety undergoes constant examination.

The following should be sufficient:
- Communication on all levels
- Safety culture
- Procedures and documentation
- Quality assurance and motivation for it.

5. References

[1] IAEA TECDOC-1329, "Safety culture in nuclear installations"
[2] IAEA Safety reports series No.11, "Developing safety culture in nuclear activities (practical suggestions)"
[3 IAEA INSAG-15, "Key practical issues in strengthening Safety Culture"
[4] IAEA INSAG-13, "Management of operational safety in Nuclear Power Plants"
[5] IAEA Safety reports series No.1, "Examples of safety culture practices"
[6] IAEA TECDOC-1479, "Human performance improvement in organizations: Potential application for the nuclear industry"
[7] WANO GL 2006-02, "Principles for a Strong Nuclear Safety Culture"
[8] WANO GL 2001-01, "Guidelines for the Organisation and Administration of Nuclear Power Plants"
[9] WANO GL 2002-02, "Principles for Excellence in Human Performance"
[10] WANO GL 2006-03, “Guidelines for Effective Nuclear Supervisor Performance”
[11] INPO SER 3-05, “Weaknesses in Operator Fundamentals”
[12] Kim Vicente, “The Human Factor: Revolutionizing the Way People Live with Technology”

Human Performance to Avoid Failures and to Improve Reliability

Günter Bäro, Thomas H. Dent, Dirk Ebert, Bernd Wilkes
Westinghouse Electric Germany GmbH

Dudenstrasse 44, 68167 Mannheim

Reasons and Goals

Human Performance is a program that has been recommended to the US operators of nuclear power plants by INPO the Institute of Nuclear Power Operators. The reason is to increase the reliability and hence the availability of a plant. Having this in mind, the overall goal is to prevent errors and to avoid failures. If we reduce the failure rate, we will increase the reliability and therefore the availability of a plant[1]. In principle, we know such a phenomenon from accident pyramids. These pyramids show us that there seems to be a unique relationship for events of different significances. We are going to encounter 1 serious event per 10 significant events, 30 near misses and 600 minor incidents. The numbers may change per organization, but the principle holds. If we have less minor incidents, we will reduce the probability of increased risks for larger problems, accidents or catastrophies, automatically.

What can be done to reduce the number of failures and the failure rates. Within the Human Performan Program of INPO, there are several methods and tools, to accomplish this goal. In Europe, there has been some reluctance to employ the Human Performance Program, despite the fact that WANO the World Association of Nuclear Operators supported the utilization of the tools and methods recommended by INPO. One of the essentials of this program is a standardized process with structured procedures, structured briefings and debriefings as well as a structured communication to strive for an exclusion of misunderstandings.

Westinghouse noted that a large portion of the problems which are encountered during the execution of a project seems to be due to communication problems. Such problems are enhanced if you work in an international environment, in which people have to cooperate who do not have a common mother tongue and a common cultural background. Potentially country-specific attitudes and methods to accomplish a communication have to be unified and structured such that misunderstandings are nearly excludable in our international work environments. In addition, a standardized and structured communication helps to avoid emotional problems between people who are working in such groups.

This paper presents the program that Westinghouse employed to improve the performance of her employees and how this program is being implemented and realized in Germany and in Europe.

---

[1] Human Performance Improvement – Overview Training, W. Earl Carnes, 2006 DOE Price-Anderson Coordinator Training April 4-6, 2006, http://www.eh.doe.gov/enforce/2006presentations/day3/Carnes(5).pdf

Human Performance – Basic Considerations

The primary goal of the INPO program of Human Performance is to prevent errors which could jeopardize safety respectively the execution of a task. During the execution of a project, each deviation or even each irritation indicates that there is a deviation of the originally qualified parameters. A correction of such an irritation or deviation requires an additional effort and enhances the risk of a failure, because of the extension to unknown parameters which have not been qualified, so far. This by itself may create problems which have not been considered and which could create unexpected disturbances at other sites respectively process steps. Such properties and such a performance are known from manufacturing materials. Changing the manufacturing parameters changes the material properties. In case of highly automated systems, this effect is known, too. Slight disturbances may be indicators or even causes of unexpected and sometimes even dramatic results. Those who work with complex databases know that the solution of a problem in one part of the program may create a new problem at another unexpected part of the program.

Fig. 1: INPO Information about Human Performance Improvement - Overview Training by W. Earl Carnes, 2006 DOE Price-Anderson Coordinator Training, April 4-6, 2006

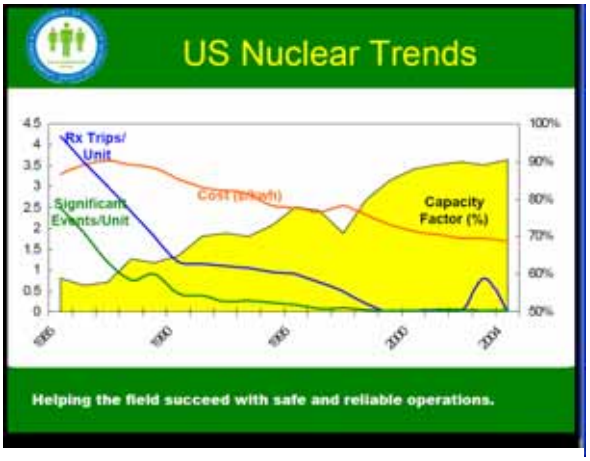

Fig. 2: INPO Information about Human Performance Improvement - Overview Training by W. Earl Carnes, 2006 DOE Price-Anderson Coordinator Training, April 4-6, 2006

INPO showed that the interaction between man, machine and organization needs to be understood, to improve the performance of complex, profoundly jeopardized systems. Human errors account for about 80% of the occurrences, and 70 % of these human errors are due to latent organizational weaknesses. In other words, there are only 20% of occurrences or events due to equipment or material failures. We eliminate technically risky products before they fail unexpectedly utilizing regular, preventive and corrective maintenance, surveillances as well as inspection and audit results. A safe and reliable, disturbance free operation increases the capacity factor and the availability. This is what drives us to go for methods and tools which reduce human errors and failures significantly.

Event-free work and reliability are a product that is achieved by the own performance at work and the achieved results. If we are going to make mistakes or failures en route, we have to encounter additional work time and furthermore irritation and annoyance of the customer. This customer irritation and annoyance by itself is creating extra time efforts and, hence, extra costs.

On top of all of this, there are customer expectations to do specific tasks and provide deliveries, which have neither been specified nor agreed upon, explicitly. Such a delivery could be file records of a documentation, a specific warning signal of a switch or button, or the explicitly defined extended limits of service deliveries, which is interpreted differently by the parties involved. An early common understanding is

needed, to increase the rate of being without errors and to get such unexpressed expectations under control.

The process to avoid errors and failures has the very first priority and the complete management has to fulfill the assigned role within this process. This means that the management has to ensure that all of the regulatory rules, the Westinghouse policies and procedures, as well as the product specific processes and guidelines are to be met, followed up and if necessary trained repeatedly.

Avoiding Failures and Errors – Definitions and Methods

An error is an action that unintentionally departs from an expected behavior. A violation is a deliberate, intentional act to evade a known policy or procedure requirement for personal advantage usually adopted for fun, comfort, expedience, or convenience.

Up to now we had the following view of a human error: A human error is the cause of accidents. To explain a failure you must seek failure. You must find people's inaccurate assessments, wrong decisions, and bad judgments. However, human errors are often symptoms of trouble deeper inside a system. Therefore, the new view is to explain the failure, and not to try to find where people went wrong. We are trying to find how people's assessments and actions made sense at the time, given the circumstances that surrounded them. It is more important to find the reasons that caused the error than the people.

Human Performance describes a behavior to achieve a work according to well described processes without running into errors or failures. If we understand and accept the situations for actions and decisions, we are enabled to develop tools that help us to avoid errors and failures. It is obvious that we have to agree on standard behavior patterns to avoid failures and errors due to communication problems within an international work group with people of different mother tongues and business / work cultures.

Process Based Leadership is an indispensable process to assure that the procedural adherence has the first priority. Managers have to reinforce the use of methods and tools employed within this process.

Tools to Optimize the Human Performance of Westinghouse

- Avoid errors by applying
    - Procedure use, adherence, placekeeping, i.e. use standardized processes and check lists
    - 3-way-communication
    - time out and collaborate in case of doubts
    - create situational awareness by monitoring tasks to identify undesirable situations
- reinforce exchanges of ideas and what is done by
    - verbalizing and challenging - share own ideas with employees/colleagues when acting
    - briefings and debriefings
- reveal and eliminate error causing organizational weaknesses by
    - self and peer checking
    - persistent, repeated observation of working procedures & employees
    - persistent, repeated registration of error events
    - active participation in the Root Cause Analysis (RCA)
- to support continuous enhancement in a learning environment
    - to coach and support efficient and error preventive practices
    - to communicate error solutions and behaviors
    - to provide resources and tools

It is the task of the management to get involved with the work which is performed by their employees. This is essential for a manager or a lead, in order to coach and to identify themselves with the work done. Therefore, the application of these tools is to be watched, to assure the persistent implementation and usage of them. For that purpose, the management will reveal their observations in a database without violating the employee's right of privacy applying a top down process. So called Learning Clocks and Human Performance Event Investigations shall demonstrate how Westinghouse applies and uses the same procedures worldwide, in order to reveal and to remedy defects. In each European country an organizational entity is established serving the site management to take care and to observe the implementation of the procedures. For the European locations, a coordinating entity assures that in all sites the same tools and methods are applied as in the US and that local management persistently reinforces the implementation and usage of the measures/actions. When implementing the process barriers and obstacles because of regional cultural and linguistic phenomena are to be identified and overcome by the local groups and should not be disregarded. A significant amount of training is given to everybody, and especially to leads and managers. By getting involved the management and the leads will support the application, observe and coach their personnel and reinforce the use of methods and tools.

Barriers in Germany

The mentioned tools are well known since years. But we have difficulties to apply them. We face cultural and mental barriers/difficulties, which might be different in each country. It is very important that the managers including the directors are getting involved and clarify that we are not looking for the guilty ones but for the latent system and organizational errors. They have to commit themselves to follow up the measures, to record observations and events and to enhance the application of the tools. Typical German barriers have been:

- Observations are not done to find something to be blamed for
- Differences in education and culture
- Differences in management systems
- Linguistic incorrectness in the translations
- Missing error culture (acticle in the FAZ dtd. 04-06-06)

Only setting good examples and the persistent usage of the mentioned tools can eliminate these barriers and change the mindset. Managers must set a good example in order to overcome those barriers as well as to assure the procedure.

Summarization

Early error perception and prevention has a top priority since several years. The procedure to enhance the work performance safety and reliability, e.g. in order to avoid errors, is being introduced as a top down procedure within Westinghouse. A prerequisite for the persistent implementation is the management's attitude that must do their utmost to realize and support the procedure. Within Westinghouse the worldwide implementation of identical tools and methods is assuring a harmonized procedure. The management is committed to follow up and to assure the application and usage of the predefined tools and methods. They record any respective observation, while events and errors and related corrective actions are published.

MONITORING THE EFFECTIVENESS OF MAINTENANCE PROGRAMMES THROUGH THE USE OF PERFORMANCE INDICATORS

P. VAISNYS, M. BIETH, P CONTRI

Institute for Energy, Joint Research Center, European Commission
Westerduinweg 3, NL-1755 LE Petten, Niederlands

ABSTRACT

Optimization of the maintenance strategy, enhancement of the maintenance efficiency and monitoring the performance are becoming the key attributes to ensure the survival of nuclear utilities in the energy market. To monitor the maintenance performance in an effective and objective way, the relevant measurable indicators were selected and a maintenance performance monitoring framework was proposed. Three attributes associated with the excellence of the maintenance program are proposed at the top of this structure. Using the attributes as a starting point, eight key performance indicators were proposed to cover the key aspects of maintenance. Finally each key performance indicator is supported by a set of specific indicators representing the measurable metrics of the maintenance program.

1. Introduction

Economic deregulation of electricity markets in many countries has placed nuclear power plants in a new competitive environment where capital, operating and maintenance costs must be minimized. Optimization of the maintenance strategy, enhancement of the maintenance efficiency and monitoring the performance are becoming the key attributes to ensure the survival of nuclear utilities in the energy market. The maintenance performance monitoring was one of the research tasks of the SENUF (Safety of European Nuclear Facilities) network established in 2003 to facilitate the harmonization of safety cultures between the Candidate Countries and the European Union. After 4 years of successful operations, the SENUF network was integrated into the new Direct Action of the European Commission, SONIS (Safe Operation of Nuclear Installations), where research on maintenance monitoring and optimisation plays a major role. The objective of this paper is to present the results of research activities carried out by the institute of Energy in the area of the use of numerical indicators in the monitoring of maintenance performance.

To monitor the maintenance performance in an effective and objective way, the relevant measurable performance indicators should be used. However, experience has shown that focusing on any single aspect of performance is ineffective and can be misleading. A range of specific leading and lagging indicators should be considered in order to provide a general sense of the overall performance of a maintenance programme and its trend over time. The best performance measurement systems contain a mix of lagging and leading indicators. When dealing with the maintenance performance monitoring we apply the business process approach to the maintenance function. This concept of process management is based on the assumption that the process itself produces the desired results and therefore the process has to be managed and measured. This approach ensures successful management of the maintenance process in order to achieve optimal levels of equipment reliability, availability and cost effectiveness. For the maintenance application, the leading indicators measure the effectiveness of the maintenance process, while lagging indicators measure results. The necessity for tracking the maintenance performance indicators other than just equipment reliability and availability is to pinpoint areas responsible for negative trends (leading indicators). In addition the performance indicators should not be considered just a measure/demonstration of success but should be used as a tool to manage successfully. The utilities should utilize performance indicators to identify opportunities for improvement rather than measures of success or failure.

2. Maintenance performance indicators (MPI) system

As a first step in the development of the maintenance performance monitoring framework, we consider the definition of the maintenance monitoring concept. It is assumed that the maintenance monitoring system is established at the power plant with the aim to achieve the maintenance excellence, by removing the existing or potential deficiencies. The proposed approach to monitoring of maintenance performance is presented in Fig. 1. On the top of the maintenance performance hierarchical structure we propose the Maintenance Excellence, from which we develop three attributes that are associated with the excellence of the maintenance programme:

- Preventive character of maintenance (including predictive maintenance);
- Maintenance management;
- Maintenance budget.

Using the attributes as a starting point, a set of maintenance performance indicators is proposed. The key performance indicators are envisioned to provide overall evaluation of relevant aspects of maintenance performance. Below each attribute, key performance indicators are established. Each key performance indicator is supported by a set of specific indicators, some of which are already in use in the industry. Specific or plant specific indicators represent quantifiable measures of performance. Specific indicators are chosen for their ability to identify declining performance trends or problem areas quickly, so that after proper investigation the management could take corrective actions to prevent further maintenance performance degradation.

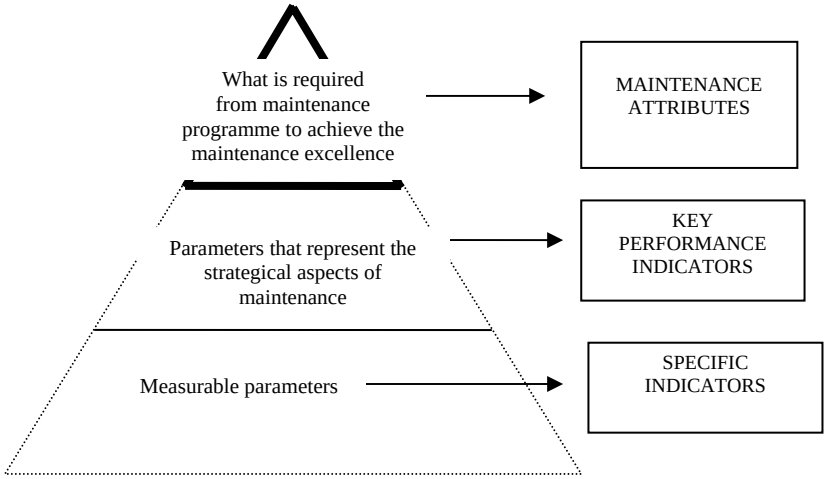

Fig 1. An approach to the monitoring of maintenance performance

3. Key performance indicators

3.1 Preventive maintenance

For the preventive attributes of maintenance the following three key indicators are proposed:

- System and equipment availability;
- Reliability of the systems and components;
- Effectiveness of preventive maintenance.

The performance indicators structure for preventive maintenance is shown in Fig. 2.

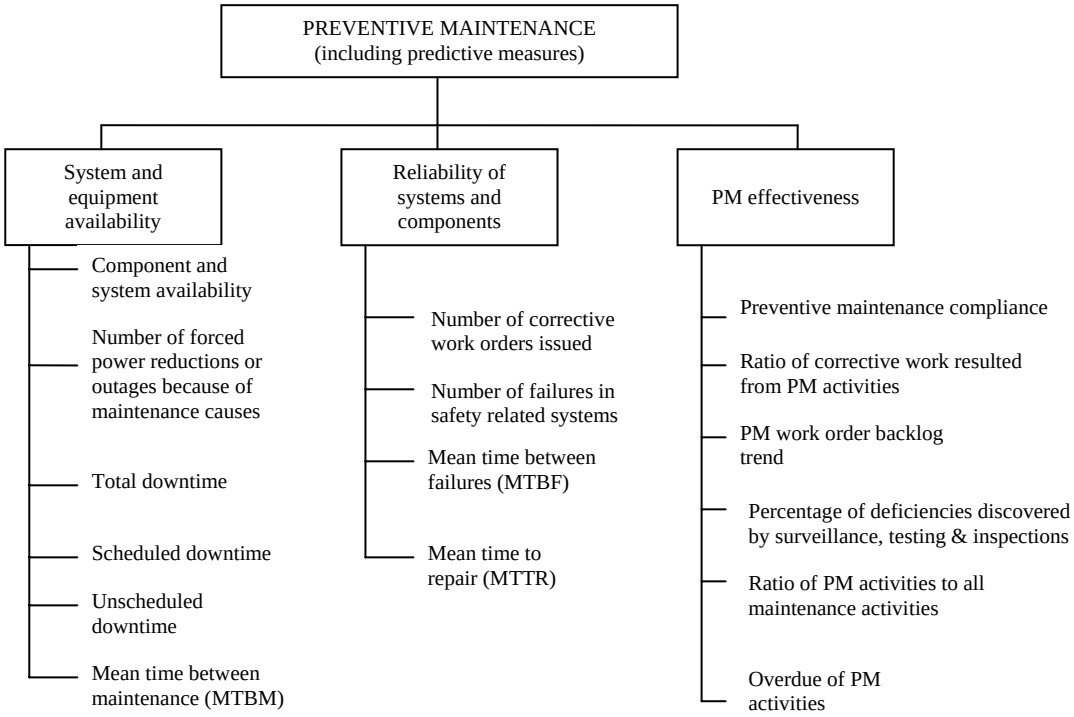

Fig 2. Performance indicators for the preventive maintenance

Preventive maintenance programs are established at the majority of nuclear facilities to maintain equipment within design operating conditions and/or to extend equipment life. In conjunction to the predictive maintenance measures, preventive maintenance helps to correct many potential problems before they occur. Preventive maintenance allows equipment to be repaired at times that do not interfere with production schedules, thereby removing one of the largest factors from downtime cost, increasing profitability. Preventive maintenance activities can be planned in advance facilitating the control of the backlog at the reasonable level.

3.2 Maintenance management

A comprehensive work planning and control system applying the defense in depth principle should be implemented so that maintenance activities can be properly authorized, scheduled and carried out by either plant personnel or contractors, in accordance with appropriate procedures, and can be completed in a timely manner. The maintenance management system should ensure the allocation on and off the site of the resources necessary to efficiently accomplish the maintenance activities. Effective coordination should be established among different maintenance groups and among the different departments of the plant. To reflect the maintenance management aspects we propose the following key indicators:

- Planning and scheduling;
- Interface with operations;
- Work control;
- Material management.

The structure of the performance indicators to reflect the maintenance management is presented in Fig. 3.

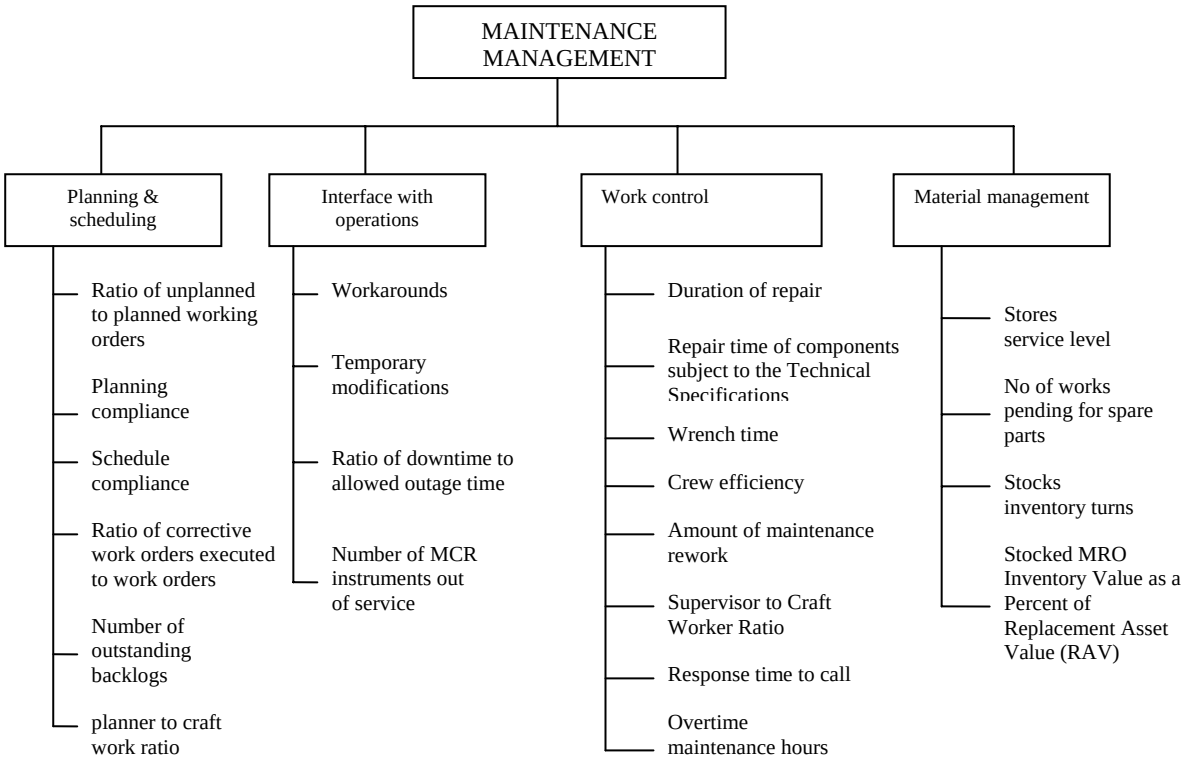

Fig 3. Indicators structure for the maintenance management

3.3 Maintenance budget

The objective of the plant management of nuclear generating utility is to maximize production of electricity at the lowest cost, the highest quality and within the established safety standards. The maintenance budget is an increasingly important aspect in the new economical environment in the energy market. Reducing the production costs, including the maintenance costs in particular is the condition of survival in the competitive energy market. Figure 4 shows the proposed indicators structure for the maintenance budgeting.

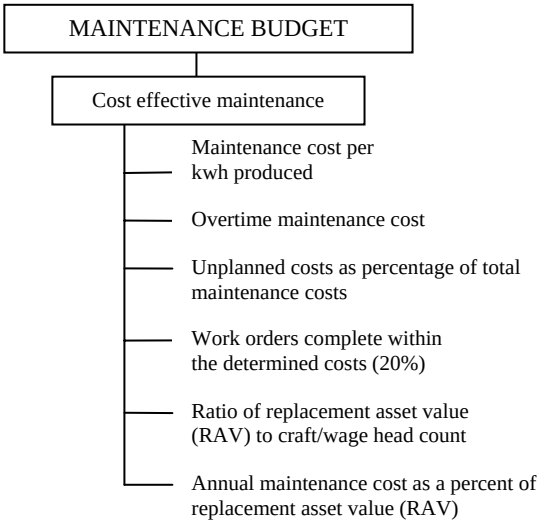

Fig4. Indicators for the maintenance budget

However we realize that because the main emphasis in our approach was put on the safe operation of a power plant, the economic effectiveness of the maintenance program, despite its unquestionable importance, was not developed in such a depth that is sufficient to represent all the budgetary aspects of a cost-effective maintenance.

4. Conclusions

The proposed system for the maintenance performance indicators is the initial step in the development of the framework for the monitoring of the maintenance efficiency using measurable performance indicators. As a further step, the pilot studies should be initiated in order to validate the applicability, usefulness and viability of the approach for implementation of proposed system of maintenance indicators at nuclear power plants. Not all indicators proposed in this paper will be found meaningful at the specific power plant. The establishing of clear and simple definition for each selected indicator is a key part of the programme implementation. When selecting the indicators for the validation studies at certain power plant it is recommended to review each indicator and to modify to plant specific definition if necessary. The elaboration of the best definition for the selected indicator is a very challenging task as it provides the evidence on how meaningful is that indicator for the power plant. More information on the proposed maintenance monitoring framework including the definitions of the selected performance indicators can be found in the EU Summary Report EUR 22602 [1]. The Report also provides recommendations to nuclear power plants for the implementation of the proposed maintenance performance monitoring system.

5. References

[1] P.Vaisnys, P.Contri, C.Rieg & M. Bieth, Monitoring the effectiveness of maintenance programs through the use of performance indicators, DG JRC-Institute of Energy Summary Report EUR 22602, 2006.
[2] R. Smith, Key performance Indicators, Leading or Lagging and when to use them, (2003) www.reliabilityweb.com.
[3] A. Mc Neeney, Selecting the Right Key Performance Indicators, Meridium, 2005.
[4] R.Smith, Key performance Indicators - Leading or Lagging and when to use them, (2003) www.reliabilityweb.com.
[5] IAEA, Operational safety performance indicators for nuclear power plants, IAEA-TECDOC-1141, IAEA, Vienna, 2000.
[6] WANO, 2005 Performance indicators, Coordinating Centre, London, UK, 2006.
[7] IAEA, Maintenance, Surveillance and In-Service Inspection in Nuclear Power Plants, Safety Standards Series No.NS-G-2.6, IAEA, Vienna, (2002).
[8] The Society for Maintenance & Reliability Professionals (SMRP), Best Practice Metrics, www.smrp.org.
[9] IAEA, Integrated approach to optimize operation and maintenance costs, IAEA-TECDOC 1509, Vienna, 2006.
[10] IAEA, Economic Performance Indicators for Nuclear Power plants, Technical Report Series No. 437, Vienna, 2006.
[11] T. Ahren, A study of maintenance Performance indicators for the Swedish Railroad System, Licentiate thesis, Lulea university of Technology, Sweden, 2005.
[12] L. Swanson, Linking maintenance strategies to performance, International Journal of Production Economics, 70**,** 237-244, 2001.
[13] E.Lehtinen, B.Wahlstrom, A.Piirto, Management of Safety through performance indicators for operational maintenance, Proceedings of IAEA Specialist meeting on Methodology for Nuclear power plant performance and Statistical Analysis, Vienna, 1996.

Session 19.3.2

Waste

RADIO ACTIVE WASTE PLANTS – BACK TO THE FUTURE

J. E. EARP, ASSOCIATE DIRECTOR STRATEGY, D.R.THOMPSON, SENIOR PRINCIPAL ENGINEER

Aker Kvaerner Engineering Services

Richardson Road, Stockton-on-Tees, TS18 3RE, United Kingdom

Abstract

This paper outlines the potential to provide smaller, potentially modular radwaste plants, suitable for new reactor proposals, within increasingly strict environmental control regimes, and with reduced discharge authorisations. Aker Kvaerner have been involved in the design, build and commissioning of radwaste plants over many years and provided the plant for Sizewell B, one of the last major PWR's to be built anywhere in the world. Unit operations and design characteristics of radioactive waste processing plant are discussed. It is concluded that these have changed little in the past 30 years. The traditional build characteristics and metrics of large radioactive waste processing facilities are described in both the reprocessing and the power generation industries. New reactor and fuel characteristics are described and used to highlight areas of potential design improvement, reducing the size, complexity, construction programme and cost of future power reactor radwaste facilities.

1. Introduction

The historical process design of large waste facilities has changed little in the past 30 years, the principal unit operations are given in Figure 1:

SOLID	LIQUID	GAS
Incinerate	Ion Exchange	Filtration
Compact	Precipitation / Filtration	Adsorption
Encapsulate	Evaporation	

Table 1. Unit Operations

Some Examples of these processes are given below:

2. Conventional Design Practice

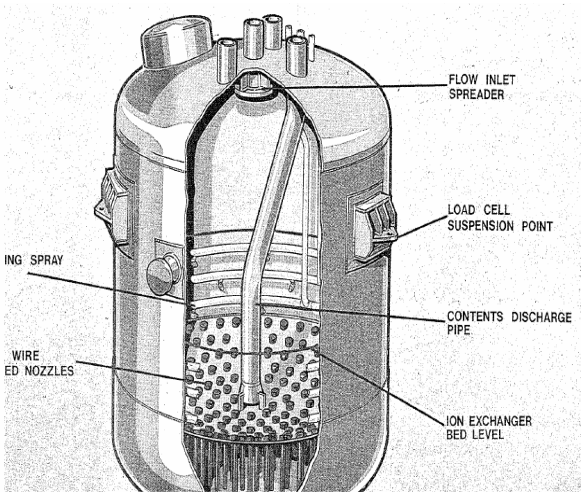

Figure 1. SIXEP Universal Vessel

At Sellafield, the Site Ion Exchange Effluent Plant (SIXEP) is an early generation of Radwaste plant for the treatment of site magnox sourced liquid effluents, designed in the late 1970's, and based on the use of filtration and ion exchange. The plant is monolithic, some 100m x 50m x 30m and the processing capacity some 4000m3/day. 70,000 te of concrete were used in construction.

Figure 1 shows a view of a Universal Vessel designed for the SIXEP facility at Sellafield. This common vessel was designed for operation with both media filtration and ion exchange.

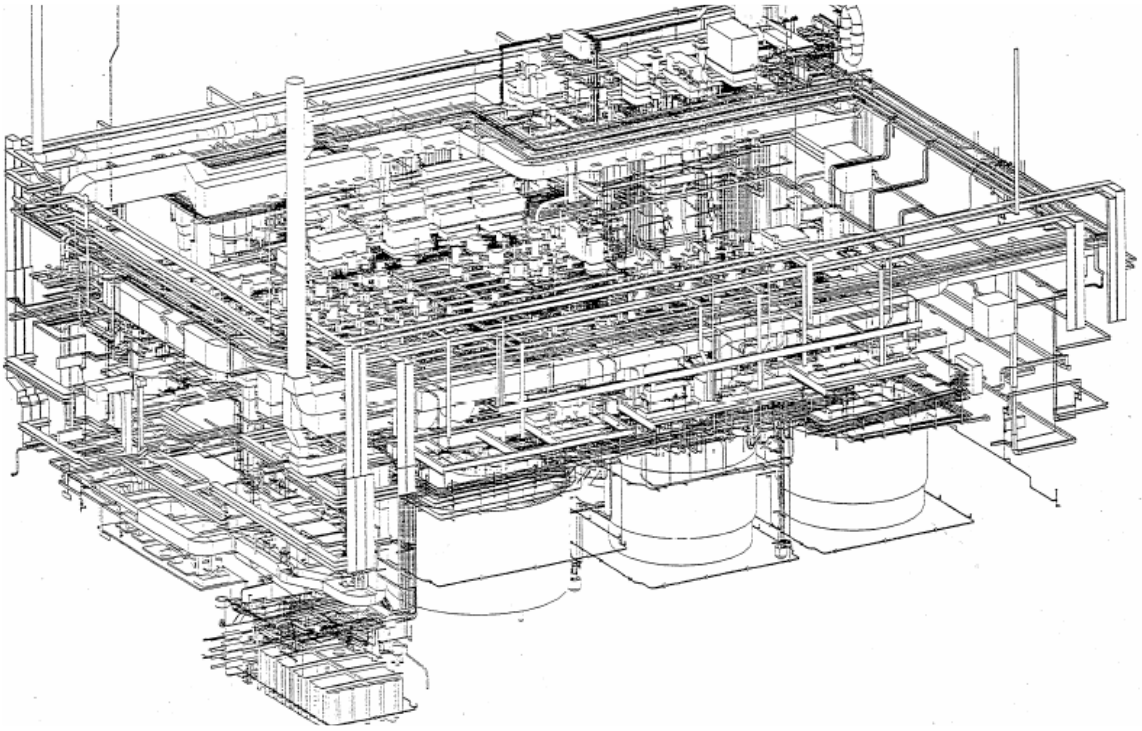

1.

Figure 2 shows a view of the Enhanced Actinide Removal Plant (EARP) processing plant. This large (65m x 45m x 35m) effluent treatment facility at Sellafield is still in service, and was constructed to meet waste requirements for medium and low active waste streams. The process basis for this facility was advanced chemical adsorption, and ultrafiltration, engineered to meet exacting operational and performance standards. High DF's were achieved for Actinides, Cs, Sr and Co. This plant is also monolithic, and used some 60,000 te of concrete, with over 30 km of pipework and 50 km of cabling.

Sizewell B Radwaste Plant is a fully integrated facility, designed in the late 1980's, and of similar size to the previous examples. In contrast, this plant uses the whole range of available process technologies for the treatment of gaseous, liquid and solid wastes from the operation of the Sizewell B PWR. This facility has nearly 400 cells, and processes almost all the active wastes on the site.

3. Process Performance

These plants have had a significant effect on operational performance. Figure 3 shows the reduction in historical Discharges from Sellafield in relation to SIXEP and EARP.

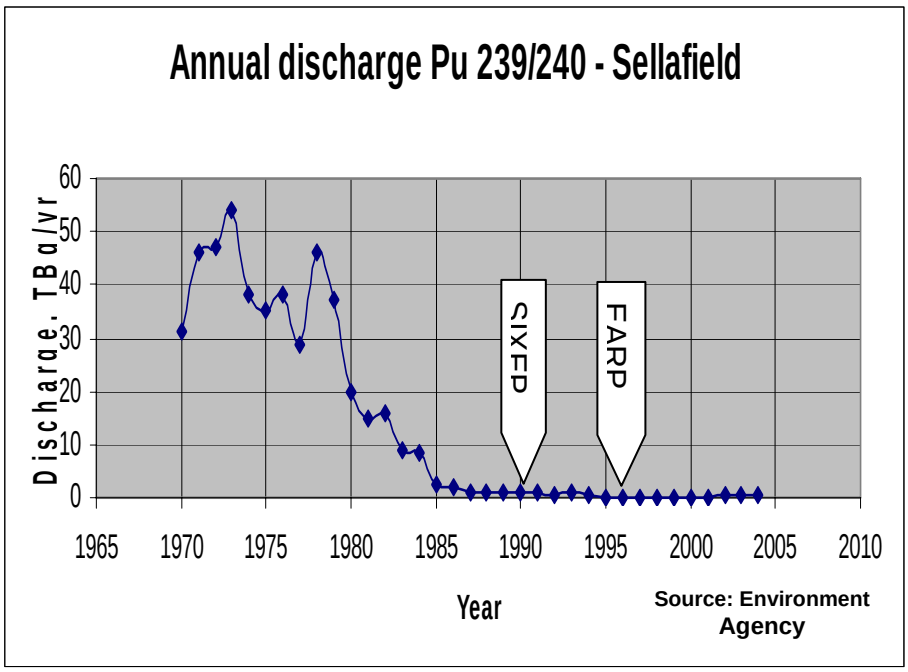

Figure 3. Historical Discharges at Sellafield

4. Commonalities

These examples serve to illustrate the similarities:

- All use the basic unit operations to provide very effective operation
- All these facilities required large buildings of bulk poured concrete, with Monolithic construction
- All contained many interacting and inter-related systems, requiring a long and complex design and build.

5. Impact of New Technologies

We now have new or intensified technologies in a number of areas such as ion exchange and filtration. These have allowed performance improvements on a scale we could not conceive just a few years ago.

6. UK Energy Supply Issues

In the face of global energy demand, global warming and security of supply economics, the development of safe, economic advanced reactor designs is now of great importance.
In the historical context above, conventional radwaste plant may not at first sight meet improved safety, cost and construction objectives.
Accordingly, this paper describes how improved safety, cost and performance objectives can be achieved in radwaste processing for advanced reactors..

7. Advanced Reactor Design

For illustration, the AP1000 design basis has been used to assess the design of a future radwaste facility:
Figure 4 shows the design metrics for the AP1000 compared with previous generation PWR technology: These achievements will deliver improvements in safety, operability, shortened construction programme and reduced cost.
.

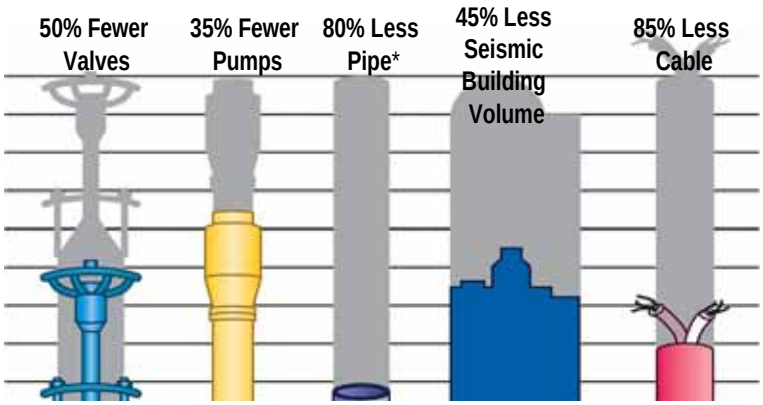

Figure 4. AP1000 Metrics. Source: Westinghouse

In applying these metrics to a future radwaste plant design, we also note the following:

a) Fabricated PWR Fuel Quality is now higher than ever; the operational design basis for Sizewell expressed as %Failed Fuel can now be exceeded by up to x100. This produces reductions in fission product activity.
b) Materials development and improved water chemistry have lead to much reduced corrosion product formation.
c) These in turn lead to much reduced primary and secondary coolant activities, giving:
    - Reduced shielding requirement in normal operation.
    - Reduced environmental impact, lower activity discharge.
d) The use of conventional effluent treatment processes as described earlier is now significantly enhanced by the availability of new materials in Ion Exchange and membrane technology.

8.0 Summary: Implications for Design

Taking these factors into account, we can now expect that compared to Sizewell B radwaste plant, it is possible to match the AP1000 metrics given in Figure 4 above.

This would deliver a building and plant volume of the order of one third to one half of that for Sizewell. It may be possible to make larger reductions in building volume although this is primarily due to the removal of evaporation and relocation of gaseous waste processing.

Figure 5 shows a view of one process area of a simplified future radwaste plant, designed with these principles:

Figure 5. Cutaway view of New Radwaste Facility

The expected improvements are:

- Reduced complexity and interactions significantly improve operational safety
- Process intensification and close alignment of processes against reactor waste streams deliver reduced plant size.

- Accelerated construction; this becomes possible because of reduced building size, and improved, fit-for-purpose building design.
- Programme: The use of skid mounted package plant, modular ‘pack’ systems for filters and ion exchangers, can shorten construction time.
- Allowance for sub contractor support service, by provision of Docking Bays and subcontractor Laydown areas, allows the future use of specialist waste services.
- Environmental; Reduced operational source terms gives potential for significantly reduced liquid and gaseous effluent levels.
- Solid Waste; improved ion exchange processes deliver equivalent performance with reduced waste volumes.
- New Radwaste plants need not be large monolithic structures, and can make more use of modular design and skid mounted systems.
- As a whole, these allow optimal design for the whole life cycle.
- Although more intensive, the processes have still not changed from those of the past. Hence, ***Back to the Future.***

References:

1. M. Howden , Progress in the reduction of radioactive discharges from Sellafield, BNFL

A 3-DIMENSIONAL HOMOGENIZED MODEL OF COUPLED THERMO-HYDRO-MECHANICS FOR NUCLEAR WASTE DISPOSAL IN GEOLOGIC MEDIA

I. CAÑAMÓN VALERA
Departamento de Ingeniería Civil: Infraestructura del Transporte, Universidad Politécnica de Madrid
E.U.I.T. Obras Públicas, C./ Alfonso XII nº 3 & 5, 28014 Madrid – Spain

R. ABABOU
Institut de Mécanique de Fluides de Toulouse, Institut National Polytechnique de Toulouse
Allée du Professeur Camille Soula, 31400 Toulouse – France

F. J. ELORZA TENREIRO
Departamento de Matemática Aplicada y Métodos Informáticos, Universidad Politécnica de Madrid
E. T. S. I. de Minas, C./ Rios Rosas. nº 21, 28003 Madrid – Spain

ABSTRACT

The present work is devoted to near-field coupled modelling of a hypothetical underground high level waste disposal in fractured granitic rock ("In-situ" experiment, FEBEX Project), performed at the Grimsel Test Site (GTS, Switzerland). First, a 3-dimensional reconstruction of the fractured network surrounding the FEBEX gallery is performed by Monte Carlo simulation, taking into account geomorphological data. Then, we estimate the equivalent coefficients of the fractured network by applying a superposition method [1]. Finally, a continuum equivalent model for 3D coupled Thermo-Hydro-Mechanics (THM) is developed and transient simulations of the excavation of the FEBEX gallery and the heating experiment are conducted using the Comsol Multiphysics ® software (3D finite elements). Preliminary comparisons of simulation results with time series data collected during the "In-situ" experiment yield encouraging results.

1. Introduction

FEBEX I and II is a demonstration and research project [2], which was carried out by an international consortium led by the Spanish agency ENRESA and co-funded by the European Commission and performed as part of the fifth EURATOM framework program, key action Nuclear Fission (1998-2002). This project aims to simulate the components of the engineering barrier system in accordance with the ENRESA's AGP ('Almacenamiento Geológico Profundo', deep geological disposal) Granite reference concept. The project includes tests on three scales: an 'In-situ' test at full scale in natural conditions; a 'Mock-up' test at almost full scale in controlled conditions; and a series of laboratory tests to complement the information from the two large-scale experiments.

The 'In-situ' experiment is being performed within a new drift which was excavated in the northern zone of the underground laboratory Grimsel Test Site (GTS), managed by NAGRA in Switzerland [3]. An important part of the demonstration experiment lays in the modelling tasks. Being able to model the processes occurring in such coupled and complex conditions is a fundamental step to assess this kind of disposals as a feasible and safe solution for the nuclear waste management.

This work aims to model both the near field (fractured rock) and the coupled Thermo-Hydro-Mechanical (THM) processes occurring in the FEBEX 'In-situ' experiment at the GTS.

2. Monte Carlo simulation of the 3D fractured network

A reconstruction of the 3D fracture network in a 70 m×200 m×70 m block surrounding the FEBEX gallery was obtained by Monte Carlo simulation, taking into account the geo-morphological data collected in exploratory boreholes. The following information was available [2, 3]:

- *Fracture orientation*. Four different families of fractures were defined according to both morphological (exploratory boreholes measurements) and genetic criteria. Uniform distributions within specific angle intervals were used for the dip (maximum slope direction) and the plunge. Figure 1 shows the stereonet of the family classification;
- *Fracture aperture*. Data on fracture aperture are only qualitative. Measurements in the main tunnel of the GTS only distinguish between filled, open and wet fractures (Figure 2). Initial values for aperture were assigned to each class and were later fitted to hydraulic measurements;
- *Fracture density*. The fracture density of the 2D map of traces (Figure 3) of the cylindrical drift, taken as (Σ trace length / intersecting plane area), was adjusted. Moreover, an anisotropic density was obtained by considering five different density zones in the trace map;
- *Fracture location*. A homogeneous Poisson process was used to define the coordinates of the fracture centres. However, the distribution of centres in the proximities of the drift was locally adapted to fit the non-uniform fracture density observed in the trace map;

…and the following parameters were optimized:

- *Fracture size*. The power law distribution was used. There are three parameters in this distribution: R_{min}, R_{max} and the exponential coefficient b. The R_{max} was set to a fixed value of 100m. The other two parameters were optimized to fit the geologic data.

An optimization procedure based on Simulated Annealing was used to adjust fracture size distribution so as to minimize the discrepancy between synthetic fractured medium and real fractured medium. The optimum values of the fracture size distribution are R_{min}=0.1985m, R_{max}=100m, and b=3.3048. Figure 4 shows a 3D view of the optimized 3D fracture network with N = 2906474 disc fractures.

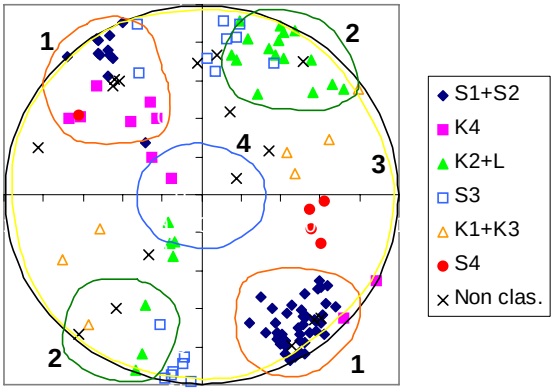

Fig 1: Families classification of the fracture data coming from exploratory boreholes.

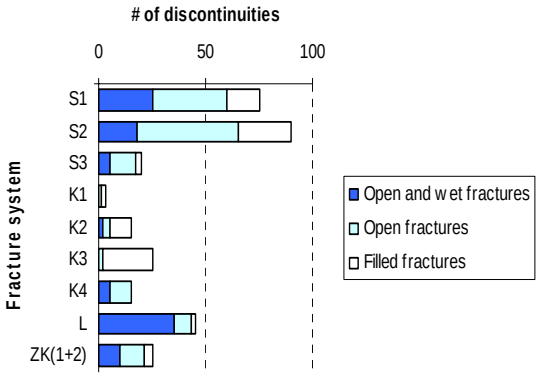

Fig 2: Fracture aperture frequency in the GTS tunnel (from [3]).

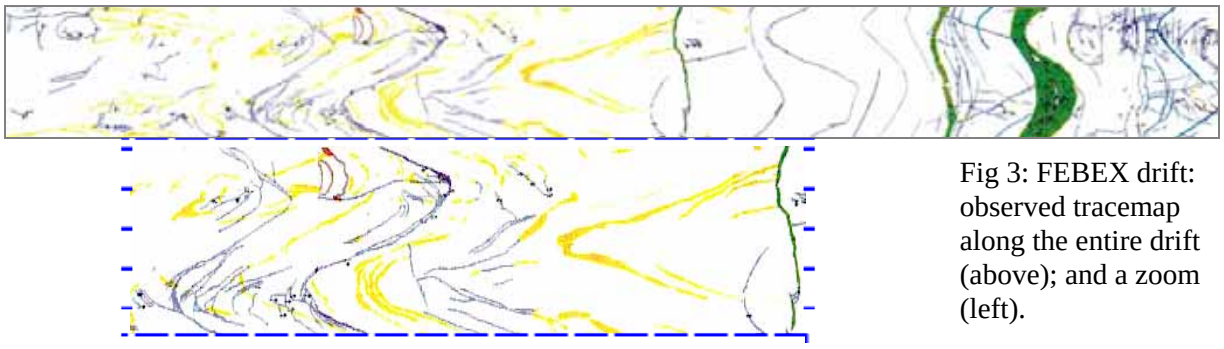

Fig 3: FEBEX drift: observed tracemap along the entire drift (above); and a zoom (left).

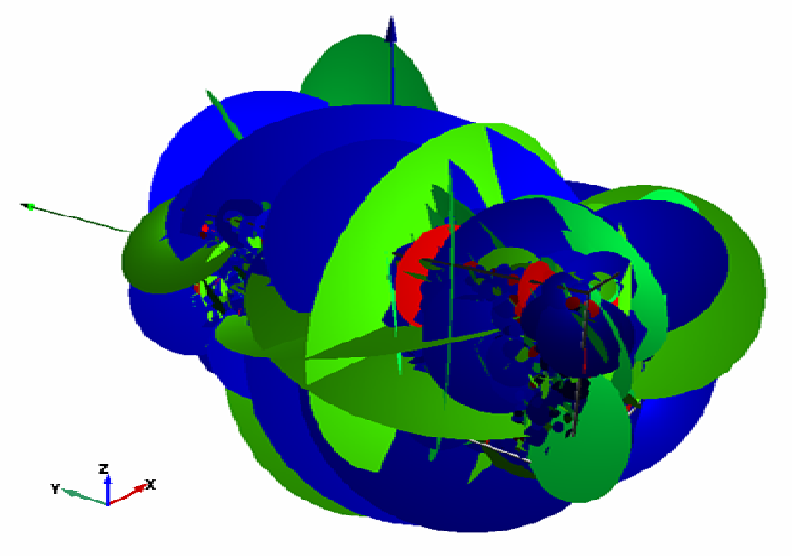

Fig 4: 3D view of the simulated fractured medium.

3. THM simulation of the FEBEX "In-situ" experiment

A continuum equivalent model for 3D coupled THM processes was developed based on [4], including: hydro-mechanical coupling via tensorial Biot equations (non-orthotropic), a Darcian flow in an equivalent porous medium (anisotropic permeability), as well as thermal stresses and heat transport by diffusion and convection, taking into account the thermal expansivity of water.

Equivalent homogenized H-M properties were determined from the simulated fractured medium based on a linear superposition approximation, which may be applied either to the whole domain, or more generally, to a partition into subdomains. The superposition approach leads to a conversion of the discrete 3D fractured medium into an equivalent continuum, by summing up all the individual contributions due to each singular fracture [1]. Equivalent coefficients such as hydraulic conductivity and mechanical stiffness were computed. The treatment followed during all the mathematical and physical developments considers conductivity and stiffness as tensors in the 3D space.

The simulation domain is the 70x200x70m^3 block mentioned above, with the Geographic North oriented towards –X and the origin of coordinates in the block centre. There are three connected drifts: the Main tunnel, the Laboratory tunnel and the FEBEX drift, the last one being centred in the origin of coordinates (Figure 5). In the test zone of the FEBEX drift there exist a heating process defined here by a temperature gradient from 100ºC at r=0m to 35ºC at r=1.14m, being r the radial direction in the FEBEX drift. Comsol Multiphysics® was used to perform the simulations.

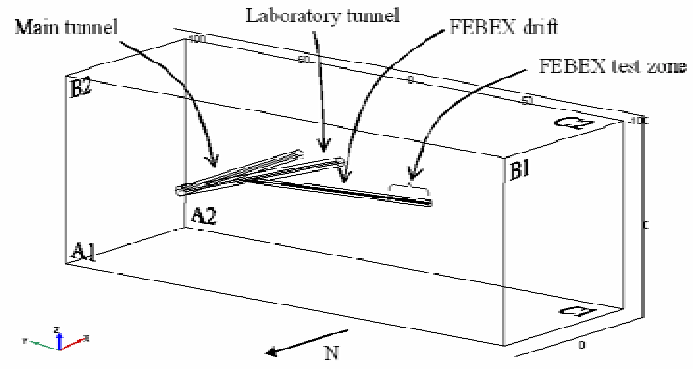

Fig 5: Domain of the THM simulation and boundary nomenclature.

The problem was simulated for different conditions of the rock (homogeneous isotropic, homogeneous anisotropic or heterogeneous anysotropic), and for three different stages:

- *Hydro-lithostatic equilibrium of the rock mass*: at this stage, there is no drift and a fully saturated 365m rock mass is assumed to be lying over the upper boundary of the domain. Both the hydrostatic and the lithostatic loads were imposed gradually for the time-dependent analysis. Relative fluid pressure was computed in all the models.
- *Drifts excavation simulation*: the HM response of the fractured rock is analyzed during the excavation of the drifts, which was modelled by gradually decreasing both the normal stresses and the fluid pressure in the boundaries of the excavated tunnels. Real hydraulic conditions existing in the GTS were used in this case.
- *Heating experiment simulation*: at this stage, the full THM model is used. A 3-year heating process is simulated around the FEBEX test zone (last 17 m of FEBEX drift). Heat load profile was determined from FEBEX "In-situ" experiment. The test zone was filled with bentonite [2].

We only present here some results of the *heating experiment simulation* (third stage). Figure 6 shows the final state of the fluid pressure in the 3D domain, as well as the flow lines at z = 0m. Figure 7 shows the Von-Misses stress at a cross-section through the FEBEX gallery axis, where the effect of thermal stresses can be appreciated. Finally, Figure 8 shows a comparison of measured and simulated temperatures at different distances in a radial borehole drilled in the test zone.

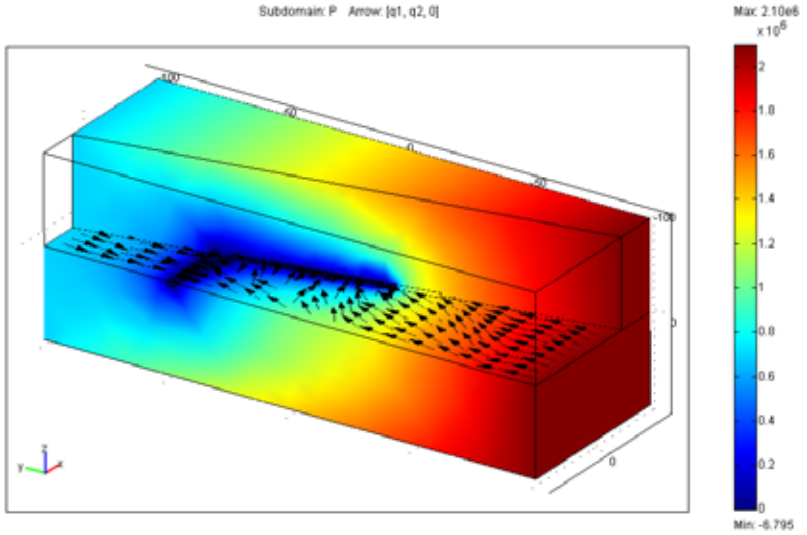

Fig 6: Final state of the fluid pressure in the heating experiment simulation.

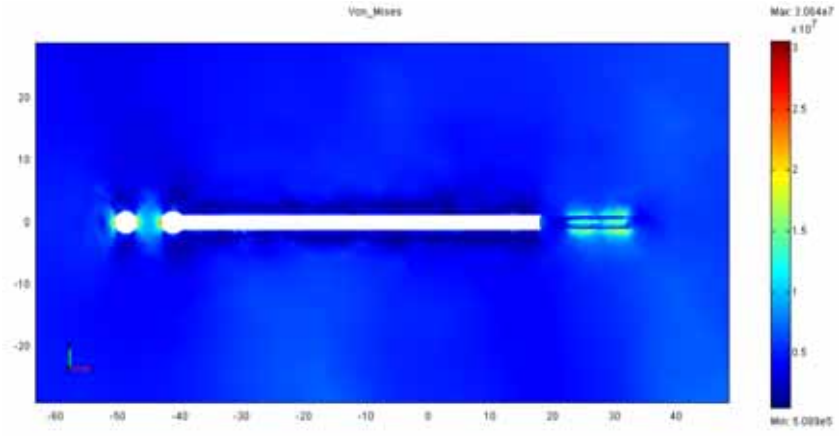

Fig 7: Final state of the Von-Misses stress (cross-section) in the heating experiment simulation.

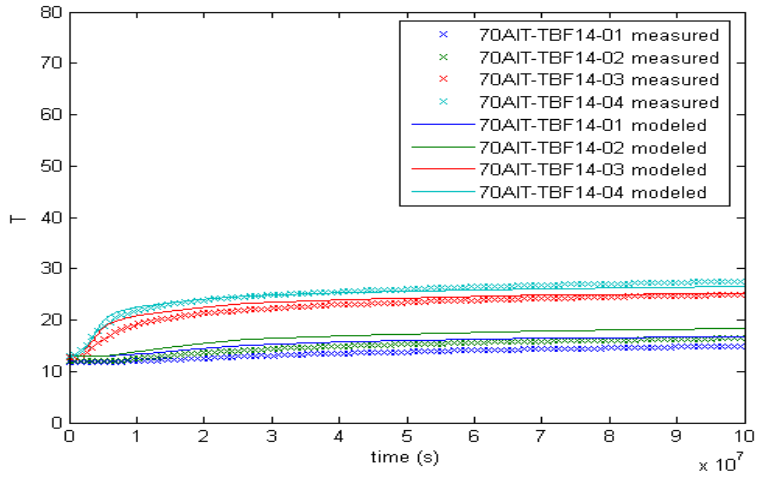

Fig 8. Comparison of measured and simulated temperatures in the heating experiment simulation at radial borehole 70AIT-TBF14.

4. Conclusions

This work develops an integrated methodology to model coupled processes occurring in a hypothetical radioactive waste underground repository in crystalline fractured rock (FEBEX "In-situ" experiment).

First, the 3D fractured network was simulated based on geomorphological information, and the locally heterogeneous fracture density around the FEBEX drift was notably well reproduced. Then, a continuum thermo-hydro-mechanical model was developed and implemented in the Comsol Multiphysics® numerical package. An up-scaling methodology was used to feed the numerical model with homogenized coefficients computed from the simulated fractured network. The advantage of the continuum approach is that it can be used for modelling coupled THM processes in the presence of many, variously oriented fractures, while a discrete fractures approach would become rapidly intractable as the number of fractures and their geometrical complexity increases. Fully anisotropic (non-orthotropic) spatially variable homogenized coefficients were computed to feed the model.

Three different stages were simulated with this modelling approach. Here, we focused mainly on the simulation of the FEBEX "In-Situ" heating experiment. The preliminary comparisons of simulations with time series data collected during the experiment yield encouraging results, and provide a good starting point to assess the validity of such models for nuclear waste underground disposals.

5. References

[1] Ababou R., A. Millard, E. Treille, M. Durin, F. Plas : Continuum Modeling of Coupled Thermo-Hydro-Mechanical Processes in Fractured Rock. Comput. Methods in Water Resour. (CMWR'94 Heidelberg), Kluwer Acad. Publishers, A. Peters et al. eds., Vol.1, Chap.6, pp.651-658, 1994.

[2] Huertas F. et al. *Full Scale Engineered Barriers Experiment for a High-level Radioactive Waste in Crystalline Host Rock (FEBEX Project)*. Final Report. European Commission. Report EUR 19147 EN. 2000.

[3] Keusen H.R., Ganguin J., Schuler P. & Buletti M. Grimsel Test Site. Geology. NAGRA, NTB 87-14E. 1989.

[4] Noorishad J., et al. Coupled thermo-hydro-elasticity phenomena in variably saturated fractured porous rocks: Formulation and numerical solution. *Dev. in Geot. Eng.: Coupled T-H-M Proc. of Fract. Media*. (O. Stephansson, L. Jing & C-F. Tsang, eds.) 79: pp. 93-134. Elsevier. 1996.

USE OF INORGANIC HIGHLY SELECTIVE ION EXCHANGE MATERIALS FOR MINIMIZATION OF LIQUID WASTE VOLUMES AT THE LOVIISA NPP IN FINLAND

ESKO TUSA
Fortum Nuclear Services Ltd
POB 100, 00048 FORTUM, Finland

ABSTRACT

Loviisa Nuclear Power Plant uses evaporation for treatment of different waste waters. With highly selective ion exchanger radioactive cesium is removed from concentrates for storage and disposal. After treatment the processed liquid can be released to the sea.

Highly selective inorganic ion exchange materials, CsTreat® for cesium, SrTreat® for strontium, and CoTreat for cobalt and other corrosion products, were developed. Several industrial applications have proven their efficiency for different waste types. Typically decontamination factors of several thousands can be achieved.

Since 1991 only 160 liters of CsTreat®, has been used to purify about 1100 m^3 of evaporator concentrates at the Loviisa NPP. This volume reduction has created good savings in treatment, conditioning and disposal costs.

Selective ion exchangers are typically used in small columns. Spent ion exchange columns can be disposed of in concrete containers. In the Loviisa NPP 12 pieces of columns are sealed into one concrete container with inner volume of one cubic meter.

1. Introduction

Fortum's (formerly: Imatran Voima Oy, IVO) Loviisa Nuclear Power Plant has two VVER-type pressurised water reactor units. The commercial operation of Loviisa 1 (LO1) began on May 9, 1977, and that of Loviisa 2 (LO2) on January 5, 1981.

Many improvements have been made over the years at the Loviisa NPP. The electrical power of the Loviisa NPP has been increased to a nominal output of 2x488 MW_e (net), and the life time has been extended to 50 years. The load factors of the Loviisa NPP have always been high, e.g. in 2006, they were 93.3 % for LO1 and 88.6 % for LO2.

Many improvements in radioactive waste management have been made, too. The goal has been to optimize the whole waste management from collection of waste to its final disposal. One very important area was treatment of waste waters and liquid wastes by effective volume reduction.

The evaporators for floor drain waters have been modified in 1986, in order to reach a salt content of 350 g/liter in concentrates. A Nuclide Removal System (NURES), based on the use of inorganic ion exchange material in columns, has been in operation since 1991 for removal of cesium from evaporator concentrates. A solidification plant (based on cementation and using concrete containers as final disposal packages) has been designed and constructed, and it will be commissioned in 2007. The underground final repository for LILW is situated at the site of the Loviisa NPP. It was licensed in 1998, and after 1 January 2007 about 7000 drums (each 200 litres) have been disposed of.

Treatment of liquid wastes by highly selective ion exchangers separates radioactive elements for storage and disposal. Even from high salt solutions radioactive target nuclides can be removed. After treatment the processed liquid can be released.

Since 1991, the NURES technology has been exported also to foreign customers. A mobile NURES-unit has been constructed and used in two projects, and highly selective materials have been used in tens of different projects in various countries. Over 200 test cases have been realized. Best benefit for users come from high volume reduction of waste and from high decontamination of purified liquid.

2. Treatment of evaporator concentrates at the Loviisa NPP

Evaporator concentrates are collected into the liquid waste storage, which is situated in a separate building. Annually 50-70 m^3 of evaporator concentrates and 10-15 $m^3$of spent resins are collected. Four 300 m^3 stainless steel storage tanks for evaporator concentrates and four similar tanks for spent resins are located in concrete blocks with inside stainless steel linings.

The large liquid waste storage capacity made it possible to store the evaporator concentrates for many years prior to additional treatment, i.e. cesium removal and release to the sea, or solidification. On 1st January 2007 the accumulated amounts of concentrates were 691.5 m^3 with 1297 GBq.

Due to natural decay, the amount of short lived radionuclides decreases considerably during the storage period. Most corrosion products settle onto the bottom of the tanks. During the 1980s, it was found that over 50% of the content of radionuclides in the evaporator concentrates consisted of Cs-137 and Cs-134, and over 90% of a total solution activity was of Cs. The second dominating radionuclide, Co-60, was associated with the solid precipitates on the tank bottom. By removing cesium from the tank solution, the purified liquid could be released within licensed release limits, and Co-60 would be left in a small waste volume on the bottom of the tank.

Fortum and the Radiochemistry Laboratory of the Helsinki University developed together a cesium selective inorganic ion exchange material CsTreat®, which is stable, granular material (with very high total ion exchange capacity and extremely high selectivity for cesium). In the nuclide removal system, CsTreat® is typically used in granular form in columns. In the column use CsTreat® is normally used in the grain size of 0.3-0.85 mm, and it can be used in pH area 1-13 in high salt (up to 400 g/l) liquids and in pH 2-11.5 in very low salt solutions. Later on two other highly selective ion exchangers, SrTreat® for strontium, and CoTreat for cobalt and other corrosion products, were developed.

3. Nuclide Removal System (NURES)

The principle of NURES is simple (Figure 1). The first phase is efficient particle filtering, which removes particle bound radioactivity as totally as possible and protects the ion exchange bed from plugging, and the second phase is ion exchange with selective material to remove ionic radioactivity. The full size NURES, as constructed in the Loviisa NPP, is also shown in Figure 1.

Table 1 shows the results for the purification of five tanks of evaporator concentrates at the Loviisa NPP since 1991 (2). After treatment of fourth tank the average processing capacity for about 900 m^3 was about 12.2 m^3/kg. After the fifth tank about 1100 m^3 has been treated, and the average processing capacity is about 10.4 m^3/kg. Processing capacity for the fifth tank was much lower than that for the previous tanks. Probable reason for this was noticed to be higher amount of solids in the waste liquid. In the case of fifth tank there was about 3.4 mg/l of solid material with very small particle size. 0.1 µm particle filter probably could not remove enough solid particles, which led to plugging of part of ion exchange capacity. Because of this more columns were used for purification of this tank than for other tanks. Efficient filtering before ion exchange is essential for nuclide removal.

A final disposal container for spent ion exchange columns has the same outer dimensions (height and diameter 1.3 m) as the container for solidified waste, having 12 disposal holes in the concrete filling of the container (Figure 2). Spent columns are sealed with lead plugs into holes of the concrete container. When all holes are full, a concrete cover is cast on top of the container.

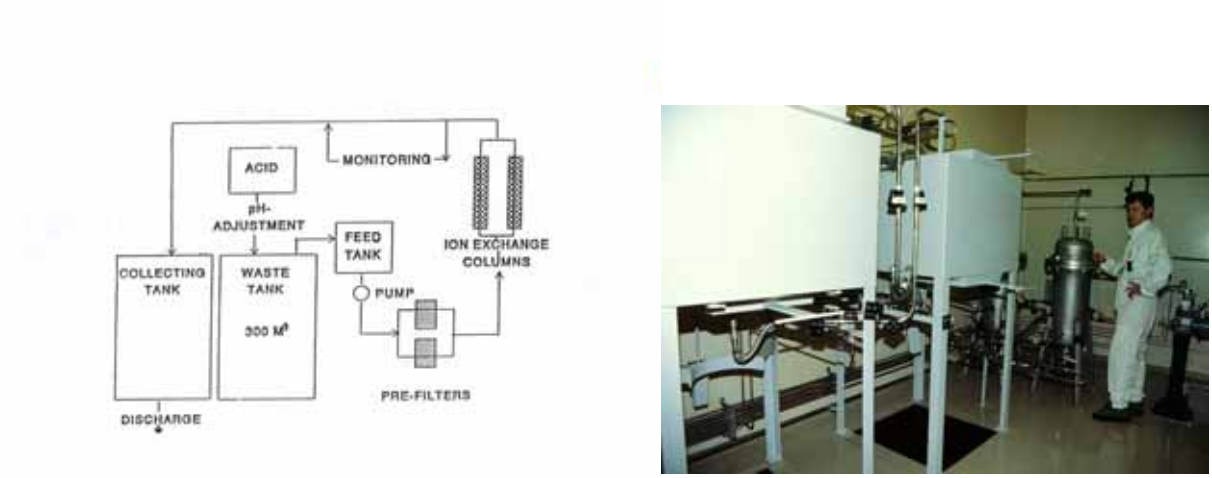

Figure 1. Principle of NURES and its realization at the Loviisa NPP.

Figure 2. The final disposal container for spent ion exchange columns.

In treatment of about 1100 m^3 of evaporator concentrates in Loviisa NPP the average decontamination factors have been well over 1000 [1, 2]. Figure 3 gives a typical performance curve for one 8 liter column. DF is relatively low in the beginning of treatment of high salt liquids, but it rather soon reaches good decontamination levels (DF = 10 000 or above). After some time, in the case of Fig. 3 after about 40 m^3, DF starts to decrease, because of exhaustion of the ion exchange capacity. At any level the operator can decide, which level he accepts for final shut-down of the column.

	Treated in	Volume treated, m^3	IX mass used. liters	Total salt conc., g/l	Decontamination factor, DF	Processing capacity, l/kg	Volume reduction factor VRF
Tank 1	1991-92	253	24	240	>2000	16 000	2000
Tank 2	1993	210	32	176	>2000 max 30 000	10 000	1260
Tank 3	1995	230	24	228	>1000	15 000	1840
Tank 4	2000	202.6	32	220	>1000 max >28 500	9600	1200
Tank 5	2002 -03	200.7	48	>220	>1000 max >16 100	6400	800

Table 1. Results from purification of five evaporator concentrate tanks at the Loviisa NPP

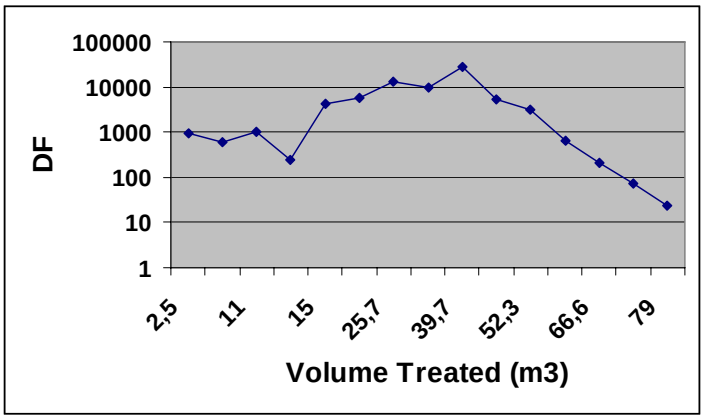

Fig. 3. Decontamination factor (DF) for one eight liter column during its operation time

4. Volume reduction of waste with the use of selective ion exchanger

Highly selective ion exchangers can be utilized in many different ways. Most efficient way is to use compact columns with volume of 2-12 liters. Until now, totally 1100 m^3 of evaporator concentrates have been purified at the Loviisa NPP by CsTreat® with only 20 pieces of 8-liter columns. Between 1991 and 2006, 112.7 GBq of Cs-137 and 2.6 GBq of Cs-134 (calculated on 25th April 2007) were removed from liquid to CsTreat®, and the purified liquid was released to the sea.

The volume reduction factor (VRF) of the waste itself, comparing the volume of the original liquid to the volume of the CsTreat® columns, is close to 7000.

Cementation of 1100 m^3 of concentrates would result in about 2310 m^3 of solid concrete product, i.e. 2310 pieces of concrete containers. Present amount of 20 spent columns will not fully occupy even two containers. Thus, the volume reduction of packed waste is close to 1400.

5. Savings due to selective ion exchange

Selective ion exchange and release of purified liquid gives economic savings due to decreased cementation needs, due to some reduction in storage costs, due to reduced transportation costs, and due to reduction in final disposal volume.

Remarkable savings have been achieved at the Loviisa NPP, when cementation of about 1100 m^3 of evaporator concentrates has been avoided.

Estimating that about 3-5 m^3 of sludge is left for cementation from annual 50-70 m^3 of concentrate collection, well over 90 % of total cementation, storage and transportation needs are avoided.

In final disposal the savings come from reduction of disposal cavern. Low- and intermediate-level wastes from the Loviisa NPP are disposed of in a repository constructed in the bedrock of the power plant site. By 1st January 2007, already a total of about 7000 steel drums (each 200 litres) of maintenance waste have been disposed of. In the design and construction of a cavern for solidified waste the reduction of cemented waste due to treatment with selective ion exchange was taken into account.

The cavern for solidified waste was constructed for 5040 concrete containers. When cementation of 1100 m^3 was avoided, about 2310 containers were eliminated from final disposal. From annual concentrate collection of 50-70 m^3 additionally about 100-140 containers are eliminated annually. Without the use of selective ion exchange materials the length of the cavern for solidified waste, which is now about 84 meters long, would have been at least 50 % longer.

6. Foreign applications of the NURES system

The NURES technology has been applied successfully also in various foreign applications. A mobile NURES unit was constructed, too, and it was first used in Paldiski in Estonia to purify 760 m^3 of low active waste liquid. After that NURES unit was used in Murmansk in Russia to remove mainly cesium and strontium from radioactive waste waters accumulated from nuclear-powered ice-breakers.

Typical floor drain waters were purified for example in the Callaway NPP (PWR), MI, USA, and at the Olkiluoto NPP (BWR) in Finland. Continuous purification is going on at some NPPs in USA. Pool waters have been purified for example at the US DOE's Savannah River Site and at Sellafield's reprocessing plant in UK.

Reprocessing waste liquids were purified at Japan Atomic Energy Research Institute's (JAERI) site in Tokai-mura in Japan. An interesting application of CsTreat has been at UKAEA's Dounreay site to remove cesium from Prototype Fast Reactor's sodium coolant.

The construction of a new liquid waste treatment system, including utilization of CsTreat®, has been completed at the Paks NPP (VVER-440) in Hungary, and the operation is scheduled to start in 2007. The system is quite similar to that used at the Loviisa NPP. Over 2000 m^3 of evaporator concentrates and other liquids will be purified (240 l/h) with this system. A boric acid recovery system has also been installed. 70-90% of boric acid will be recovered from the existing liquid wastes.

Additionally, plenty of smaller applications of these highly selective ion exchange materials are operating for special needs.

7. Conclusions

Fortum has taken many practices into use to minimize the amount of wastes going to the on-site repository for final disposal. The whole waste management chain has been optimized from waste collection to final disposal. High capacities of treatment equipment and existing systems have made it possible to store and treat liquid wastes in a different way than at many other power plants.

Treatment of evaporator concentrates included originally the greatest potential for savings. Selective removal of radionuclides was developed and taken into use. It has proven to be a very efficient way to minimize the volumes of evaporator concentrates and to reduce the volume of final disposal. Since 1991, selective removal of radionuclides has purified 1100 m^3 of evaporator concentrates with only 160 liters of selective ion exchange material, giving a volume reduction factor of about 1400 for packed waste. Avoidance of cement solidification of the original waste volume has brought remarkable savings in the cost of treatment, conditioning, storage and final disposal. In the construction of the underground repository, which is already in operation at the Loviisa NPP site, reduction in the volume of evaporator concentrate has been taken into account.

Based on Fortum's own experience in the operation of the Loviisa NPP, several practices and systems are now also used at many nuclear sites around the world.

References

1. E. Tusa, A. Paavola, R. Harjula and J. Lehto, Ten years' successful operation of nuclide removal system in Loviisa NPP, Finland, Proceedings of ICEM 01 Conference, Bruges, Belgium, 30.9.-4.10.2001, Paper 40-3.

2. E. Tusa, R. Harjula, and P. Yarnell, Fifteen Years of Operation with Inorganic Highly Selective ion Exchange Materials, to be published in Proceedings of Waste Management 2007, Tucson, AZ, February 25 - March 1, 2007

ENC 2007 European Nuclear Conference
16-20 September 2007, Brussels, Belgium

European Nuclear Society
Rue de la Loi 57
1040 Brussels, Belgium
Telephone +32 2 505 3 50
Fax + 32 2 502 39 02
ens@euronuclear.org
www.euronuclear.org

Layout and Design: Marion Brünglinghaus, ENS